

The ellipticity (H/V -ratio) of Rayleigh surface waves

Dissertation

zur Erlangung des akademischen Grades doctor rerum naturalium
(Dr. rer. nat.)

vorgelegt dem Rat der Chemisch-Geowissenschaftlichen Fakultät der
Friedrich-Schiller-Universität Jena

von Master-Mechanics Tran Thanh Tuan
geboren am 09. Sep 1980 in Hanoi, Vietnam

Gutachter:

1. Prof. Dr. Peter Malischewsky, FSU Jena
2. Prof. Dr. Frank Scherbaum, University of Potsdam
- 3.

Tag der öffentlichen Verteidigung: 04 February 2009

Zusammenfassung

Seit langem ist bekannt, dass die von Erdbeben hervorgerufenen Zerstörungen in menschlichen Ansiedlungen erheblich von den lokalen Bodeneigenschaften und von anderen Faktoren wie die unregelmäßige Oberflächentopographie und die Untergrundmorphologie abhängen. Eine der effektivsten Verfahren zur Charakterisierung der Untergrundeigenschaften ist die H/V -Methode, die eine Abschätzung des Verhältnisses der Fourieramplitudenspektren der horizontalen (H) und vertikalen (V) Komponenten der von der natürlichen Bodenunruhe erzeugten und mit einer einzelnen Station aufgezeichneten Schwingungen liefert.

Indem angenommen wird, dass die am meisten dominanten Beiträge der natürlichen Bodenunruhe von den Oberflächenwellen stammen, obwohl die exakte Zusammensetzung von den speziellen Gegebenheiten abhängen kann, ist das Ziel dieser Dissertation ein tieferes Verständnis des Verhaltens des H/V -Verhältnisses von Rayleighwellen, und sie trägt somit zur weiteren Entwicklung dieser etablierten H/V -Methode bei. Die in der Dissertation angewandte Methode zum Studium des H/V -Verhältnisses von Rayleighwellen führt von einfachen zu komplexen Modellen. Die Komplexität dieser Modelle reicht vom einfachen Modell "homogener Halbraum" zum allgemeinsten Modell "inhomogene Schicht über homogenem Halbraum".

Die Dissertation konzentriert sich auf die Spitzen und Täler der H/V -Kurven, die eine wichtige Rolle beim H/V -Formalismus spielen, und wie bestimmte Parameter diese beeinflussen. Zusätzlich studiere ich auch die Bewegung eines individuellen Teilchens. Es ist gut bekannt, dass die Teilchenbewegung im homogenen Halbraum immer retrograd ist, und ich zeige in dieser Dissertation, dass prograde Bewegung für das Modell "Impedanzoberfläche", welches einer dünnen Schicht über einem Halbraum entspricht, nicht möglich ist. Dagegen wird prograde Bewegung im Modell "Schicht mit festem Boden" beobachtet, welches ein Spezialfall des Modells "Schicht über Halbraum" für sehr hohen Impedanzkontrast ist. Es werden Karten konstruiert, die die Frequenzbeziehungen der Spitzen und Täler von H/V mit den Modellparametern demonstrieren, und es werden Anwendungen dieser Karten für das Studium von Naturkatastrophen vorgeschlagen.

Der "Oskulationspunkt" der Phasengeschwindigkeitskurven ist der Punkt, wo sich die individuellen Kurven von zwei Moden zu kreuzen scheinen. Ich zeige in dieser Dissertation, dass der Oskulationspunkt auch ein Punkt ist, an dem das H/V -Verhältnis seine Eigenschaft ändert: von zwei Spitzen zu einer Spitze und einem Nullpunkt. In der Umgebung dieses Punktes ist das Verhalten von H/V sehr empfindlich: es kann sich dramatisch ändern bei einer sehr kleinen Änderung irgendeines Parameters. Diese Eigenschaft wird analytisch bewiesen für das Modell "Schicht mit festem Boden", und einige der wichtigsten Klassen von Oskulation-

spunkten werden mit einfachen Formeln beschrieben. Für das allgemeine Modell "Schicht über Halbraum" kann nur eine Näherungsformel für die Menge der Oskulationspunkte angegeben werden.

Die Dissertation ist auch der Bestimmung von H/V einer einfallenden Raumwelle gewidmet, die aus der Tiefe des Substrats kommt, z. B. von einem Erdbeben. Ich zeige die Ähnlichkeit von H/V in diesem Szenarium mit H/V von einer einfallenden Raumwelle mit turbulentem Noise. Es stellt sich heraus, dass diese beiden H/V -Verhältnisse dann identisch sind, wenn die Scheingeschwindigkeit mit der Rayleighwellengeschwindigkeit übereinstimmt. Allerdings ist diese Bedingung nur theoretischer Natur, weil die Scheingeschwindigkeit der einfallenden Raumwellen immer größer ist als die S-Wellen-Geschwindigkeit im Halbraum, die für die Rayleigh-Oberflächenwellen eine obere Grenze darstellt.

Für die inhomogene Schicht benutze ich eine Technik von Vrettos zur Bestimmung der Eigenwerte und Eigenfunktionen. Das Ergebnis wird mit dem Modell einer homogenen Schicht verglichen, in dem die Parameter der Mittelwert von denjenigen im Modell der inhomogenen Schicht sind. Für die numerische Überprüfung des inhomogenen Modells wird Herrmanns (1994) [22] Programmpaket für Oberflächenwellen benutzt, das für die Berechnung synthetischer Noise-Daten in einem homogenen Vielschichtmodell über einem Halbraum entwickelt wurde. Die Ergebnisse stimmen gut mit den theoretischen Resultaten überein.

Abstract

It has long been observed that damage to human settlements during earthquakes depends greatly both on the local properties of the soil, and on other features such as irregular surface topography and underground morphology. One of the most efficient ways to define the soil properties is the H/V -method, which yields an estimation of the ratio between the Fourier amplitude spectra of the horizontal (H) to vertical (V) components of the ambient noise vibrations recorded at one single station.

Considering that the most dominant contributions to ambient vibrations are known to come from surface waves, although the exact composition may change depending on the particular site, the aim of this thesis is to more deeply investigate the behavior of the H/V -ratio curve of Rayleigh waves, and thereby contribute to the further development of the established H/V -method. The method of the thesis is to study the H/V -ratio of Rayleigh waves, working from simple to complex models. The model complexity ranges from the easiest model, “homogeneous half-space”, to the most general model: “inhomogeneous layer over homogeneous half-space”.

The thesis concentrates on the peaks and the troughs of H/V curves which play an important role in the H/V calculation, and how specific parameters affect them. I additionally study the motion of an individual particle. It is well-known that in homogeneous half-space, the particle motion is always retrograde, and in this thesis I show that the prograde is impossible in the model “impedance surface”, which is a thin layer over half-space. Prograde motion is observed in the model “layer with fixed bottom”, which is a special case of “layer over half-space” when the impedance contrast is very high. In studying the peaks and troughs, I construct maps showing their frequency relationships with parameters of the model and propose applications to the study of natural disasters.

The “osculation point” of the phase velocity curve is the point where the individual curves of two modes seem to cross. In this thesis, I show that the osculation point is also the point at which the H/V -ratio changes its property from having two peaks to having one peak and one zero point. Around this point, the property of H/V -ratio is very sensitive: it can change dramatically with a very small change of any parameter. This property is proved analytically in the model “layer with fixed bottom”, and some of the most important classes of osculation points are described with simple formulas. With the general model “layer over half-space”, only an approximate formula is determined for the set of osculation points.

The thesis is also devoted to determining the H/V -ratio of a body incident wave which is generated from deep inside the substrate, for example by an earthquake. I show the similarity of the H/V -ratio in this scenario to the H/V -ratio of a surface wave with a turbulence noise.

It turns out that these two H/V -ratios are identical if the phase velocity is that of a Rayleigh wave. However, this condition at present exists only in theory because the apparent phase velocity of incident body waves is always greater than S-wave of the half-space which is the upper bound value of Rayleigh surface waves.

For the inhomogeneous layer, I use a technique from Vrettos to determine the eigenvalue and eigenfunctions. I then compare the result with a model of the homogeneous layer in which the parameters are the mean value of those for the inhomogeneous layer model. To check the numerical calculations for the inhomogeneous model, I use a surface wave package distributed by Herrmann (1994) [22], which was created to construct synthetic data generating from the noise of a multi-homogeneous-layer over a half-space, and the results agree well with the theoretical results.

Contents

Zusammenfassung	i
Abstract	iii
Introduction and Motivation	xi
1 Two simple models	1
1.1 Plane waves	1
1.2 The homogeneous half-space (HS)	4
1.2.1 Eigen-value problem	4
1.2.2 H/V -ratio	6
1.3 The impedance wave	8
1.3.1 The dispersion equation	8
1.3.2 The H/V -ratio formula	10
2 Layer with fixed bottom (LFB)	15
2.1 Homogeneous layer	15
2.1.1 The eigen-value problem	16
2.1.2 Dispersion law	17
2.1.3 Displacements	19
2.1.4 H/V ratio	20
2.1.5 Particle motion	24
2.2 Inhomogeneous layer	26
2.2.1 The eigenvalue problem	26
2.2.2 The eigen functions	33
2.2.3 H/V -ratio	38
2.3 Conclusions	38

3	Layer over half-space (LOH)	41
3.1	Homogeneous layer	41
3.1.1	The eigen-value problem	41
3.1.2	Dispersion of zero-frequency Rayleigh waves	44
3.1.3	Displacements	51
3.1.4	H/V -ratio	52
3.1.5	Particle motion	62
3.1.6	H/V -ratio in the depth	66
3.2	Inhomogeneous layer over half-space	68
3.2.1	Application for synthetic data	75
3.3	Incident body waves	76
3.3.1	Formulas of H/V -ratios of incident body waves	78
3.3.2	Real incident angles	81
3.3.3	The relation between body wave and Rayleigh wave	84
3.4	Conclusions	86
4	Osculation points	89
4.1	Layer with fixed bottom	89
4.1.1	The case: $t_1^2 = t_2^2$	90
4.1.2	The case: $t_1^2 = 1$, $t_2^2 \neq 1$	91
4.1.3	Solutions of (4.12)	92
4.1.4	Solution of (4.13)	92
4.1.5	Numerical results	93
4.1.6	Get the Tolstoy's formula again from LBF's secular equation	93
4.2	Osculation points of LOH	94
	General conclusions and perspectives	97
	Appendix	101
	Curriculum Vitae	115
	Acknowledgements	117
	Selbstständigkeitserklärung	119

List of Figures

1.1	Rayleigh waves velocity as a function of Poisson's ratio ν : exact curve (continuous), Achenbach's approximation (dashed), Bergman's approximation (dotted)	6
1.2	H/V -ratio of Rayleigh waves as a function of Poisson's ratio	7
1.3	Model "Impedance wave"	9
1.4	Contour line of $P(y, \gamma_2)$	13
2.1	Homogeneous bottom fixed layer	15
2.2	Velocity curves of three modes with $\nu = 1/3$	17
2.3	The ellipticity for the model layer with fixed bottom (LFB) in dependence of frequency and Poisson's ratio: retrograde motion (dark gray) and prograde motion (light gray)	24
2.4	Inhomogeneous layer with fixed bottom model	26
2.5	Shear modulus functions in layer	32
2.6	Dispersion curves for three different values of Poisson's ratio. (0) fundamental mode, (1) first higher mode	34
2.7	Attenuation with depth of the horizontal and vertical displacement at representative frequencies for $\mu_\infty = 2000m/s$ and three different Poisson's ratios. (0) fundamental mode, (1) first higher mode	35
2.8	H/V -ratio curves for three different values of Poisson's ratio. (0) fundamental mode, (1) first higher mode	36
2.9	The ellipticity for the model inhomogeneous layer with fixed bottom in dependence of frequency and Poisson's ratio: retrograde motion (dark gray) and prograde motion (light gray)	37
3.1	Homogeneous layer over half-space	41
3.2	Isolines $K_1 = 0$ in dependence on ν_1 and r_s for different values of ν_2 . The position of three example models M_1 , M_2 , M_3 is indicated by stars.	49
3.3	Dispersion curves $\bar{C}(\bar{f}) = c(\bar{f})/\beta_2$ for the models M_1 , M_2 , M_3	49
3.4	Dispersion curves $\bar{C}(\bar{f}) = c(\bar{f})/\beta_2$ for the models M_1 , M_3 : Exact (continuous), Tiersten (dash), B6vik (dot) and Taylor expansion (dash-dot)	50

3.5	Dispersion analysis of synthetic data for a two-layer model with f-k (data1) and SPAC (data2). Comparison with the exact dispersion curve (solid) and the approximation (dashed)	51
3.6	H/V curve of Model 1 in Table 3	54
3.7	Contour of $\bar{f}_p/0.25$. The blue line is the curve of function $F(\nu_1)$ and it divides the domain into two parts: continuous red lines are for the singularities and dotted brown lines for maximum points.	56
3.8	Four different characters of H/V ratio. The curve of function $F(\nu_1)$ is blue and the curve of function $G(\nu_1)$ is green.	56
3.9	Contour of \bar{f}_z	59
3.10	Contour of \bar{f}_z/\bar{f}_p	59
3.11	Tokimatsu[1997] [55]	60
3.12	Contour of $\bar{f}_p/0.25$ as a function of r_s and \bar{f}_z/\bar{f}_p in region R_1	61
3.13	Contour of $\bar{f}_p/0.25$ as a function of r_s and \bar{f}_z/\bar{f}_p in region R_3	62
3.14	Contour of $\bar{f}_p/0.25$ as a function of ν_1 and \bar{f}_z/\bar{f}_p	63
3.15	2D graph of the domain of prograde motion (red) as a function of \bar{f} and r_s for the incompressible Model 2 (Table 3)	64
3.16	2D graph of the domain of prograde motion (white) as a function of \bar{f} and r_s for different values of ν_1 (contours) and for r_d and ν_2 of Model 3 (Table 3)	65
3.17	2D graph of the domain of prograde motion (white) on the interface as a function of \bar{f} and r_s for different values of ν_1 (contours) and for r_d and ν_2 of Model 1 (Table 3)	65
3.18	Peak frequency of H/V -ratio curve with respect to the depth	67
3.19	Three approximation of shear modulus in the layer: linear $G_1(x_3)$ (continuous), quadratic $G_2(x_3)$ (dashed) and third power polynomial $G_3(x_3)$ (dotted)	71
3.20	Phase velocity and H/V ratio curves of $G_1(x_3)$, $G_2(x_3)$ and $G_3(x_3)$	73
3.21	The phase velocity curve using Vrettos's technique (continuous), Newlands's (dashed) and Herrmann's program (dotted)	73
3.22	$\nu_1 = 0.4375$ for figure a, c and $r_s = 1/6$ for figure b, d	74
3.23	Deviation of singularity frequency between the actual model and the simple equivalent model "Layer over half-space" with the average shear wave velocity of the layer is calculated by (3.95)	75
3.24	Synthetic H/V -ratio data and two maps defining the value of Poisson's ratio and S-wave velocity contrast	77
3.25	Peak frequency of H/V -ratio of incident body waves	82
3.26	Ratio between peak and trough frequencies of H/V -ratio of incident body wave	83

List of Tables

2.1	The value of μ_∞ corresponding to the degree of approximation polynomial function	32
3.1	Parameters for models under consideration	42
3.2	Model parameters for the models M_1 , M_2 , M_3 with the derivatives of \bar{C} for $\bar{f} = 0$	48
3.3	Parameters for the "two-layer over half-space" model in Liège, Belgium . . .	76

Introduction and Motivation

There are many cities built on soft sediments, and a large number of them are unfortunately located in seismic areas, emphasizing the need for a careful and reliable assessment of site amplification phenomena. This issue has long been addressed by scientists and engineers who have developed many techniques to identify the main characteristics of site responses for soft deposits (i.e., resonance frequencies and amplification factor). Beside the classical geophysical and geotechnical tools (such as seismic refraction, seismic reflection, boreholes, penetrometers, etc.) which suffer severe limitations in urbanized areas, mainly because of their cost and their environmental impact that is less and less accepted by communities (use of explosives, drilling, etc.), the H/V technique, based on ambient noise recordings, has become more and more popular over the last decades. This technique, first applied by Nogoshi and Igarashi in 1971 [44] and popularized by Nakamura (1989 [40], 1996 [41], 2000 [42]), offers a convenient, practical and low-cost tool to be used in urbanized areas. It uses information about the peak and trough frequency of the H/V -ratio curve (the spectral ratio between horizontal and vertical components) of microtremors measured at the ground surface to estimate fundamental periods and amplification factors of a site. One question which must be addressed here is: what is the meaning of the H/V peak and trough frequency, and under what conditions is it allowed to assume the approximate equivalence of the H/V peak frequency and the peak frequency of the transmission response of a medium? These questions turn out to be surprisingly challenging theoretically even for very simple models and they have only rarely been addressed in the literature (e. g. Malischewsky and Scherbaum, 2004 [35], Malischewsky et al., 2008 [38]). To answer these questions, we need to more deeply understand the properties of H/V -ratio curve.

Since microtremors observed at the ground surface are thought to consist of body and surface waves with their proportions unclarified, it is unclear what constitutes the peak and trough of H/V -ratio curve. However, Lachet and Bard (1994) [29] indicated with numerical simulation that the H/V -ratios at the longer periods were governed by fundamental mode Rayleigh waves. In addition, based on f-k analysis of ambient vibration, Scherbaum et al. (2003) [50] found strong evidence for treating H/V -ratios as Rayleigh wave ellipticities. Based on these facts, in this thesis, I study mainly the ellipticity of Rayleigh waves, concentrating on the peak and trough frequency.

The S-wave resonance in soft surface layers is a key parameter to be determined, and many experimental works (Tokimatsu 1997 [55], Scherbaum et al. 2002 [49], Parolai et al. 2004 [46], Bonnefoy-Claudet et al. 2006 [9], Souriau et al. 2007 [3], etc.) have found that the H/V spectral ratios and H/V peak frequency agree fairly well with the natural site frequency. It is then necessary to know when the peak frequency of the Rayleigh wave ellipticity can be

regarded as the natural site frequency.

Objectives

The objective of this thesis is to answer all the questions addressed above. Achieving this objective requires building better knowledge of the peaks and troughs of the Rayleigh H/V -ratio curve, especially regarding their amplitudes, frequencies and to what degree they depend on different parameters. Since a typical H/V spectral ratio of the ambient noise vibrations recorded at one single station often shows a peak and sometimes a trough from which some important information about the structure are retrieved – such as the S-wave velocity of the layer, the impedance contrast or the Poisson’s ratio – it is also important to find the link between information about the peaks and trough, and parameters of the structure. This will help seismologist to determine necessary information from the H/V spectral ratios.

Thesis outline

The thesis consists of four chapters.

The first chapter is devoted to Rayleigh waves in homogeneous half-space (HS) and a half-space deposited by a thin layer called “impedance wave”. The H/V -ratio of Rayleigh waves in homogeneous half-space has been studied thoroughly in (for example) Malischewsky and Scherbaum (2004) [35], and it has been shown that the Rayleigh wave is always non-dispersive and the particle motion is always retrograde. In this chapter, I only recall some basic properties of plane waves and the important features of the H/V -ratio of Rayleigh waves in half-space, which is considered as the first simple model. The next step is for “impedance wave” model, which is a half-space deposited by a thin layer. It was investigated by Tiersten (1969) [54] and Bøvik (1996) [12]. Tiersten used the elastic theory of a thin plate to replace the homogeneous boundary conditions in the surface of half-space by special non-homogeneous boundary conditions. In this chapter, I use these special boundary conditions in a low frequency to simulate an approximation of the behavior of Rayleigh waves, and I prove that although the Rayleigh waves are dispersive in this model, the motion of the particles is always retrograde, the same as in half-space. The H/V -ratio curve might have a maximum, but no singularity or zero points are observed.

The behavior of Rayleigh waves in a layer with a stress-free surface and fixed bottom with both homogeneous and inhomogeneous material is studied in Chapter 2. Some features of the H/V -ratio of this model have been studied, e.g in Giese (1957) [19]. In this chapter I demonstrate that the H/V -ratio does not depend on the density of mass, and with the homogeneous layer, I determine formulas for the frequency of the singularity and the zero-point with the condition of Poisson’s ratio of the layer in which the singularity or the zero point exists. I then derive a general picture showing the retrograde and prograde motion of the particles. From the numerical calculations, simple linear formulas for singularity and zero point frequency are presented from which we can calculate the broad range of frequency for prograde motion.

In the third chapter, I study the most general model, “layer over half-space” (LOH). Donat

Fäh et al. (2002) [17] shows that the H/V -ratio can be used to determine reasonable S-wave velocity models for a site, if the structure is characterized by a large velocity contrast between bedrock and sediments, and as long as the site can be approximated by a layered structure. Therefore, a thorough theoretical understanding of Rayleigh surface waves of even a single layer over half-space is not only of theoretical, but also of considerable practical interest. There is a rich literature on the H/V -ratio which is discussed in detail by Bonneyfoy-Claudet et al. (2006) [10], and a list of which may be found in Kudo (1995) [27], Bard (1998) [4], Stephenson (2003) [53], Malischewsky and Scherbaum (2004) [35] and Bonnefoy-Claudet (2004) [8]. In 2002, Malischewsky et al. [33] proposed to use the H/V -ratio in non-destructive testing with acoustic surface waves and in 2004, Malischewsky and Scherbaum [35] specified the exact formula of H/V for a 2-layer model of compressible media to investigate its properties for several models. In this chapter, by using the exact H/V -ratio formula of Malischewsky, I focus on the analysis of some more difficult properties of the H/V -ratio. The half-space in this model is always homogeneous, but the layer can be inhomogeneous. The first section is for the homogeneous layer and I use the exact H/V -ratio formula to investigate the H/V -ratio curve, concentrating on the peak and trough frequency, which are key parameters in the H/V -method. Since the phase velocity is another key parameter and has the greatest affect on the H/V -ratio, the first results of this section are a simple formula of the derivative of the phase velocity curve at zero frequency. This formula can classify three states of phase velocity curve at zero frequency: normal, anomalous or zero dispersion, depending on the parameter systems. The first peak of the H/V curve, especially its amplitude and frequency, plays an important role in the H/V -ratio method, so it is necessary to know whether it is a singularity with very high amplitude or only a maximum point. In the H/V spectral ratio, it usually has a sharp peak, but sometimes it exhibits a broad peak (Giulio et al. 2006 [20]). This broad peak may be connected with the maximum point of the H/V -ratio curve. In this section, I present a simple formula condition of the structure parameters defining the existence of singularity or only maximum point. Although this formula is constructed on numerical calculation, its accuracy is very good.

In the analysis of local seismic hazards, dynamic ground shaking and permanent ground failure are the two most important effects, at least with respect to building and lifelines. Dynamic ground shaking is the important factor for building. Ground shaking refers to the amplitude, frequency, composition and duration of the horizontal and vertical components of the vibration of the ground produced by seismic waves arriving at a site. These effects depend largely on the local geological ground condition. With the high impedance contrast between the deposit and the bedrock of the site, the singularity frequency is approximately the resonant frequency of the S-wave of the layer which is considered as the “dangerous” frequency. However, the properties may vary among and within sites, so it is necessary to determine the dangerous ranges of frequency for all possible structures by observing whether the peak frequency of the H/V spectral ratio is close to the resonant frequency of the S-wave in the layer. For this reason, I present several maps of peak and trough frequency of the H/V -ratio curve of Rayleigh waves dependent on particular parameters. The parameters here are the Poisson’s ratio and the impedance contrast which represent the conditions at each site. From these maps, some applications are proposed such as defining the parameters of the site by the information of peak and trough frequency in H/V spectral ratio.

The second section in Chapter 3 is devoted to the inhomogeneous layer. In this section, I keep

the density of mass and the Poisson's ratio in the layer constant and let the shear modulus vary. Three functions of shear modulus in the layer are investigated. The linear variation of shear modulus in the layer has already been studied by Newlands and Stoneley (1950) [39], and in this section I study the linear, quadratic and the third polynomial form of shear wave velocity using the Vrettos technique (1990) [57]. The effect of inhomogeneity on the H/V -ratio is studied, and I compare the peak and trough frequencies between the actual inhomogeneous layer model with the simple equivalent homogeneous model to determine when we can use the simple model to replace the complicated one while maintaining reasonable accuracy.

In the last section in Chapter 3, I study the H/V -ratio of body incident waves (SV wave and P wave) which might be generated from the deep depths of the Earth. The H/V -ratio formulas of these body incident waves are presented, and by using these formulas, I show that, in most cases, the H/V peak frequencies are close to the S-wave resonant frequency of the layer. I also point out the theoretical similarity between H/V -ratio of incident body waves and of the Rayleigh surface waves.

The osculation point is one of the important features of the phase velocity curve. This is the point at which two curves of different modes seem to cross each other. In this thesis, I show that the osculation point of the fundamental mode is a special point at which the H/V -ratio curve changes its property from having two singularities to having one singularity and one zero point. This phenomenon is proven analytically for LFB and shown numerically for LOH. In Chapter 4, the osculation point of the phase velocity curve is analytically investigated for the model "layer with fixed bottom" by using the ray theory of Tolstoy & Usdin [56], and numerically for the model "layer over half-space". For "layer with fixed bottom", three of the most important classes of osculation point are found with simple forms, and for "layer over half-space", an approximate formula for osculation point is presented.

Chapter 1

Two simple models

In this chapter, we will begin to investigate Rayleigh waves with the simplest model, “homogeneous half-space”, which has been very thoroughly investigated. When analyzing seismic diagrams, seismologists found a new kind of wave whose velocity was less than the transversal wave speed. This wave has the facial property, meaning that the oscillation amplitude strongly decreases with depth. The dissipation of energy of this wave is slower than for longitudinal and transversal waves. These two latter waves propagate from the stimulating source center, such as an earthquake, in every direction, while the surface wave only concentrates on the surface and propagates in 2D-space. Thus, we can consider it as a plane wave far from the source center. In 1885, Lord *Rayleigh* (England) predicted, from theory, the existence of elastic surface waves.

1.1 Plane waves

It will be convenient to recall something about the plane wave, which constitutes the Rayleigh wave. A plane displacement wave propagating with phase velocity c in a direction defined by the unit propagation vector \mathbf{p} is represented by

$$\mathbf{u} = f(\mathbf{x} \cdot \mathbf{p} - ct)\mathbf{d} . \quad (1.1)$$

In this equation \mathbf{d} and \mathbf{p} are unit vectors defining the directions of motion and propagation, respectively. The vector \mathbf{x} denotes the position vector, and $\mathbf{x} \cdot \mathbf{p} = \text{constant}$ describes a plane normal to the unit vector \mathbf{p} . Eq. (1.1) thus represents a plane wave whose planes of constant phase are normal to \mathbf{p} and which propagates with velocity c .

In the absence of body forces the components of the displacement vector in a homogeneous, isotropic, linearly elastic medium are governed by the following system of partial differential equations:

$$\mu \nabla^2 \mathbf{u} + (\lambda + \mu) \nabla \nabla \cdot \mathbf{u} = \rho \ddot{\mathbf{u}} , \quad (1.2)$$

where λ and μ are Lamé’s elastic constants, and ρ is the mass density. The vector operator ∇ is defined as

$$\nabla = i_1 \frac{\partial}{\partial x_1} + i_2 \frac{\partial}{\partial x_2} + i_3 \frac{\partial}{\partial x_3} , \quad (1.3)$$

and ∇^2 is the Laplacian. We will substitute the expression for the plane wave, Eq. (1.1), into the system of field equations (1.2). After some transformations, we obtain

$$[\mu \mathbf{d} + (\lambda + \mu)(\mathbf{p} \cdot \mathbf{d})\mathbf{p} - \rho c^2 \mathbf{d}] f''(\mathbf{x} \cdot \mathbf{p} - ct) = 0 ,$$

or

$$(\mu - \rho c^2)\mathbf{d} + (\lambda + \mu)(\mathbf{p} \cdot \mathbf{d})\mathbf{p} = 0 . \quad (1.4)$$

Since \mathbf{p} and \mathbf{d} are two different unit vectors, Eq. (1.4) can be satisfied two ways only:

$$\text{either } \mathbf{d} = \pm \mathbf{p} , \quad \text{or } \mathbf{p} \cdot \mathbf{d} = 0 .$$

If $\mathbf{d} = \pm \mathbf{p}$, we have $\mathbf{d} \cdot \mathbf{p} = \pm 1$, and Eq. (1.4) yields

$$c = c_L = \left(\frac{\lambda + 2\mu}{\rho} \right)^{\frac{1}{2}} . \quad (1.5)$$

In the case that the motion is parallel to the direction of propagation, the wave is called a *longitudinal* wave. The components of the rotation $\nabla \wedge \mathbf{u}$ are

$$e_{klm} \partial_l u_m = e_{klm} p_l d_m f' ,$$

and thus

$$\nabla \wedge \mathbf{u} = (\mathbf{p} \wedge \mathbf{d}) f'(\mathbf{x} \cdot \mathbf{p} - ct) = 0 .$$

The rotation thus vanishes, which has motivated the alternative terminology *irrotational* wave. This type of wave is also often called a dilatational wave, a pressure wave, or a P-wave (primary, pressure).

If $\mathbf{p} \neq \pm \mathbf{d}$, both terms in (1.4) vanish independently, yielding

$$\mathbf{p} \cdot \mathbf{d} = 0 \quad c = c_T = \left(\frac{\mu}{\rho} \right)^{\frac{1}{2}} . \quad (1.6)$$

Now the motion is normal to the direction of propagation, and the wave is called a *transverse* wave. This type of wave is often called a *rotational* wave, a shear wave, or an S-wave (secondary, shear).

We can consider a decomposition of the displacement vector in Eq. (1.2) of the form

$$\mathbf{u} = \nabla \varphi + \nabla \wedge \psi , \quad (1.7)$$

where

$$\nabla \cdot \psi = 0 . \quad (1.8)$$

Substitution of the displacement representation (1.7) into Eq. (1.2) yields

$$\mu \nabla^2 [\nabla \varphi + \nabla \wedge \psi] + (\lambda + \mu) \nabla \nabla \cdot [\nabla \varphi + \nabla \wedge \psi] = \rho \frac{\partial^2}{\partial t^2} [\nabla \varphi + \nabla \wedge \psi] . \quad (1.9)$$

Since $\nabla \cdot \nabla \varphi = \nabla^2 \varphi$ and $\nabla \cdot \nabla \wedge \psi = 0$, we obtain, upon rearranging terms

$$\nabla[(\lambda + 2\mu)\nabla^2 \varphi - \rho\ddot{\varphi}] + \nabla \wedge [\mu\nabla^2 \psi - \rho\ddot{\psi}] = 0. \quad (1.10)$$

Clearly, the displacement representation (1.7) satisfies the equation of motion if

$$\nabla^2 \varphi = \frac{1}{c_L^2} \ddot{\varphi} \quad (1.11)$$

and

$$\nabla^2 \psi = \frac{1}{c_T^2} \ddot{\psi}, \quad (1.12)$$

which are the phase velocity of the longitudinal and transverse wave, respectively.

The stresses can be determined by Hooke's law

$$\tau_{i,j} = \lambda \epsilon_{kk} \delta_{ij} + 2\mu \epsilon_{ij} \quad (1.13)$$

with the strain-displacement relations

$$\epsilon_{ij} = \frac{1}{2} (u_{i,j} + u_{j,i}). \quad (1.14)$$

Although the scalar potential φ and the components of the vector potential ψ are generally coupled through the boundary conditions, which still causes substantial mathematical complications, the use of the displacement decomposition generally simplifies the analysis. To determine the solution of a boundary-initial value problem, one may simply select appropriate particular solutions of Eqs. (1.11) and (1.12) in terms of arbitrary functions or integrals over arbitrary functions. If these functions can subsequently be chosen so that the boundary conditions and the initial conditions are satisfied, then the solution to the problem has been found. The solution is unique by virtue of the uniqueness theorem, which will not be discussed here.

A plane harmonic displacement wave propagating with phase velocity c in a direction defined by the unit propagation vector p is represented by

$$\mathbf{u} = A \mathbf{d} \exp[ik(\mathbf{x} \cdot \mathbf{p} - ct)], \quad (1.15)$$

where $i = \sqrt{-1}$ and it is understood that the actual displacement components are the real or imaginary parts of the right-hand side. The amplitude A may be real or complex, but it is independent of \mathbf{x} and t . $\omega = kc$ is the circular frequency and k is the wave-number. These quantities are related to the period T and the wavelength λ by $\omega = 2\pi/T$ and $k = 2\pi/\lambda$, respectively.

Eq. (1.15) is a special case of (1.1). Thus we have two types of plane harmonic waves: longitudinal and transverse waves, propagating with phase velocities c_L and c_T , respectively. Since the wavenumber k does not appear in the expression for the phase velocities, plane harmonic waves in an unbounded homogeneous, isotropic, linearly elastic medium are not dispersive.

1.2 The homogeneous half-space (HS)

Rayleigh waves propagating over the surface of homogeneous and inhomogeneous elastic half-spaces are a well-known and prominent feature of wave theory. They are vector waves, which are confined to the region near the surface, and are polarized in the sagittal plane. This means that the displacement has a horizontal component, which is parallel to the direction of propagation, and a vertical component directed into the half-space. The dimensionless ratio of these components of H/V at the surface, the so-called ellipticity, is an important parameter which reflects fundamental properties of the elastic material. In this section, the 2D-Rayleigh wave motion is described in a Cartesian coordinate system with its origin located on the surface of the half-space. The x_1 -axis points in the direction of propagation, while the x_3 -axis is directed into the half-space.

1.2.1 Eigen-value problem

The Rayleigh waves equation can be found in many textbooks such as [24], [6], [2], [14] but we consider the expression of the potentials

$$\varphi = Ae^{-px_3}e^{ik(x_1-ct)} \quad (1.16)$$

and

$$\psi = [0, Be^{-qx_3}e^{ik(x_1-ct)}, 0], \quad (1.17)$$

respectively. A and B are integral constants. Substitution of the potentials Eqs. (1.16) and (1.17) into (1.11) and (1.12), respectively, yields

$$p = k \left(1 - \frac{c^2}{\alpha^2}\right)^{\frac{1}{2}}, \quad q = k \left(1 - \frac{c^2}{\beta^2}\right)^{\frac{1}{2}} \quad (1.18)$$

in which β and α are the shear-wave and the longitudinal-wave velocity, respectively.

Substituting the potential expressions into (1.7) yields the displacements

$$u_1 = U_1(x_3)e^{ik(x_1-ct)}, \quad (1.19)$$

$$u_2 = 0,$$

$$u_3 = U_3(x_3)e^{ik(x_1-ct)} \quad (1.20)$$

with

$$\begin{aligned} U_1(x_3) &= ikAe^{-px_3} + qBe^{-qx_3}, \\ U_3(x_3) &= -pAe^{-px_3} + ikBe^{-qx_3} \end{aligned} \quad (1.21)$$

and wave number k , phase velocity c , and the time t . The real part of p is supposed to be positive, so that the displacements decrease with increasing x_3 and tend towards zero as x_3 tends towards infinity.

Substitution of Eqs. (1.19)-(1.20) into the stress formula (1.13) yields

$$\tau_{13} = S_{13}(x_3)e^{ik(x_1-ct)} , \quad (1.22)$$

$$\tau_{33} = S_{33}(x_3)e^{ik(x_1-ct)} \quad (1.23)$$

with

$$\begin{aligned} S_{13}(x_3) &= \mu \left(U_1'(x_3) + ikU_3(x_3) \right) , \\ S_{33}(x_3) &= (\lambda + 2\mu)U_3'(x_3) + ik\lambda U_1(x_3) . \end{aligned} \quad (1.24)$$

The prime $()'$ denotes differentiation with respect to x_3 and λ, μ are Lamé's constants of the half-space.

The boundary conditions at the free-surface are

$$S_{13}(0) = S_{33}(0) = 0 . \quad (1.25)$$

By substituting (1.24) into (1.25), we obtain

$$2pikA - (q^2 + k^2)B = 0 , \quad (1.26)$$

$$[p^2 - (1 - 2\gamma)k^2]A - 2ik\gamma qB = 0 \quad (1.27)$$

with $\gamma = \beta^2/\alpha^2$. For a non-trivial solution the determinant of the coefficients of A and B must vanish, which yields the following well-known equation for the phase velocity of Rayleigh waves:

$$4pq - k^2\left(2 - \frac{c^2}{\beta^2}\right)^2 = 0 . \quad (1.28)$$

Substituting p, q from (1.18) yields

$$4\sqrt{1 - \frac{c^2}{\beta^2}}\sqrt{1 - \frac{c^2}{\alpha^2}} - \left(2 - \frac{c^2}{\beta^2}\right)^2 = 0 . \quad (1.29)$$

If we substitute $c = \beta$ into the left-hand side of (1.29), we obtain unity. Substitution of $c = \epsilon\beta$, where ϵ is a very small number, yields $-2[1 - \gamma]\epsilon^2$, which is always negative. Hence (1.29) has at least one real root lying between $c = 0$ and $c = \beta$. Achenbach [1] proved that there exists only one positive root of (1.29). He also made a good approximation of c_R/β as a function of Poisson's ratio ν

$$\frac{c_R}{\beta} = \frac{0.862 + 1.14 \nu}{1 + \nu} . \quad (1.30)$$

There are some analytical formulas for the Rayleigh phase velocity which have been recently proposed, and we use the Bergman formula [7]

$$\frac{c_R}{\beta} = \frac{0.87 + 1.12 \nu}{1 + \nu} , \quad (1.31)$$

and Malischewsky's formula [34]

$$x(\nu) = \frac{2}{3} \left[3 - \sqrt[3]{h_3(\gamma)} + \frac{2(1-6\gamma)}{\sqrt[3]{h_3(\gamma)}} \right] \quad (1.32)$$

with these auxiliary functions

$$\begin{aligned} h_1(\gamma) &= 3\sqrt{33 - 186\gamma + 321\gamma^2 - 192\gamma^3}, \\ h_3(\gamma) &= 17 - 45\gamma + h_1(\gamma). \end{aligned} \quad (1.33)$$

In formula (1.32), the main values of the cubic roots are to be used. Alternatively, x can be determined by using Malischewsky's approximation (see Pham Chi Vinh and Malischewsky [48]), which is also valid for auxetic material with negative Poisson ratio [like the exact formula (1.32)]:

$$x(\nu) = 0.874 + 0.196 \nu - 0.043 \nu^2 - 0.055 \nu^3. \quad (1.34)$$

Fig. 1.1 shows the root of equation (1.29) compared to the approximation of Achenbach (1.30) and Bergman (1.31). We can see that Bergman's approximation is very good, but

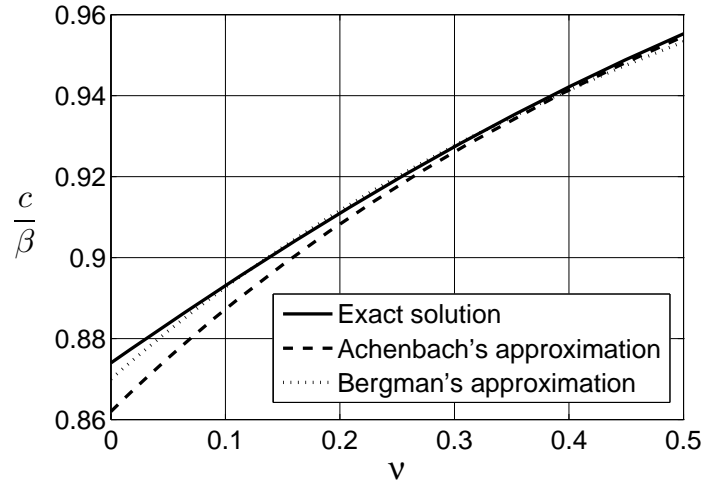


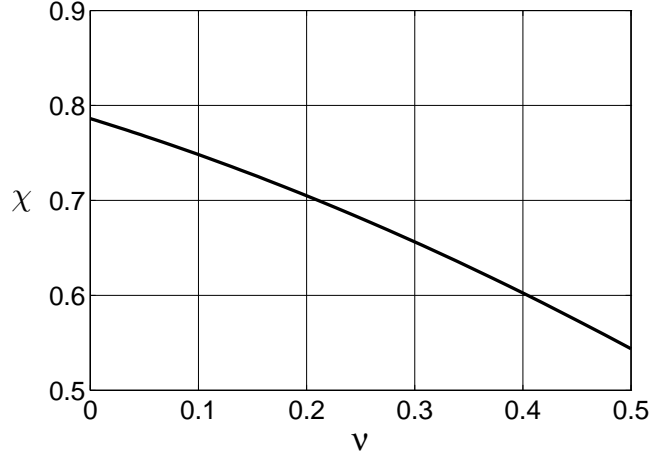
Figure 1.1: Rayleigh waves velocity as a function of Poisson's ratio ν : exact curve (continuous), Achenbach's approximation (dashed), Bergman's approximation (dotted)

Achenbach's is only good for large values of ν . The Malischewsky approximation is not displayed here because it is almost identical to the exact solution.

1.2.2 H/V -ratio

The H/V -ratio is formulated as ratio of horizontal to vertical displacement amplitudes

$$\chi = \left| \frac{U_1(0)}{U_3(0)} \right| = \left| \frac{ikA + qB}{-pA + ikB} \right|. \quad (1.35)$$

Figure 1.2: H/V -ratio of Rayleigh waves as a function of Poisson's ratio

From the boundary condition (1.26)-(1.27), we have

$$B = \frac{2pik}{q^2 + k^2} A. \quad (1.36)$$

By substituting B in (1.36) into (1.35), we obtain

$$\chi = \left| \frac{k q^2 + k^2 + 2pq}{p q^2 + k^2 + 2k^2} \right|. \quad (1.37)$$

Using the dispersion equation (1.29) and formulas of p and q (1.18), we have a simple formula of H/V

$$\chi = \sqrt{\frac{p}{q}} = 2 \frac{\sqrt{1 - c^2/\beta^2}}{2 - c^2/\beta^2}. \quad (1.38)$$

The ellipticity χ depends only on Poisson's ratio ν . In terms of Malischesky's formula for phase velocity (1.32), the H/V -ratio can be expressed analytically as a function of Poisson's ratio ν in the form

$$\chi(\nu) = \frac{\sqrt{1 - 2g_4(\nu)}}{1 - g_4(\nu)} \quad (1.39)$$

with the auxiliary functions g_4 defined by

$$g_3(\nu) = 17 + 3\sqrt{33 - 24\bar{\nu}^3 + \frac{321}{4}\bar{\nu}^2 - 93\bar{\nu} - \frac{45}{2}\bar{\nu}}, \quad (1.40)$$

$$g_4(\nu) = \frac{1}{3} \left[4 + \frac{2(1 - 3\bar{\nu})}{\sqrt[3]{g_3(\nu)}} - \sqrt[3]{g_3(\nu)} \right] \quad \text{and} \quad (1.41)$$

$$\bar{\nu} = 1 - \frac{\nu}{1 - \nu} \quad (1.42)$$

where the main values of cubic root should be used.

This ellipticity $\chi(\nu)$ is a positive function for $-1 \leq \nu \leq 0.5$ as a result of retrograde particle motion (see Malischewsky et al. [36]). Fig. 1.2 shows the well-known behaviour of χ dependent on ν for all possible values of Poisson's ratio.

1.3 The impedance wave

The Rayleigh wave in an isotropic, elastic half-space is non-dispersive and there is only one straight-crested surface wave propagating, but if a layer of a different material is deposited on the half-space, an infinite number of straight-crested surface waves is possible, all of which are dispersive, including that corresponding to the Rayleigh wave. For a thin layer, H. F. Tiersten [54] used the approximate equations of low-frequency extension and flexure of thin plates to account for the motion of the layer. These approximate equations enable the entire effect of the layer to be treated as a boundary condition at the surface of the substrate. Tiersten also showed that the accuracy of the approximation is excellent in the small frequency range. In this section, we will use the Tiersten technique to investigate impedance waves.

1.3.1 The dispersion equation

Our model is displayed as in Fig. 1.3.1. We use index 1 for the layer and index 2 for the half-space. The thickness of the layer is d , and it is considered to be small. The 2D-Rayleigh wave motion is described in a Cartesian coordinate system with its origin located on the interface between layer and half-space. The x_1 -axis points into the direction of propagation while the x_3 -axis is directed into the half-space. As for the model "half-space", we choose the potential expression of the half-space as in (1.16-1.17), so the expression of the displacements and the stresses of the half-space are the same as in (1.21) and (1.24). However, the boundary conditions are quite different. Instead of the homogeneous conditions of the free stresses at the surface in the model "half-space", the stresses at the interface between the layer and half-space of new model must be taken from Tiersten's approximations as

$$S_{13} + \epsilon_1 U_1 = 0, \quad S_{33} + \epsilon_3 U_3 = 0 \quad \text{for } x_3 = 0, \quad (1.43)$$

with

$$\epsilon_1 = d\rho_1\omega^2 \left[1 - \frac{4(\mu_1 + \lambda_1)}{2\mu_1 + \lambda_1} \frac{\beta_1^2}{c^2} \right] \quad \text{and} \quad \epsilon_3 = d\rho_1\omega^2. \quad (1.44)$$

μ_1 , α_1 and ρ_1 are the Lamé's constants and the density of mass of the layer, respectively. Details of this boundary replacement can be found in [31]. Substitution the formulas of the displacements (1.21) and stresses (1.24) into the Tiersten's boundary condition (1.43) yields

$$\begin{aligned} & 2i \left[-g_\alpha C + r_d r_s^2 \pi \bar{f} (C^2 - 4(1 - \gamma_1)) \right] A \\ & + \left[-C(2 - C^2) + 2r_d r_s^2 \pi \bar{f} g_\beta (C^2 - 4(1 - \gamma_1)) \right] B = 0 \end{aligned} \quad (1.45)$$

and

$$\left[(2 - C^2) - 2C r_d r_s^2 \pi \bar{f} g_\alpha \right] A + 2i(-g_\beta + C r_d r_s^2 \pi \bar{f}) B = 0 \quad (1.46)$$

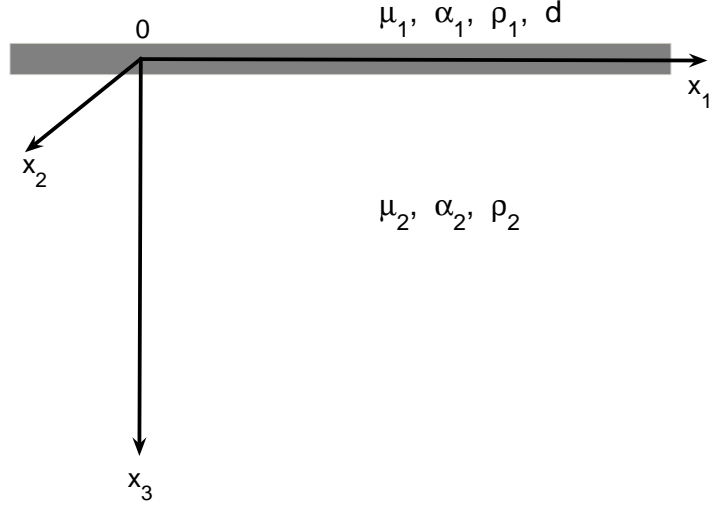


Figure 1.3: Model "Impedance wave"

with $i = \sqrt{-1}$, $C = c/\beta_1$, $r_d = \rho_1/\rho_2$, $r_s = \beta_1/\beta_2$ for the density ratio and the impedance ratio, respectively. γ_1 , γ_2 are the squared ratios of the shear wave to the longitudinal wave and they are functions of Poisson's ratio, respectively, as

$$\gamma_1 = \left(\frac{\beta_1}{\alpha_1}\right)^2 = \frac{1-2\nu_1}{2(1-\nu_1)}, \quad \gamma_2 = \left(\frac{\beta_2}{\alpha_2}\right)^2 = \frac{1-2\nu_2}{2(1-\nu_2)}. \quad (1.47)$$

We use here a non-dimensional frequency \bar{f} , defined by

$$\bar{f} = \frac{d}{\lambda_{\beta_1}}, \quad (1.48)$$

where d is the thickness of the layer and λ_{β_1} is the wavelength of shear waves in the layer. We also denote g_α and g_β as

$$g_\alpha = \sqrt{1 - \frac{c^2}{\alpha_2^2}} = \sqrt{1 - C^2 r_s^2 \gamma_2}, \quad g_\beta = \sqrt{1 - \frac{c^2}{\beta_2^2}} = \sqrt{1 - C^2 r_s^2}. \quad (1.49)$$

The nontrivial solution for this system of equations of A and B corresponds to the determinant equals zero which leads to the secular equation

$$A_0(C) + A_1(C)\bar{f} + A_2(C)\bar{f}^2 = 0 \quad (1.50)$$

with abbreviations

$$\begin{aligned} A_0(C) &= (2 - C^2 r_s^2)^2 - 4g_\beta g_\alpha, \\ A_1(C) &= 2C r_d r_s^4 \pi [C^2(g_\beta + g_\alpha) + 4g_\beta(-1 + \gamma_1)], \\ A_2(C) &= 4r_d^2 r_s^4 \pi^2 (-1 + g_\beta g_\alpha)(-4 + C^2 + 4\gamma_1). \end{aligned}$$

The zero-frequency velocity

When $\bar{f} = 0$, Eq. (1.50) becomes

$$(2 - C^2 r_s^2)^2 - 4\sqrt{1 - C^2 r_s^2} \sqrt{1 - C^2 r_s^2 \gamma_2} = 0. \quad (1.51)$$

Denote $\bar{C} = C^2 r_s^2 = c^2/\beta_2^2$, Eq. (1.51) becomes

$$(2 - \bar{C})^2 - 4\sqrt{1 - \bar{C}} \sqrt{1 - \bar{C}\gamma_2} = 0. \quad (1.52)$$

This is the Rayleigh-wave equation of the half-space, so the phase velocity at zero frequency is the Rayleigh wave velocity of the substrate.

1.3.2 The H/V -ratio formula

Suppose that the velocity is found and the ellipticity can be determined from

$$\chi = \frac{U_1(0)}{iU_3(0)} = \frac{ikA + qB}{-ipA - kB}. \quad (1.53)$$

The relation between constants A and B can be determined from (1.45) and (1.46), so we can have two formulas for the H/V -ratio.

From (1.45), we have

$$\frac{B}{A} = -\frac{2i[-g_\alpha C + r_d r_s^2 \pi \bar{f}(C^2 - 4(1 - \gamma_1))]}{[-C(2 - C^2) + 2r_d r_s^2 \pi \bar{f} g_\beta(C^2 - 4(1 - \gamma_1))]}, \quad (1.54)$$

so

$$\chi_1(\bar{f}, \nu_1, \nu_2, r_s, r_d) = -C \frac{M_0(C)}{N_0(C) r_s^2} \quad (1.55)$$

where

$$\begin{aligned} M_0(C) &= -2 + C^2 r_s^2 + 2\sqrt{1 - C^2 r_s^2} \sqrt{1 - C^2 r_s^2 \gamma_2}, \\ N_0(C) &= C^3 \sqrt{1 - C^2 r_s^2 \gamma_2} \\ &\quad + 2r_d \pi (-1 + \sqrt{1 - C^2 r_s^2} \sqrt{1 - C^2 r_s^2 \gamma_2}) (-4 + C^2 + 4\gamma_1) \bar{f}. \end{aligned}$$

On the other hand, the relation between A and B can be determined from (1.46) as

$$\frac{B}{A} = -\frac{(2 - C^2) - 2C r_d r_s^2 \pi \bar{f} g_\alpha}{2i(-g_\beta + C r_d r_s^2 \pi \bar{f})} \quad (1.56)$$

and we derive another formula of the H/V -ratio

$$\chi_2(\bar{f}, \nu_1, \nu_2, r_s, r_d) = -C r_s^2 \frac{M_1(C)}{N_1(C)} \quad (1.57)$$

where

$$\begin{aligned} M_1(C) &= C \sqrt{1 - C^2 r_s^2} + 2r_d \pi (-1 + \sqrt{1 - C^2 r_s^2} \sqrt{1 - C^2 r_s^2 \gamma_2}), \\ N_1(C) &= M_0(C). \end{aligned}$$

These two formulas of H/V -ratio, (1.55) and (1.57), are dependent on each other, i.e., each of them can be obtained from the other and the dispersion equation.

Proposition 1. *The secular equation (1.50) can be determined from the relation:*

$$\chi_1 = \chi_2 .$$

Proof. From $\chi_1 = \chi_2$ and the formulas (1.55) and (1.57), we have:

$$M_1(C)N_0(C)r_s^4 - N_1(C)M_0(C) = 0 .$$

But we can express

$$M_1(C)N_0(C)r_s^4 - N_1(C)M_0(C) = \Delta(\bar{f})(-1 + \sqrt{1 - C^2 r_s^2} \sqrt{1 - C^2 r_s^2 \gamma_2})$$

with $\Delta(C, \bar{f}) = A_0 + A_1 \bar{f} + A_2 \bar{f}^2$ from the dispersion equation. We always have

$$-1 + \sqrt{1 - C^2 r_s^2} \sqrt{1 - C^2 r_s^2 \gamma_2} \neq 0 , \quad (1.58)$$

if $c^2 \neq \alpha_2^2 + \beta_2^2$ and because of assumption that $c < \beta_2$ so

$$\Delta(C, \bar{f}) = 0 .$$

□

Zero-frequency ellipticity

When $\bar{f} = 0$, we use the second formula of the H/V -ratio (1.57) and it becomes

$$\chi_2 = - \frac{\bar{C} \sqrt{1 - \bar{C}}}{\bar{C} + 2(-1 + \sqrt{1 - \bar{C}} \sqrt{1 - \bar{C} \gamma_2})} \quad (1.59)$$

where $\bar{C} = c/\beta_2$. We proved that \bar{C} is Rayleigh wave of the substrate when $\bar{f} = 0$ so \bar{C} satisfies the Rayleigh equation as

$$(2 - \bar{C})^2 - 4\sqrt{1 - \bar{C}} \sqrt{1 - \bar{C} \gamma_2} = 0 \quad (1.60)$$

thus,

$$\chi_2 = \frac{2\sqrt{1 - \bar{C}}}{2 - \bar{C}} . \quad (1.61)$$

Similar to phase velocity, the H/V -ratio at zero-frequency is the H/V -ratio of the substrate, and it depends only on γ_2 or ν_2 .

Particle motion

It is shown in the model “half-space” that the phase velocity is non-dispersive and the particle motion is always a retrograde ellipse. However, the phase velocity of the impedance wave is dispersive, so we consider the possibility that the particle motion is prograde. We proved that the ellipticity at zero frequency is positive, which means the motion at zero frequency is retrograde. Now we will prove that H/V -ratio keeps its sign with other frequencies.

Because the phase velocity is a continuous function of the frequency, the H/V -ratio can only change its sign if it has a zero point or a singularity. Suppose that the H/V -ratio has a singularity at \bar{f}_p . The corresponding phase velocity is C_p . We will use the formula χ_1 of H/V -ratio, and the condition that χ_1 has singularity yields the denominator $N_0(C) = 0$ or

$$C_p^3 \sqrt{1 - C_p^2 r_s^2 \gamma_2} + 2r_d \pi (-1 + \sqrt{1 - C_p^2 r_s^2} \sqrt{1 - C_p^2 r_s^2 \gamma_2}) (-4 + C_p^2 + 4\gamma_1) \bar{f}_p = 0 \quad (1.62)$$

thus,

$$\bar{f}_p = - \frac{C_p^3 \sqrt{1 - C_p^2 r_s^2 \gamma_2}}{2r_d \pi (-1 + \sqrt{1 - C_p^2 r_s^2} \sqrt{1 - C_p^2 r_s^2 \gamma_2}) (-4 + C_p^2 + 4\gamma_1)}. \quad (1.63)$$

The pair (\bar{f}_p, C_p) must satisfy the secular equation (1.50). Substituting (\bar{f}_p, C_p) into the secular equation yields

$$\frac{8 + C_p^4 r_s^4 (1 + 4\gamma_2) + 4(C_p^2 r_s^2 - 2) \sqrt{1 - C_p^2 r_s^2} \sqrt{1 - C_p^2 r_s^2 \gamma_2} - 4C_p^2 r_s^2 (2 + \gamma_2)}{-1 + \sqrt{1 - C_p^2 r_s^2} \sqrt{1 - C_p^2 r_s^2 \gamma_2}} = 0. \quad (1.64)$$

The left side of this equation can be re-written by denoting $y = C_p^2 r_s^2 = c_p^2 / \beta_2^2$ as

$$P(y, \gamma_2) = \frac{8 + (1 + 4\gamma_2)y^2 + 4(y - 2)\sqrt{1 - y}\sqrt{1 - y\gamma_2} - 4y(2 + \gamma_2)}{-1 + \sqrt{1 - y}\sqrt{1 - y\gamma_2}}. \quad (1.65)$$

We observe that the function $P(y, \gamma_2)$ only depends on two arguments y and γ_2 and does not depend on any parameters of the layer. This makes it much easier to determine whether $P(y, \gamma_2) = 0$ has a solution. Because $\gamma_2 \in [0, 0.5]$, and we assume that $c < \beta_2$ or $y < 1$, we have a picture showing the contour of $P(y, \gamma_2)$ as in Fig. 1.3.2. We can see that $P(y, \gamma_2)$ never reaches the 0 value, except at $y = 0$ or $c = 0$. This solution is trivial, so we cannot find any value of the phase velocity at which H/V has a singularity. That means that the H/V -ratio does not contain any singularities for any parameter systems of layer and half-space.

By analogy, we suppose that the H/V -ratio has a zero-point at \bar{f}_z and C_z . We use the second formula of the H/V -ratio χ_2 in (1.57) and the condition for the H/V -ratio having a zero point is $M_1(C) = 0$ or:

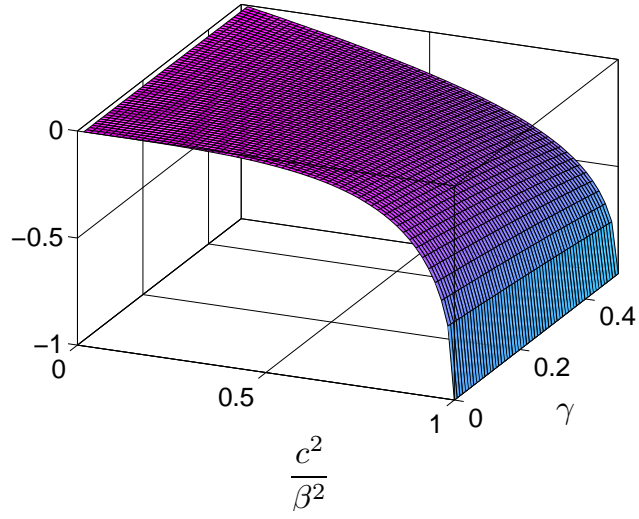
$$C_z \sqrt{1 - C_z^2 r_s^2} + 2r_d \bar{f}_z \pi (-1 + \sqrt{1 - C_z^2 r_s^2} \sqrt{1 - C_z^2 r_s^2 \gamma_2}) = 0.$$

Thus,

$$\bar{f}_z = - \frac{C_z \sqrt{1 - C_z^2 r_s^2}}{2r_d \pi (-1 + \sqrt{1 - C_z^2 r_s^2} \sqrt{1 - C_z^2 r_s^2 \gamma_2})}. \quad (1.66)$$

Substituting this \bar{f}_z into the dispersion equation (1.50) we have:

$$\frac{8 + C_z^4 r_s^4 (1 + 4\gamma_2) + 4(C_z^2 r_s^2 - 2) \sqrt{1 - C_z^2 r_s^2} \sqrt{1 - C_z^2 r_s^2 \gamma_2} - 4C_z^2 r_s^2 (2 + \gamma_2)}{-1 + \sqrt{1 - C_z^2 r_s^2} \sqrt{1 - C_z^2 r_s^2 \gamma_2}} = 0. \quad (1.67)$$

Figure 1.4: Contour line of $P(y, \gamma_2)$

The left side of this equation can be consider as a function $Q(t, \gamma_2)$ with $t = c_z^2/\beta_2^2$. Comparing $Q(t, \gamma_2)$ with $P(y, \gamma_2)$, we realize that these functions are identical. Thus, $Q(t, \gamma_2)$ does not have any solutions in our domain of interest, t and γ_2 , or the H/V -ratio does not have any zero points.

So, the ellipticity is always positive with all values of ν_2 , or the motion of the particle on the surface is always retrograde.

Chapter 2

Layer with fixed bottom (LFB)

Our model now is one layer with a fixed bottom. The thickness of the layer is d . The length and the width are large enough for the surface of the layer to be considered as a plane. The surface of the layer is free while the bottom is fixed. In this chapter, I will investigate both the cases of homogeneous and inhomogeneous layer.

2.1 Homogeneous layer

In homogeneous case, the Poisson ratio is ν , the shear wave velocity is β , the density of mass is ρ and they are constant in the layer. This model is a special case of model "Layer over half-space" (LOH) when the impedance contrast between the layer and half-space is very high. We choose the coordinate system as in Fig. 2.1. The waves (P and SV) propagate in the plane $(x_1 O x_3)$.

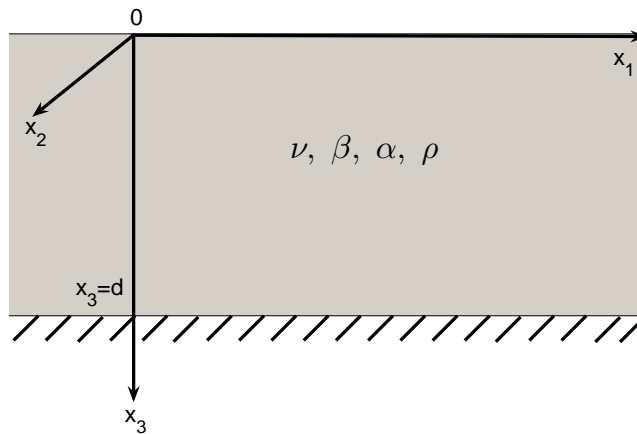


Figure 2.1: Homogeneous bottom fixed layer

2.1.1 The eigen-value problem

Suppose that the surface wave propagates along the x_1 -axis with the phase velocity c . The displacement is characterized by two components, u_1 and u_3 , while $u_2 = 0$. The corresponding complex amplitudes of potentials are described by

$$\begin{aligned}\varphi &= \Phi(x_3) \exp[i(kx_1 - \omega t)] , \\ \psi &= \Psi(x_3) \exp[i(kx_1 - \omega t)] .\end{aligned}\tag{2.1}$$

We choose a solution of $\Phi(x_3)$ and $\Psi(x_3)$ which satisfies the motion equation:

$$\Phi(x_3) = A_1 \sin(px_3) + A_2 \cos(px_3) ,\tag{2.2}$$

$$\Psi(x_3) = B_1 \sin(qx_3) + B_2 \cos(qx_3) ,\tag{2.3}$$

where

$$p^2 = \frac{\omega^2}{\alpha^2} - k^2 = k^2 \left(\frac{c^2}{\alpha^2} - 1 \right) , \quad q^2 = \frac{\omega^2}{\beta^2} - k^2 = k^2 \left(\frac{c^2}{\beta^2} - 1 \right) .\tag{2.4}$$

In the expression for the displacement and the stress components, which are obtained from (2.1), the term $\exp[i(kx_1 - \omega t)]$ appears as a multiplier. Since the exponential appears in all of the expressions, it does not play a further role in the determination of the frequency equation and it is therefore omitted in the following equations. Thus we write the displacement and stress amplitudes as

$$U_1 = ik\Phi - \frac{d\Psi}{dx_3} ,\tag{2.5}$$

$$U_3 = \frac{d\Phi}{dx_3} + ik\Psi\tag{2.6}$$

and

$$\tau_{31} = \rho\beta^2 \left[\frac{dU_1}{dx_3} + ikU_3 \right] ,\tag{2.7}$$

$$\tau_{33} = \rho\alpha^2 \left[\frac{dU_3}{dx_3} + ik(1 - 2\gamma)U_1 \right] .\tag{2.8}$$

Boundary conditions at the free surface and at the fixed bottom are

$$\tau_{31} = \tau_{33} = 0 \quad \text{on } x_3 = 0 ,\tag{2.9}$$

and

$$U_1 = U_3 = 0 \quad \text{on } x_3 = d .\tag{2.10}$$

By substituting the displacement and stress formulas into the boundary conditions (2.9)-(2.10) we obtain a system of equations defining the constants A_1, A_2, B_1 and B_2 in the matrix form

$$\begin{bmatrix} 2ig_\alpha & 0 & 0 & -1 + g_\beta \\ 0 & -1 + 2\gamma - g_\alpha^2 & 2i\gamma g_\beta & 0 \\ i \sin(g_\alpha dk) & i \cos(g_\alpha dk) & -g_\beta \cos(g_\beta dk) & g_\beta \sin(g_\beta dk) \\ g_\alpha \cos(g_\alpha dk) & -g_\alpha \sin(g_\alpha dk) & i \sin(g_\beta dk) & i \cos(g_\beta dk) \end{bmatrix} \begin{bmatrix} A_1 \\ A_2 \\ B_1 \\ B_2 \end{bmatrix} = 0\tag{2.11}$$

where $g_\alpha = p/k = \sqrt{\gamma C^2 - 1}$, $g_\beta = q/k = \sqrt{C^2 - 1}$. The non-trivial solution corresponding to the determinant of A_1 , A_2 , B_1 and B_2 to zero results in the secular equation

$$\Delta(C, \bar{f}) = A_0(C) + B_0(C) \sin\left(\frac{2\pi \bar{f} g_\alpha}{C}\right) \sin\left(\frac{2\pi \bar{f} g_\beta}{C}\right) + C_0(C) \cos\left(\frac{2\pi \bar{f} g_\alpha}{C}\right) \cos\left(\frac{2\pi \bar{f} g_\beta}{C}\right) \quad (2.12)$$

where

$$\bar{f} = d/\lambda_\beta, \quad C = c/\beta \quad (2.13)$$

and the auxiliary functions $A_0(C)$, $B_0(C)$, $C_0(C)$ are given by

$$\begin{aligned} A_0(C) &= -4g_\alpha g_\beta (C^2 - 2), \\ B_0(C) &= C^4(4\gamma + 1) - 4C^2(\gamma + 2) + 8, \\ C_0(C) &= -g_\alpha g_\beta (C^4 - 4C^2 + 8). \end{aligned} \quad (2.14)$$

2.1.2 Dispersion law

The secular equation (2.12) depends on the frequency \bar{f} , phase velocity C and Poisson's ratio ν . It does not depend on the density of mass. Figure 2.2 shows dispersion curves for several modes of the layer with Poisson's ratio $\nu = 1/3$. We can see that each mode has a cut-off frequency, even the fundamental mode. This is the case because a surface wave satisfying the fixed bottom condition cannot exist at small frequencies or long wavelengths. In this small range of frequencies, there is only the complex solution of phase velocity given by Eq. (2.12) corresponding to the leaking wave, which we do not consider here. The phase velocity at

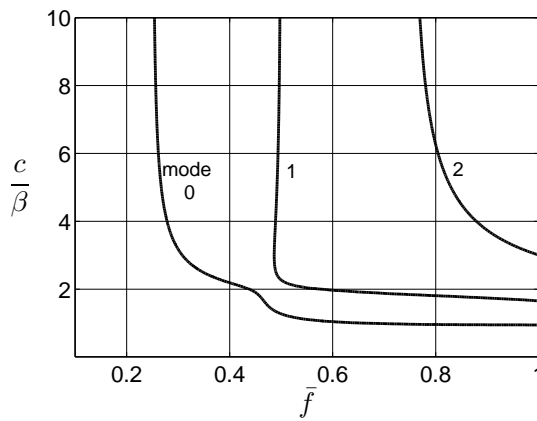


Figure 2.2: Velocity curves of three modes with $\nu = 1/3$

the cut-off frequency is observed as infinite. To find these cut-off frequencies we substitute the phase velocity as infinity into the secular equation. When phase velocity $C \rightarrow +\infty$, the

left-hand side of Eq. (2.12) tends to infinity and we have the approximations

$$\begin{aligned} A_0 &\approx -4\sqrt{\gamma}C^4, \\ B_0 &\approx (4\gamma + 1)C^4, \\ C_0 &\approx -\sqrt{\gamma}C^6, \end{aligned}$$

thus

$$\begin{aligned} \Delta(C, \bar{f}) &\approx C^4 [-4\sqrt{\gamma} + (4\gamma + 1) \sin(2\pi\bar{f}\sqrt{\gamma}) \sin(2\pi\bar{f}) + \sqrt{\gamma}C^2 \cos(2\pi\bar{f}\sqrt{\gamma}) \cos(2\pi\bar{f})] \\ &\approx \sqrt{\gamma}C^6 \cos(2\pi\bar{f}\sqrt{\gamma}) \cos(2\pi\bar{f}). \end{aligned}$$

The necessary condition of \bar{f} for $C \rightarrow +\infty$ is a solution of the secular equation:

$$\cos(2\pi\bar{f}\sqrt{\gamma}) \cos(2\pi\bar{f}) = 0, \quad (2.15)$$

or

$$\begin{cases} \bar{f} = \frac{1}{4} + \frac{k}{2} \\ \bar{f} = \frac{1}{4\sqrt{\gamma}} + \frac{l}{2\sqrt{\gamma}}, \quad k, l \in N. \end{cases} \quad (2.16)$$

From numerical results, we can see that the singularity of the fundamental mode always corresponds to $k = 0$ in (2.16). The corresponding frequency is $\bar{f} = 0.25$. This frequency is exactly the resonant frequency of the shear wave in the layer. In figure 2.2 in which we plot phase velocity curves with $\nu = 1/3$, we can use the formula (2.16) to find the cut-off frequency for other higher modes. For example, the cut-off frequency of the first higher mode is $\bar{f} = 0.5$ corresponding to $l = 0$ and of the second higher mode is $\bar{f} = 0.75$ corresponding to $k = 1$.

High frequency

When the frequency is very high or $\bar{f} \rightarrow \infty$, the necessary condition for $\Delta(C, \bar{f})$ in (2.12) converges is g_α and g_β become imaginary number. If not so, since $\sin(x)$ and $\cos(x)$ do not converge when $x \rightarrow \infty$, $\Delta(C, \bar{f})$, so $\Delta(C, \bar{f})$ can not converge. The above conditions lead to

$$C < 1 \quad \text{or} \quad c < \beta. \quad (2.17)$$

We denote

$$t_1 = i \frac{2\pi\bar{f}g_\alpha}{C}, \quad t_2 = i \frac{2\pi\bar{f}g_\beta}{C} \quad (2.18)$$

and with the conditions $C < 1$, t_1, t_2 are real and

$$t_1 \rightarrow +\infty, \quad t_2 \rightarrow +\infty \quad \text{when} \quad \bar{f} \rightarrow \infty. \quad (2.19)$$

We transform $\Delta(C, \bar{f})$ as

$$\begin{aligned} \Delta(C, \bar{f}) &= A_0(C) - B_0(C) \sinh t_1 \sinh t_2 + C_0(C) \cosh t_1 \cosh t_2 \\ &= A_0(C) - B_0(C) \frac{e^{t_1} - e^{-t_1}}{2} \frac{e^{t_2} - e^{-t_2}}{2} + C_0(C) \frac{e^{t_1} + e^{-t_1}}{2} \frac{e^{t_2} + e^{-t_2}}{2} \end{aligned}$$

and we have

$$\Delta(C, \bar{f}) \approx \frac{e^{t_1+t_2}}{4} [C_0(C) - B_0(C)] \quad (2.20)$$

when $\bar{f} \rightarrow \infty$. The necessary condition of C to be a solution of the secular equation when $\bar{f} \rightarrow \infty$ is

$$C_0(C) - B_0(C) = 0. \quad (2.21)$$

By substituting $B_0(C)$ and $C_0(C)$ from (2.14) into this equation we obtain the equation defining the phase velocity of a Rayleigh wave with high frequency in “layer with fixed bottom”:

$$C^4(4\gamma + 1) - 4C^2(\gamma + 2) + 8 + (C^4 - 4C^2 + 8)\sqrt{C^2\gamma - 1}\sqrt{C^2 - 1} = 0. \quad (2.22)$$

Proposition 2. *The Rayleigh wave velocity is a solution of equation (2.22).*

Proof. Suppose that $C = C_R$. Because it must satisfy the Rayleigh wave equation, we have

$$(2 - C_R^2)^2 - 4\sqrt{1 - C_R^2}\gamma\sqrt{1 - C_R^2} = 0, \quad (2.23)$$

and therefore

$$(2 - C_R^2)^2 = 4\sqrt{1 - C_R^2}\gamma\sqrt{1 - C_R^2} = -4\sqrt{C_R^2\gamma - 1}\sqrt{C_R^2 - 1}.$$

By substituting this into (2.22) and conducting some simple algebraic transformations we have

$$(2 - C_R^2)^2 - 4\sqrt{1 - C_R^2}\gamma\sqrt{1 - C_R^2} = 0.$$

This equation exactly corresponds to the Rayleigh equation. □

From this proposition we can conclude that the Rayleigh wave of half-space represents the phase velocity when the frequency is high, and it is observed for the fundamental mode. This fact can be predicted from the skin effect in surface waves: high-frequency waves are concentrated within a thin layer near the surface.

2.1.3 Displacements

Suppose that we have the phase velocity. From (2.5) and (2.6) we have the displacement in the layer

$$U_1(x_3) = ik [A_1 \sin(px_3) + A_2 \cos(px_3)] - q [B_1 \cos(qx_3) - B_2 \sin(qx_3)], \quad (2.24)$$

$$U_3(x_3) = p [A_1 \cos(px_3) - A_2 \sin(px_3)] + ik [B_1 \sin(qx_3) + B_2 \cos(qx_3)]. \quad (2.25)$$

The relation between A_1 , A_2 , B_1 and B_2 can be determined from three of four boundary condition equations. After some simple algebraic transformations we obtain

$$\frac{U_1(x_3)}{U_3(0)} = \frac{C^2 - 2}{\gamma_\alpha C^2} \frac{D(x_3)}{M}, \quad (2.26)$$

$$\frac{U_3(x_3)}{U_3(0)} = \frac{C^2 - 2}{C^2} \frac{E(x_3)}{M} \quad (2.27)$$

where

$$M = (1 - g_\beta^2) [2\gamma g_\alpha g_\beta \sin(g_\alpha dk) + (-1 + 2\gamma - g_\alpha^2) \sin(g_\beta dk)] , \quad (2.28)$$

and

$$D(x_3) = D_1 \sin(g_\alpha dx_3) + D_2 \sin(g_\beta dx_3) + D_3 \cos(g_\alpha dx_3) + D_4 \cos(g_\beta dx_3) \quad (2.29)$$

for

$$D_1 = M ,$$

$$D_2 = 2g_\alpha g_\beta M / (1 - g_\beta^2) ,$$

$$D_3 = 2\gamma g_\alpha g_\beta [-2 \cos(g_\beta dk) + (1 - g_\beta^2) \cos(g_\alpha dk)] ,$$

$$D_4 = -g_\alpha g_\beta (-1 + 2\gamma - g_\alpha^2) [-2 \cos(g_\beta dk) + (1 - g_\beta^2) \cos(g_\alpha dk)] ,$$

and

$$E(x_3) = E_1 \sin(g_\alpha dx_3) + E_2 \sin(g_\beta dx_3) + E_3 \cos(g_\alpha dx_3) + E_4 \cos(g_\beta dx_3) \quad (2.30)$$

for

$$E_1 = -D_3 , E_2 = D_4 / g_\alpha g_\beta , E_3 = D_1 , E_4 = -D_2 / g_\alpha g_\beta .$$

2.1.4 H/V ratio

The H/V -ratio formula is constructed from the ratio of the horizontal displacement to the vertical displacement on the surface

$$\chi = \frac{U_1(0)}{U_3(0)} = \frac{ikA_2 - qB_1}{pA_1 + ikB_2} . \quad (2.31)$$

The relation among A_1 , A_2 , B_1 and B_2 can be derived from three of four boundary conditions, and there are three possible combinations, so we can have three formulas of the H/V -ratio:

$$\chi_1 = \frac{N_1 [1 - \cos(g_\alpha dk) \cos(g_\beta dk)] - N_2 \sin(g_\alpha dk) \sin(g_\beta dk)}{g_\alpha (1 + g_\beta^2) [g_\alpha g_\beta \cos(g_\beta dk) \sin(g_\alpha dk) + \cos(g_\alpha dk) \sin(g_\beta dk)]} \quad (2.32)$$

where

$$N_1 = g_\alpha g_\beta (-3 + g_\beta^2) ,$$

$$N_2 = 1 + (-1 + 2g_\alpha^2) g_\beta^2 ,$$

and

$$\chi_2 = \frac{(1 + g_\alpha^2) g_\beta \left[(-1 + g_\beta^2) \cos(g_\alpha dk) + 2 \cos(g_\beta dk) \right]}{\gamma (1 + g_\beta^2) \left[-2g_\alpha g_\beta \sin(g_\alpha dk) + (-1 + g_\beta^2) \sin(g_\beta dk) \right]}, \quad (2.33)$$

$$\chi_3 = - \frac{(1 + g_\alpha^2) g_\beta \left[-(-1 + g_\beta^2) \sin(g_\alpha dk) + 2g_\alpha g_\beta \sin(g_\beta dk) \right]}{\gamma g_\alpha (1 + g_\beta^2) \left[2 \cos(g_\alpha dk) + (-1 + g_\beta^2) \cos(g_\beta dk) \right]}. \quad (2.34)$$

These three formulas of χ depend on each other in the sense that each of them can be derived from one other and the secular equation, and we can obtain the secular equation by taking $\chi_2 = \chi_3$.

The first peak

For frequencies below $\bar{f} = 0.25$ there is no undamped surface-wave motion, so there is no H/V -ratio with these frequencies. When $\bar{f} = 0.25$, the phase velocity curve has a singularity. By substituting $C = +\infty$ and $\bar{f} = 0.25$ into the H/V -ratio formula χ_1 we obtain

$$\chi \approx C^4 \sqrt{\gamma} \left[1 - 2\sqrt{\gamma} \sin(\sqrt{\gamma} \frac{\pi}{2}) \right].$$

Hence $\chi \rightarrow \pm \infty$ at $\bar{f} = 0.25$. The sign depends on the value of γ . The equation

$$1 - 2\sqrt{\gamma} \sin(\sqrt{\gamma} \frac{\pi}{2}) = 0 \quad (2.35)$$

has a solution $\gamma = 0.373$ in the region $0 < \gamma < 0.5$. This value corresponds to $\nu = 0.2026$ and we conclude for the H/V -ratio at $\bar{f} = 0.25$ that

- if $0 < \nu < 0.2026$ then $\chi \rightarrow -\infty$
- if $0.2026 < \nu < 0.5$ then $\chi \rightarrow +\infty$.

High frequency

When the frequency is very high, the phase velocity reaches the velocity of Rayleigh waves $C_R = c_R/\beta_1$. Substituting C_R into the formula χ_2 (2.33) yields

$$\chi = \frac{2 - C_R^2}{2\sqrt{1 - \gamma C_R^2}} \quad (2.36)$$

and because C_R satisfies the Rayleigh waves equation as

$$(2 - C_R^2)^2 = 4\sqrt{1 - C_R^2}\sqrt{1 - \gamma C_R^2},$$

so χ can be transformed to

$$\chi = \frac{2\sqrt{1 - C_R^2}}{2 - C_R^2} \quad (2.37)$$

and we again have the formula for the H/V -ratio of model half-space. Because of $C_R < 1$, the H/V -ratio is positive.

Zero-point

Unlike the model “impedance wave”, which does not have any singularities or zero points, in the model LFB, we can observe both. The zero point occurs when the horizontal displacement vanishes and it must satisfy the secular equation. Thus the zero-point of the H/V -ratio curve is the solution of this system of equations:

$$\begin{cases} \Delta(C, \bar{f}) = 0 \\ \chi(C, \bar{f}) = 0. \end{cases} \quad (2.38)$$

We have proved that the secular equation $\Delta(C, \bar{f})$ and the three formulas of the H/V -ratio are dependent. Thus the system of equations (2.38) is equivalent to

$$\begin{cases} \chi_2(C, \bar{f}) = 0 \\ \chi_3(C, \bar{f}) = 0. \end{cases} \quad (2.39)$$

From (2.39) we have (2.38) (proved in **Appendix 1**). The details of (2.39) are:

$$\begin{cases} (C^2 - 2) \cos(g_\alpha dk) + 2 \cos(g_\beta dk) = 0 \\ (C^2 - 2) \sin(g_\alpha dk) - 2g_\alpha g_\beta \sin(g_\beta dk) = 0. \end{cases} \quad (2.40)$$

This leads to

$$\begin{cases} \cos^2(g_\beta dk) = \frac{\gamma(1-C^2)+C^2/4}{\gamma(1-C^2)+1} \\ \cos^2(g_\alpha dk) = \left(\frac{2}{C^2-2}\right)^2 \frac{\gamma(1-C^2)+C^2/4}{\gamma(1-C^2)+1}. \end{cases} \quad (2.41)$$

Proposition 3. *At the zero-point of the H/V -ratio curve, the phase velocity satisfies $1 < C < 2$.*

Proof. - If $C < 1$ then

$$\cos(g_\beta dk) = \cos\left(2\pi\sqrt{C^2-1}\bar{f}/C\right) = \cosh\left(2\pi\sqrt{1-C^2}\bar{f}/C\right) > 1,$$

but

$$\frac{\gamma(1-C^2)+C^2/4}{\gamma(1-C^2)+1} < 1.$$

It is nonsense so $C > 1$.

- Because $C > 1$, $\cos(g_\beta dk) < 1$. Therefore

$$\frac{\gamma(1-C^2)+C^2/4}{\gamma(1-C^2)+1} < 1,$$

or $C^2/4 < 1$ or $C < 2$.

So $1 < C < 2$. □

The necessary condition of γ for the existence of a solution of (2.41) is:

$$\frac{\gamma(1 - C^2) + C^2/4}{\gamma(1 - C^2) + 1} > 0 ,$$

and because

$$\gamma(1 - C^2) + C^2/4 < \gamma(1 - C^2) + 1 \quad (\text{since } C < 2) ,$$

the condition becomes

$$\left[\begin{array}{l} \gamma(1 - C^2) + C^2/4 > 0 \\ \gamma(1 - C^2) + 1 < 0 \end{array} \right] \quad \text{or} \quad \left[\begin{array}{l} C^2(\gamma - 1/4) < \gamma \\ \gamma C^2 > 1 + \gamma \end{array} \right]. \quad (2.42)$$

- If $\gamma < 1/4$, (2.42) is automatically satisfied in the first inequality.
- If $\gamma > 1/4$, (2.42) becomes

$$\left[\begin{array}{l} C^2 < \frac{\gamma}{\gamma - 1/4} \\ C^2 > \frac{1 + \gamma}{\gamma} \end{array} \right].$$

Because $1 < C < 2$ and both $\frac{\gamma}{\gamma - 1/4}$ and $\frac{1 + \gamma}{\gamma}$ are greater than 1, γ must be satisfied $\frac{\gamma}{\gamma - 1/4} > \frac{1 + \gamma}{\gamma}$ or $\gamma < 1/3$.

So $\gamma < 1/3$ or $\nu > 0.25$.

We find the zero-point from (2.41). The simpler form of it is:

$$\left\{ \begin{array}{l} \sqrt{C^2\gamma - 1} \arccos\left(\sqrt{\frac{\gamma(1 - C^2) + C^2/4}{\gamma(1 - C^2) + 1}}\right) = \sqrt{C^2 - 1} \arccos\left(\frac{2}{2 - C^2} \sqrt{\frac{\gamma(1 - C^2) + C^2/4}{\gamma(1 - C^2) + 1}}\right) \\ \bar{f} = \frac{C}{2\pi\sqrt{C^2 - 1}} \arccos\left(\sqrt{\frac{\gamma(1 - C^2) + C^2/4}{\gamma(1 - C^2) + 1}}\right) \end{array} \right. \quad (2.43)$$

The singularity of H/V -ratio

The singularity of the H/V -ratio curve is the solution of this system of equations:

$$\left\{ \begin{array}{l} \Delta(C, \bar{f}) = 0 \\ \frac{1}{\chi(C, \bar{f})} = 0 \end{array} \right. \quad (2.44)$$

This system of equations is equivalent to

$$\left\{ \begin{array}{l} \frac{1}{\chi_2(C, \bar{f})} = 0 \\ \frac{1}{\chi_3(C, \bar{f})} = 0 \end{array} \right. \quad (2.45)$$

because of the dependence between the secular equation and formulas of H/V -ratio. From (2.45) we again obtain (2.44) (Appendix 2). The details of (2.45) are:

$$\left\{ \begin{array}{l} (C^2 - 2) \cos(g_\beta dk) + 2 \cos(g_\alpha dk) = 0 \\ (C^2 - 2) \sin(g_\beta dk) - 2g_\alpha g_\beta \sin(g_\alpha dk) = 0 \end{array} \right. \quad (2.46)$$

This leads to:

$$\begin{cases} \cos^2(g_\alpha dk) &= \frac{\gamma(1-C^2)+C^2/4}{\gamma(1-C^2)+1} \\ \cos^2(g_\beta dk) &= \left(\frac{2}{C^2-2}\right)^2 \frac{\gamma(1-C^2)+C^2/4}{\gamma(1-C^2)+1}, \end{cases} \quad (2.47)$$

or

$$\begin{cases} \sqrt{C^2-1} \arccos\left(\sqrt{\frac{\gamma(1-C^2)+C^2/4}{\gamma(1-C^2)+1}}\right) = \sqrt{C^2\gamma-1} \arccos\left(\frac{2}{2-C^2}\sqrt{\frac{\gamma(1-C^2)+C^2/4}{\gamma(1-C^2)+1}}\right) \\ \bar{f} = \frac{C}{2\pi\sqrt{C^2\gamma-1}} \arccos\left(\sqrt{\frac{\gamma(1-C^2)+C^2/4}{\gamma(1-C^2)+1}}\right). \end{cases} \quad (2.48)$$

This is a system of equations defining the singularity frequencies of H/V -ratio curve.

2.1.5 Particle motion

In the two previous models, “half-space” and “impedance wave”, we do not observe any possibility for prograde particle motion; the motion is always retrograde. In the model “layer with fixed bottom (LFB)”, the H/V ratio curve has a singularity and a zero point at certain frequencies. In these frequencies, the sense of motion changes and the particle motion can be prograde. Fig. 2.3 shows a 2D graph of ellipticity χ as a function of \bar{f} and the Poisson’s

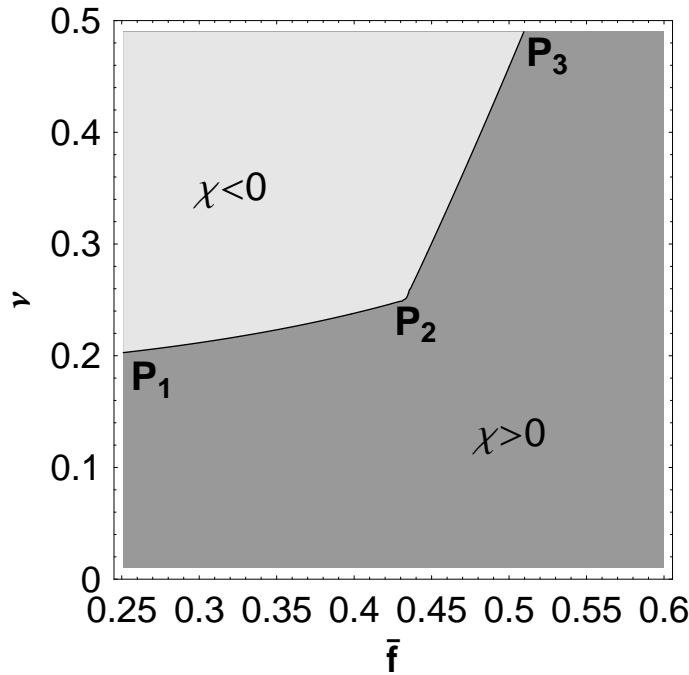


Figure 2.3: The ellipticity for the model layer with fixed bottom (LFB) in dependence of frequency and Poisson’s ratio: retrograde motion (dark gray) and prograde motion (light gray)

ratio of the layer ν . It displays the sharp partition into two regions, where $\chi > 0$ corresponds

to retrograde particle motion (dark shading) and $\chi < 0$ to prograde particle motion (light shading).

The domain of prograde motion is bounded on the left by a critical point P_1 with coordinates $(0.25, 0.2026)$ and at the top of the figure by point P_3 with coordinates $(0.5126, 0.5)$. The critical value $\nu = 0.2026$ follows from the equation (2.35). Unfortunately, there is no algebraic representation of the P_3 coordinates. The value $\bar{f} = 0.5126$ follows from the solution of the system of Eqs. (2.43) when $\gamma = 0$ or $\nu = 0.5$.

The curve P_1P_2 is the set of singularities which are solutions of the system of equations (2.48) and the curve P_2P_3 is the set of zero points which are solutions of the system of equations (2.43). By numerical calculation, we can approximate these two sets of solutions by simple linear functions of Poisson's ratio:

$$P_1P_2 : \bar{f} = 0.25 + 3.861 (\nu_1 - 0.2026) \text{ when } 0.2026 \leq \nu_1 \leq 0.25 \quad (2.49)$$

and

$$P_2P_3 : \bar{f} = \frac{\sqrt{3}}{4} + 0.318 (\nu_1 - 0.25) \text{ when } 0.25 \leq \nu_1 \leq 0.5 . \quad (2.50)$$

No prograde motion is observed for $\nu < 0.2026$. The same critical value is observed in the method used by Giese [19] for the determination of Poisson's ratio from frequency when the sense of motion changes. When $\nu > 0.2026$, the broad band of frequency range for the prograde motion becomes larger with higher value of ν . It can be calculated by the distance between $\bar{f} = 0.25$ and \bar{f} in (2.49) and (2.50).

A critical point P_2 with coordinates $(\sqrt{3}/4, 0.25)$ is located near the center of the graph. It is the point at which the H/V -ratio changes its properties dramatically from having two singularities to one singularity and one zero point. The H/V -ratio in the close vicinity of P_2 can have any value and χ at P_2 becomes indeterminate as

$$\chi = \frac{0}{0} \text{ for } \bar{f} = \sqrt{3}/4 \text{ and } \nu = 0.25 \quad (2.51)$$

with right-hand and left-hand limits

$$\lim_{\bar{f} \rightarrow \sqrt{3}/4+0} \chi = 0.4089 \text{ and } \lim_{\bar{f} \rightarrow \sqrt{3}/4-0} \chi = -7.3371 . \quad (2.52)$$

This remarkable jump had been noticed by Giese [19], among others, and is one example of the problems with mode theory. The way to avoid difficulties such as this jump is to classify the eigenfunctions or modes in another manner, as pointed out by Okal [45] in the context of the Earth's spheroidal modes. We have only considered the fundamental mode which is defined in the standard manner as the wave with the lowest phase velocity. If, instead, the branches are defined by the continuity of $dc/d\bar{f}$, allowing them to cross each other, then the discontinuity disappears.

The critical point P_2 is closely connected with a so-called osculation point of dispersion curves for fundamental and first higher modes, respectively. The properties of this kind of point will be studied in detail in Chapter 4.

When $\bar{f} > 0.5126$, no prograde motion is observed. This phenomenon is due to the skin effect of the surface waves. When \bar{f} is large enough, our model LFB can be considered to be similar to the model “half-space”, and it is well known that there exists only retrograde motion in this model.

2.2 Inhomogeneous layer

In the previous section, we investigated the LFB with a homogeneous layer. There are some remarkable features for this case. The first is that neither the phase velocity nor the H/V ratio depends on the density of mass. The second is that the cut-off frequency for real phase velocity is $\bar{f} = 0.25$, the resonant shear wave frequency. However, do these features still hold for the inhomogeneous layer? To answer this question, we make the layer inhomogeneous by continuously increasing the shear modulus, while the other parameters remain constant (Fig. 2.4).

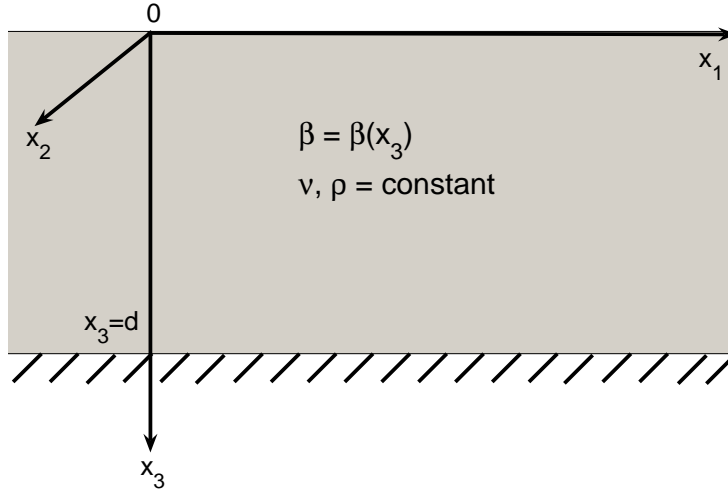


Figure 2.4: Inhomogeneous layer with fixed bottom model

2.2.1 The eigenvalue problem

Vrettos [57] investigated the surface waves in the half-space model with a special form of the variable shear modulus. This form is presented as a function of the depth

$$\mu(x_3) = \mu_0 + (\mu_\infty - \mu_0)[1 - \exp(-a x_3)] , \quad 0 < \mu_0 < \mu_\infty \quad (2.53)$$

where μ_0 and μ_∞ are the shear modulus at the surface and at infinite depth, respectively, and a is a constant with the dimension of inverse length. We will apply Vrettos' idea to our

model with the shear modulus function as in (2.54), but the domain of this function is only $0 \leq x_3 \leq d$, and

$$\mu_1 = \mu(d) \quad \text{or} \quad a \, d = \ln \frac{\mu_\infty - \mu_0}{\mu_\infty - \mu_1} . \quad (2.54)$$

When the shear modulus is a continuous function, and under the plane strain conditions, the governed motion equations follow two coupled differential equations:

$$\rho \frac{\partial^2 u_1}{\partial t^2} = \frac{2\mu(1-\nu)}{1-2\nu} \frac{\partial^2 u_1}{\partial x_1^2} + \mu \frac{\partial^2 u_1}{\partial x_3^2} + \frac{\mu}{1-2\nu} \frac{\partial^2 u_3}{\partial x_1 \partial x_3} + \frac{d\mu}{dx_3} \left[\nu \frac{\partial u_1}{\partial x_3} + \frac{\partial u_3}{\partial x_1} \right] \quad (2.55)$$

$$\rho \frac{\partial^2 u_3}{\partial t^2} = \frac{2\mu(1-\nu)}{1-2\nu} \frac{\partial^2 u_3}{\partial x_3^2} + \mu \frac{\partial^2 u_3}{\partial x_1^2} + \frac{\mu}{1-2\nu} \frac{\partial^2 u_1}{\partial x_1 \partial x_3} + \frac{2}{1-2\nu} \frac{d\mu}{dx_3} \left[\nu \frac{\partial u_1}{\partial x_1} + (1-\nu) \frac{\partial u_3}{\partial x_3} \right] \quad (2.56)$$

where $\mu = \mu(x_3)$ is defined by equation (2.54).

For steady-state plane waves of fixed circular frequency ω and wave number k propagating in the horizontal direction of increasing x_1 , we set

$$u_1(x_1, x_3, t) = \hat{u}_1(x_3) \exp[i(\omega t - kx_1)] , \quad (2.57)$$

$$u_3(x_1, x_3, t) = i \hat{u}_3(x_3) \exp[i(\omega t - kx_1)] \quad (2.58)$$

where i is the imaginary unit. The factor i in front of the displacement amplitude \hat{u}_3 implies that the path of a particle in the medium will be an ellipse, a property which holds for Rayleigh waves in a homogeneous half-space.

Substituting the trial solutions (3.67) and (3.68) into the wave equation (2.55) and (2.56), we obtain a system of couple linear differential equations for the displacement amplitudes $\hat{u}_1(x_3)$ and $\hat{u}_3(x_3)$:

$$\begin{aligned} (1-2\nu)\mu \frac{d^2 \hat{u}_1}{dx_3^2} + (1-2\nu) \frac{d\mu}{dx_3} \frac{d\hat{u}_1}{dx_3} + [(1-2\nu)\rho\omega^2 - 2(1-\nu)k^2\mu] \hat{u}_1 \\ + k\mu \frac{d\hat{u}_3}{dx_3} + (1-2\nu)k \frac{d\mu}{dx_3} \hat{u}_3 = 0 , \end{aligned} \quad (2.59)$$

$$2(1-\nu)\mu \frac{d^2 \hat{u}_3}{dx_3^2} + 2(1-\nu) \frac{d\mu}{dx_3} \frac{d\hat{u}_3}{dx_3} + (1-2\nu)(\rho\omega^2 - k^2\mu) \hat{u}_3 - k\mu \frac{d\hat{u}_1}{dx_3} - 2\nu k \frac{d\mu}{dx_3} \hat{u}_1 = 0 . \quad (2.60)$$

The stresses can be expressed in terms of the displacement amplitudes \hat{u}_1 and \hat{u}_3 by using the relations of linear elasticity

$$\sigma_{33} = \frac{2\mu}{1-2\nu} \left[\nu \frac{\partial u_1}{\partial x_1} + (1-\nu) \frac{\partial u_3}{\partial x_3} \right] , \quad (2.61)$$

$$\sigma_{13} = \mu \left[\frac{\partial u_1}{\partial x_3} + \frac{\partial u_3}{\partial x_1} \right] . \quad (2.62)$$

The free-surface conditions require vanishing traction at $x_3 = 0$ and the fixed bottom conditions require vanishing displacements at $x_3 = d$. For the SV/P waves considered here this

means that

$$\begin{aligned} \text{for } x_3 = 0 : \sigma_{33} &= 0 , \\ \sigma_{13} &= 0 , \\ \text{for } x_3 = d : u_3(d) &= 0 , \\ u_1(d) &= 0 . \end{aligned}$$

Applying (3.67-3.68) and (2.61-2.62), we obtain

$$\begin{aligned} \text{for } x_3 = 0 : \nu k \hat{u}_1 - (1 - \nu) \frac{d\hat{u}_3}{dx_3} &= 0 , \\ \frac{d\hat{u}_1}{dx_3} + k \hat{u}_3 &= 0 , \end{aligned} \tag{2.63}$$

$$\begin{aligned} \text{for } x_3 = d : \hat{u}_3(d) &= 0 , \\ \hat{u}_1(d) &= 0 . \end{aligned} \tag{2.64}$$

To treat the eigenvalue problem considered here analytically, it is convenient to introduce a subsidiary depth variable

$$\xi = H_0 \exp(-ax_3) \tag{2.65}$$

which transforms the interval $0 \leq x_3 \leq d$ onto $0 \leq H_1 \leq \xi \leq H_0 < 1$. H_0 and H_1 are the so-called inhomogeneity parameters defined by

$$H_0 = 1 - \frac{\mu_0}{\mu_\infty} , \tag{2.66}$$

$$H_1 = 1 - \frac{\mu_1}{\mu_\infty} . \tag{2.67}$$

Substituting the above transformations into the differential equations (2.59) and (2.60) we obtain

$$\xi^2(1 - \xi)\gamma \hat{u}_1'' + \xi(1 - 2\xi)\gamma \hat{u}_1' + [\gamma\theta - \beta(1 - \xi)]\hat{u}_1 - (1 - \xi)\xi\sqrt{\beta}(1 - \gamma)\hat{u}_3' + \xi\sqrt{\beta}\gamma\hat{u}_3 = 0 \tag{2.68}$$

and

$$\xi^2(1 - \xi)\hat{u}_3'' + \xi(1 - 2\xi)\hat{u}_3' + \gamma[\theta - \beta(1 - \xi)]\hat{u}_3 + (1 - \xi)\xi\sqrt{\beta}(1 - \gamma)\hat{u}_1' - \xi\sqrt{\beta}(1 - 2\gamma)\hat{u}_1 = 0 \tag{2.69}$$

where

$$\theta = \frac{\omega^2 \rho}{a^2 \mu_\infty}, \quad \beta = \frac{k^2}{a^2}, \quad \gamma = \frac{1 - 2\nu}{2(1 - \nu)}$$

and $()'$ denotes differentiation with respect to ξ . The constant γ expresses the following relation between the velocities of compression (P) and shear (S) waves, α and β , respectively:

$$\gamma = \left(\frac{\beta}{\alpha} \right)^2 = \frac{1 - 2\nu}{2(1 - \nu)} .$$

The boundary conditions transform to

$$\begin{aligned} \text{for } \xi = H_0 : \quad & \nu\sqrt{\beta}\hat{u}_1 + (1-\nu)\xi\hat{u}_3' = 0, \\ & \xi\hat{u}_1' - \sqrt{\beta}\hat{u}_3 = 0, \end{aligned} \quad (2.70)$$

$$\begin{aligned} \text{for } \xi = H_1 : \quad & \hat{u}_3 = 0, \\ & \hat{u}_1 = 0. \end{aligned} \quad (2.71)$$

Analytical solutions for the system of differential equations (2.68) and (2.69) can be found by using the Frobenius method [26] (extended power series method). Hence, we seek a solution of the form

$$\hat{u}_1(\xi) = \sum_{n=0}^{\infty} a_n \xi^{n+m}, \quad (2.72)$$

$$\hat{u}_3(\xi) = \sum_{n=0}^{\infty} b_n \xi^{n+m}. \quad (2.73)$$

Substitution of these expression and the derivatives into differential equations (2.68) and (2.69) yields, after some manipulations,

$$\begin{aligned} \sum_{n=0}^{\infty} [\gamma(n+m)^2 + \gamma\theta - \beta] a_n \xi^{n+m} - \sqrt{\beta}(1-\gamma) \sum_{n=0}^{\infty} (n+m) b_n \xi^{n+m} \\ = \sum_{n=0}^{\infty} [\gamma(n+m-1)(n+m) - \beta] a_{n-1} \xi^{n+m} \\ - \sqrt{\beta} \sum_{n=0}^{\infty} [(n+m-1) - \gamma(n+m-2)] b_{n-1} \xi^{n+m} \end{aligned} \quad (2.74)$$

and

$$\begin{aligned} \sqrt{\beta}(1-\gamma) \sum_{n=0}^{\infty} (n+m) a_n \xi^{n+m} + \sum_{n=0}^{\infty} [\gamma(\theta - \beta) + (n+m)^2] b_n \xi^{n+m} \\ = \sqrt{\beta} \sum_{n=0}^{\infty} [(1-\gamma)(n+m-1) + (1-2\gamma)] a_{n-1} \xi^{n+m} \\ + \sum_{n=0}^{\infty} [(n+m-1)(n+m) - \gamma\beta] b_{n-1} \xi^{n+m}. \end{aligned} \quad (2.75)$$

By setting the sum of the coefficients of the smallest power ξ^m to zero, we obtain the following system of equations for the coefficients a_0, b_0 :

$$a_0 [\gamma m^2 + \gamma\theta - \beta] - b_0 [(1-\gamma)m\sqrt{\beta}] = 0, \quad (2.76)$$

$$a_0 [(1-\gamma)m\sqrt{\beta}] - b_0 [m^2 + \gamma(\theta - \beta)] = 0. \quad (2.77)$$

Non-trivial solutions a_0, b_0 exist if

$$m^4 + [\theta(1+\gamma) - 2\beta] m^2 + (\beta - \theta)(\beta - \gamma\theta) = 0 \quad (2.78)$$

which is the indicial equation of the system of differential equations (2.68) and (2.69). The roots of this bi-quadratic equation are

$$m_{1,3} = \pm\sqrt{\beta - \gamma\theta}, \quad m_{2,4} = \pm\sqrt{\beta - \theta}. \quad (2.79)$$

So long as they do not differ by an integer, these roots correspond to four linearly independent solutions for \hat{u}_1 and \hat{u}_3 . Henceforth, the superscript (i) ($i = 1, 2, 3, 4$) is used to indicate the solutions corresponding to the root m_i . For

$$a_0^{(1)} = a_0^{(2)} = a_0^{(3)} = a_0^{(4)} = 1, \quad (2.80)$$

we find from equations (2.76) and (2.77)

$$b_0^{(1)} = -b_0^{(3)} = -\sqrt{\left(\frac{\beta - \gamma\theta}{\beta}\right)}, \quad b_0^{(2)} = -b_0^{(4)} = -\sqrt{\left(\frac{\beta}{\beta - \theta}\right)}. \quad (2.81)$$

The recurrence relations for a_n and b_n may be derived by equating the sums of the coefficients of each power of ξ for $n \geq 1$. Then we obtain

$$F_{11}a_n + F_{12}b_n = \bar{F}_1, \quad (2.82)$$

$$F_{21}a_n + F_{22}b_n = \bar{F}_2 \quad (2.83)$$

where

$$F_{11} = \gamma(n+m)^2 + \gamma\theta - \beta,$$

$$F_{12} = -\sqrt{\beta}(1-\gamma)(n+m),$$

$$F_{21} = \sqrt{\beta}(1-\gamma)(n+m),$$

$$F_{22} = \gamma(\theta - \beta) + (n+m)^2,$$

$$\bar{F}_1 = [\gamma(n+m-1)(n+m) - \beta]a_{n-1} - \sqrt{\beta}[(n+m-1) - \gamma(n+m-2)]b_{n-1},$$

$$\bar{F}_2 = -\sqrt{\beta}[\gamma - (n+m)(1-\gamma)]a_{n-1} + [(n+m-1)(n+m) - \gamma\beta]b_{n-1}.$$

Inserting each root m into this system of equations, the coefficients a_n and b_n are determined successively:

$$a_n = \frac{\bar{F}_1 F_{22} - F_{12} \bar{F}_2}{F_{11} F_{22} - F_{12} F_{21}}, \quad (2.84)$$

$$b_n = \frac{\bar{F}_2 F_{11} - F_{21} \bar{F}_1}{F_{11} F_{22} - F_{12} F_{21}} \quad (2.85)$$

with a_0 and b_0 given by equations (2.80) and (2.81). Thus, the complete solution for the displacement amplitudes are

$$\hat{u}_1(\xi) = A_1 \hat{u}_1^{(1)}(\xi) + A_2 \hat{u}_1^{(2)}(\xi) + A_3 \hat{u}_1^{(3)}(\xi) + A_4 \hat{u}_1^{(4)}(\xi), \quad (2.86)$$

$$\hat{u}_3(\xi) = A_1 \hat{u}_3^{(1)}(\xi) + A_2 \hat{u}_3^{(2)}(\xi) + A_3 \hat{u}_3^{(3)}(\xi) + A_4 \hat{u}_3^{(4)}(\xi) \quad (2.87)$$

where A_1 , A_2 , A_3 and A_4 are integration constants. Introducing the notation

$$\begin{aligned} RB1(i) &= \nu\sqrt{\beta} \sum_{n=0}^{\infty} a_n^{(i)} H_0^n + (1-\nu) \sum_{n=0}^{\infty} (n+m_i) b_n^{(i)} H_0^n \quad (i = 1, 2, 3, 4) , \\ RB2(i) &= \sum_{n=0}^{\infty} (n+m_i) a_n^{(i)} H_0^n - \sqrt{\beta} \sum_{n=0}^{\infty} b_n^{(i)} H_0^n \quad (i = 1, 2, 3, 4) , \\ RB3(i) &= \sum_{n=0}^{\infty} a_n^{(i)} H_1^n \quad (i = 1, 2, 3, 4) , \\ RB4(i) &= \sum_{n=0}^{\infty} b_n^{(i)} H_1^n \quad (i = 1, 2, 3, 4) \end{aligned}$$

and inserting the solutions (3.67) and (3.68) into the boundary conditions (2.63)-(2.64) we obtain

$$\begin{aligned} A_1 RB1(1) H_0^{m_1} + A_2 RB1(2) H_0^{m_2} + A_3 RB1(3) H_0^{m_3} + A_4 RB1(4) H_0^{m_4} &= 0 , \\ A_1 RB2(1) H_0^{m_1} + A_2 RB2(2) H_0^{m_2} + A_3 RB2(3) H_0^{m_3} + A_4 RB2(4) H_0^{m_4} &= 0 , \\ A_1 RB3(1) H_1^{m_1} + A_2 RB3(2) H_1^{m_2} + A_3 RB3(3) H_1^{m_3} + A_4 RB3(4) H_1^{m_4} &= 0 , \\ A_1 RB4(1) H_1^{m_1} + A_2 RB4(2) H_1^{m_2} + A_3 RB4(3) H_1^{m_3} + A_4 RB4(4) H_1^{m_4} &= 0 . \end{aligned}$$

Non-trivial solutions for the integration constants A_1 , A_2 , A_3 and A_4 exist only if the determinant of the coefficients is zero:

$$\begin{vmatrix} RB1(1)H_0^{m_1} & RB1(2)H_0^{m_2} & RB1(3)H_0^{m_3} & RB1(4)H_0^{m_4} \\ RB2(1)H_0^{m_1} & RB2(2)H_0^{m_2} & RB2(3)H_0^{m_3} & RB2(4)H_0^{m_4} \\ RB3(1)H_1^{m_1} & RB3(2)H_1^{m_2} & RB3(3)H_1^{m_3} & RB3(4)H_1^{m_4} \\ RB4(1)H_1^{m_1} & RB4(2)H_1^{m_2} & RB4(3)H_1^{m_3} & RB4(4)H_1^{m_4} \end{vmatrix} = 0 . \quad (2.88)$$

This is the characteristic equation of the eigenvalue problem considered here, and we can write is as

$$\Delta(c, \omega) = 0 . \quad (2.89)$$

This equation depends on six parameters: the Poisson ratio ν , three parameters from the function of shear modulus (μ_0 , μ_∞ and the constant a), and the layer's thickness and frequency.

By varying the parameters μ_0 , μ_∞ and the constant a , we obtain a wide range of real shear modulus variations of the layer. If the shear modulus of the layer varies from μ_0 on the surface to μ_1 at the bottom, the constant a must satisfy

$$a = \frac{1}{d} \ln \frac{H_0}{H_1} \quad (2.90)$$

degree	1	2	3	4
β_∞	2.51	1.77	1.50	1.36

Table 2.1: The value of μ_∞ corresponding to the degree of approximation polynomial function

where H_0 and H_1 are defined as in (2.66) and (2.67). Because $\mu_1 \geq \mu_0$ or $\frac{H_0}{H_1} \geq 1$, we can choose the value of a to be arbitrarily small (but $a > 0$) by varying μ_∞ . For small values of a , the function $\mu(x_3)$ can be expanded as a Taylor's expansion:

$$\mu(x_3) = \mu_0 + (\mu_\infty - \mu_0) \left[\sum_{i=1}^n (-1)^{i-1} \frac{(ax_3)^i}{i!} + o(ax_3)^n \right]. \quad (2.91)$$

If we consider that the shear modulus function in the layer is a polynomial power n , we can choose μ_∞ so that

$$(ad)^n = \left(\ln \frac{H_0}{H_1} \right)^n < 1\% \quad (2.92)$$

if we want the error to be less than 1%.

Table 2.1 shows values of μ_∞ for several approximations. In this case, we choose the layer with shear wave velocity on the surface $\beta_0 = 0.2$ km/s, at the bottom $\beta_1 = 0.8$ km/s, and mass density $\rho = 1.9$ g/cm³. Figure (2.5) shows the shear modulus function with different μ_∞ .

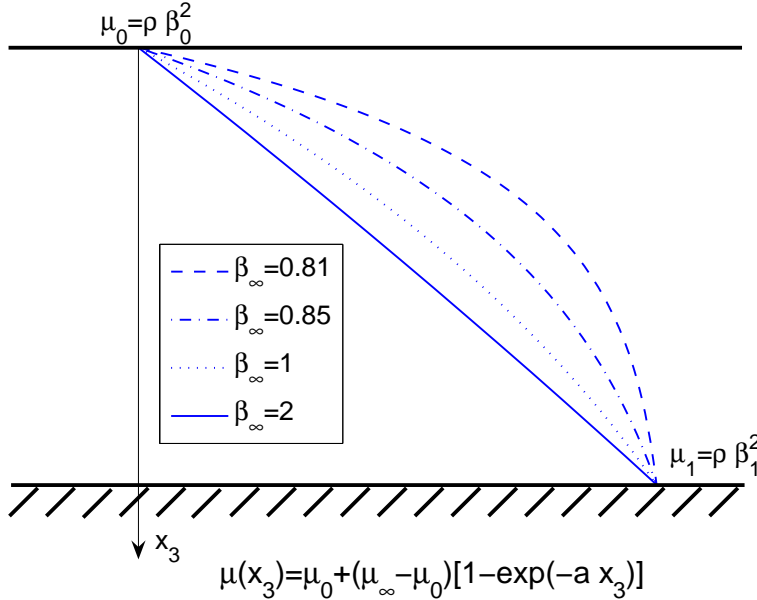


Figure 2.5: Shear modulus functions in layer

Dispersion law

For comparison with the homogeneous model, a dimensionless frequency \bar{f} and a dimensionless phase velocity C are defined:

$$\bar{f} = \frac{d \cdot f}{\bar{\beta}}, \quad C = \frac{c}{\bar{\beta}} \quad (2.93)$$

where c is the propagation velocity of the surface wave and the $\bar{\beta}$ is the mean of the shear wave velocity over the layer

$$c = \frac{\omega}{k}, \quad \bar{\beta} = \frac{1}{d} \int_0^d \sqrt{\frac{\mu(x_3)}{\rho}} dx_3. \quad (2.94)$$

From the set of the eigenvalue pairs (β, θ) the relation $C = C(\bar{f})$ can be calculated:

$$\bar{f} = \frac{\beta_\infty t}{2\pi \bar{\beta}} \sqrt{\beta}, \quad C = \sqrt{\frac{\theta}{\beta} \frac{\beta_\infty}{\bar{\beta}}}. \quad (2.95)$$

In Fig. 2.6, we choose $\beta_\infty = 2000$ m/s to plot velocity curves of the two first modes: fundamental and first higher modes with several different values of Poisson ratio. From figure (2.5) we can see that, with this value of μ_∞ , the shear modulus variation in the layer can be considered to vary linearly. From eq. (2.94), the mean velocity in this case is

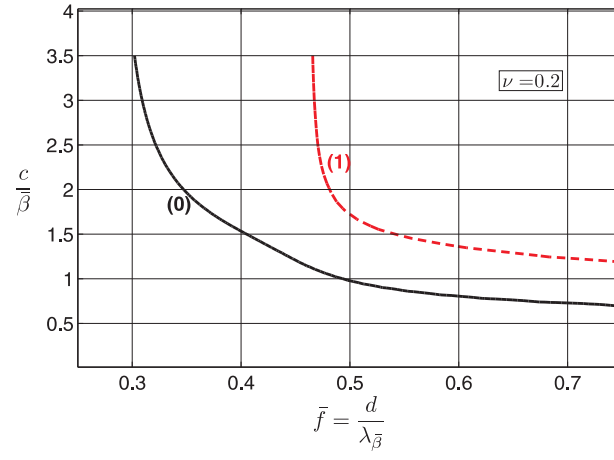
$$\bar{\beta} = 567.57 \text{ (m/s)}. \quad (2.96)$$

We see that every mode has a cut-off frequency similar to the phase velocity curve of the homogeneous layer. However, the cut-off frequencies shift to the right on the frequency axis compared to the homogeneous layer. This phenomenon is due to the inhomogeneity effect. The phase velocity at cut-off frequencies is not infinite, but β_∞ . When $\nu = 0.3525$, two velocity curves of fundamental and first higher mode seem to meet each other, and this point is similar to the osculation point of the homogeneous layer but with $\nu = 0.25$.

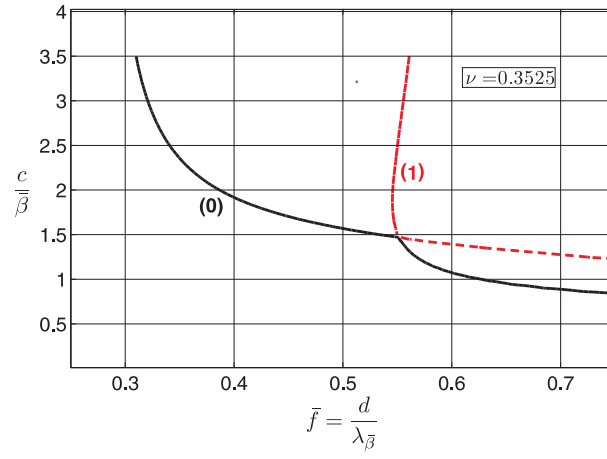
2.2.2 The eigen functions

Let us assume that (4.61) is solved and we thus have the eigenvalue in terms of (θ, β) pairs. We proceed now to determine the corresponding eigenfunctions, i.e., the displacement distributions of the particular wave modes. The variations with depth of the horizontal and vertical displacement amplitudes are given by equations (3.67) and (3.68). The relationship among the four integration constants A_1, A_2, A_3 and A_4 is obtained by the boundary conditions at the surface and the bottom. From any three of four these boundary condition equations we express, for example, A_2, A_3 and A_4 in terms of A_1 as

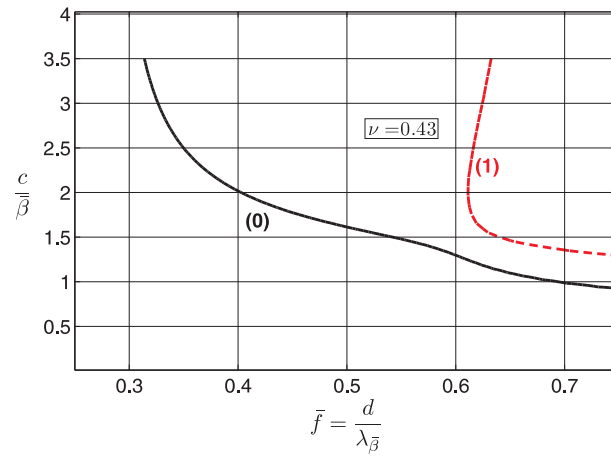
$$A_2 = l_1 A_1, \quad A_3 = l_2 A_1, \quad A_4 = l_3 A_1. \quad (2.97)$$



(a)



(b)



(c)

Figure 2.6: Dispersion curves for three different values of Poisson's ratio. (0) fundamental mode, (1) first higher mode

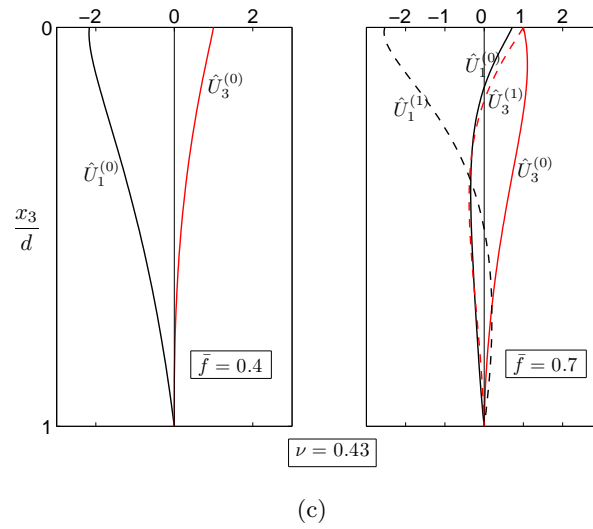
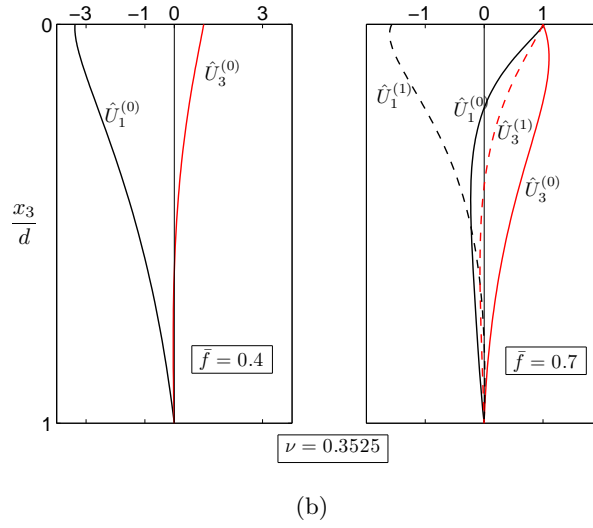
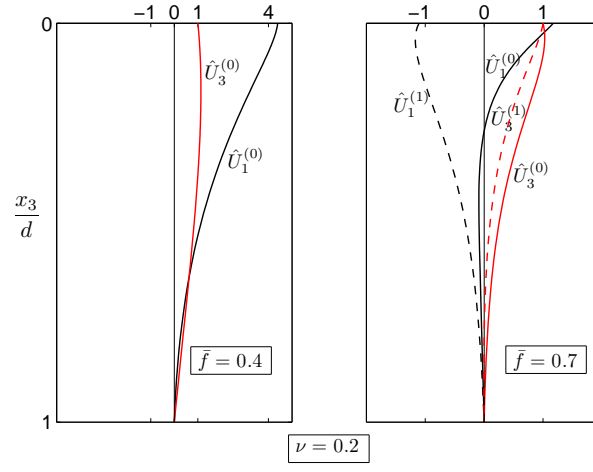
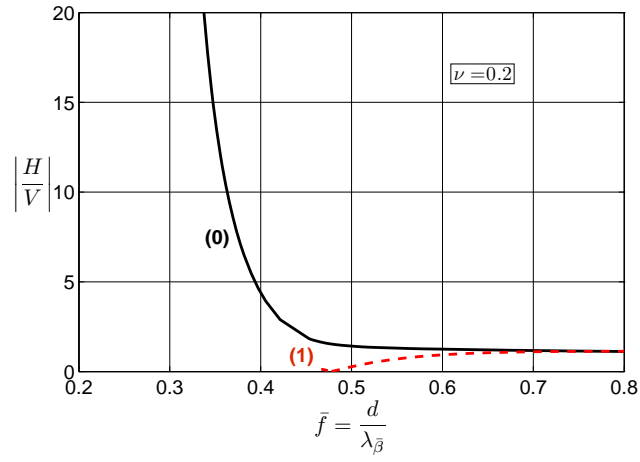
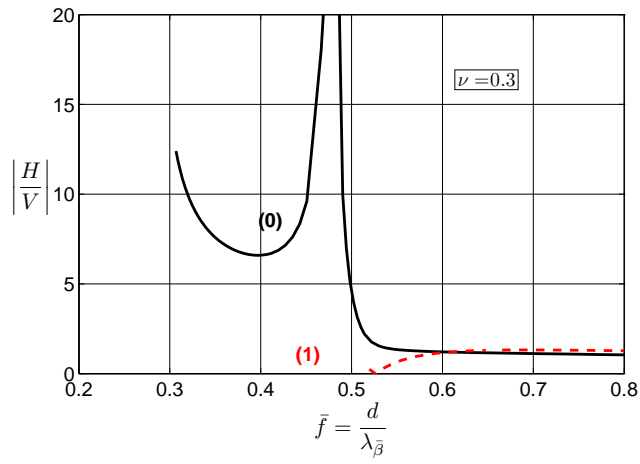


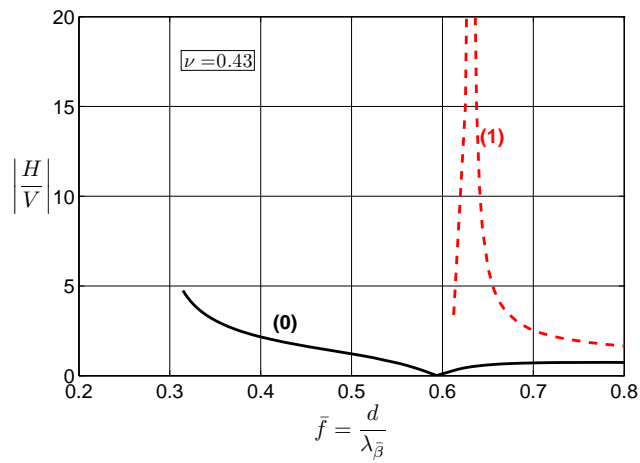
Figure 2.7: Attenuation with depth of the horizontal and vertical displacement at representative frequencies for $\mu_\infty = 2000m/s$ and three different Poisson's ratios. (0) fundamental mode, (1) first higher mode



(a)



(b)



(c)

Figure 2.8: H/V -ratio curves for three different values of Poisson's ratio. (0) fundamental mode, (1) first higher mode

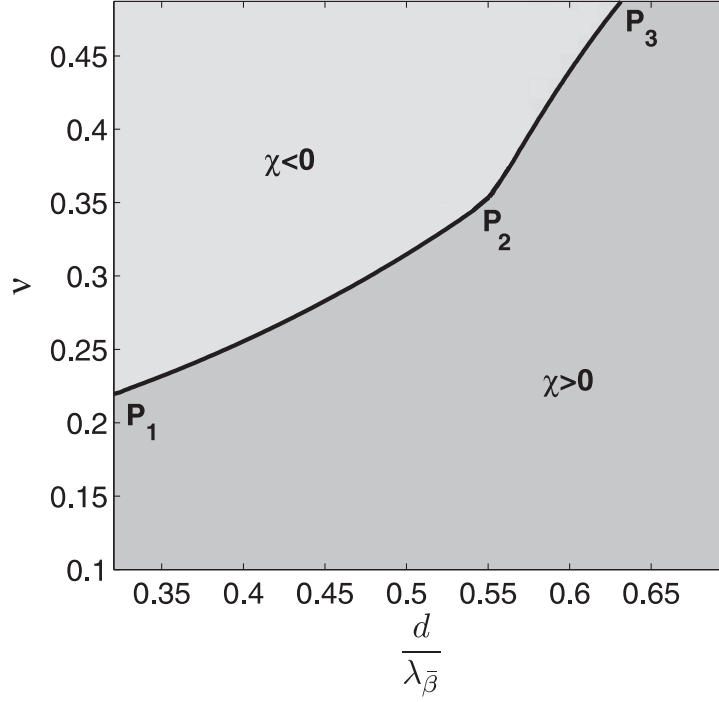


Figure 2.9: The ellipticity for the model inhomogeneous layer with fixed bottom in dependence of frequency and Poisson's ratio: retrograde motion (dark gray) and prograde motion (light gray)

The displacement amplitudes are normalized with respect to the vertical surface displacement amplitude by introducing

$$\hat{U}_1(\xi) = \frac{\hat{u}_1(\xi)}{\hat{u}_3(H_0)} = \frac{\hat{u}_1^{(1)}(\xi) + l_1 \hat{u}_1^{(2)}(\xi) + l_2 \hat{u}_1^{(3)}(\xi) + l_3 \hat{u}_1^{(4)}(\xi)}{\hat{u}_3^{(1)}(H_0) + l_1 \hat{u}_3^{(2)}(H_0) + l_2 \hat{u}_3^{(3)}(H_0) + l_3 \hat{u}_3^{(4)}(H_0)}, \quad (2.98)$$

$$\hat{U}_3(\xi) = \frac{\hat{u}_3(\xi)}{\hat{u}_3(H_0)} = \frac{\hat{u}_3^{(1)}(\xi) + l_1 \hat{u}_3^{(2)}(\xi) + l_2 \hat{u}_3^{(3)}(\xi) + l_3 \hat{u}_3^{(4)}(\xi)}{\hat{u}_3^{(1)}(H_0) + l_1 \hat{u}_3^{(2)}(H_0) + l_2 \hat{u}_3^{(3)}(H_0) + l_3 \hat{u}_3^{(4)}(H_0)} \quad (2.99)$$

and the subsidiary depth co-ordinate ξ is transformed to

$$\frac{x_3}{d} = \frac{\ln H_0 - \ln \xi}{\ln H_0 - \ln H_1} \quad (2.100)$$

where H_0 and H_1 are expressed in (2.66) and (2.67). So, for given values of the inhomogeneity parameter H_0, H_1 and the Poisson's ratio ν , the variation of the amplitude attenuation with the depth-to-thickness ratio may be computed at any frequency \bar{f} . Figure 2.7 illustrates the dependence of $\hat{U}_1(x_3/d)$ and $\hat{U}_3(x_3/d)$ on frequency and wave mode for given values of H_0, H_1 and ν . Several effects should be highlighted. The fundamental mode shapes are similar to those of Rayleigh waves in a homogeneous half-space with high frequency. The vertical displacement component \hat{u}_3 is node-free, whereas the horizontal component \hat{u}_1 has one node at $x_3 \approx 0.2 d$. This can be explained by the fact that the penetration depth of the

wave is about 1.5 times the wavelength in the model “a half-space”, so with a sufficiently high frequency or short wavelength, as long as the thickness of the layer is greater than one and a half times the wavelength, our model can be considered as a half-space. With small frequencies, it is quite different: for example, with $\bar{f} = 0.4$, at the surface both components have the same sign, which means the particle motion is retrograde when $\nu = 0.2$, but it changes to prograde motion when $\nu = 0.3525$ and $\nu = 0.43$.

2.2.3 H/V -ratio

The ellipticity of the particle motion on the surface is

$$\chi = \frac{\hat{u}_1(H_0)}{\hat{u}_3(H_0)}. \quad (2.101)$$

Figure 2.8 illustrates H/V curves with different Poisson’s ratios $\nu = 0.2, 0.3225, 0.43$. The main features of the H/V curve shown in this figure deserve mention. The H/V of the fundamental mode starts from its cut-off frequency $\bar{f} \approx 0.33$ and reaches a very large value. In the homogeneous case, this cut-off frequency is always $\bar{f} = 0.25$, and H/V is infinite at this frequency. When Poisson’s ratio is small, $\nu = 0.2$, the H/V does not change its sign, and remains positive. That means both displacement components on the surface are of the same sign, and since they are 90° out of phase the motions of the particles are retrograde ellipses. When Poisson’s ratio is increasing but less than 0.3525 , $\nu = 0.35$, H/V has a singularity. The value of Poisson’s ratio $\nu = 0.3525$ corresponds to the special case which is closely connected with a so-called osculation point of dispersion curves for the fundamental mode and first higher mode, respectively. When $\nu = 0.43$, H/V has a zero point.

As for the homogeneous case, we plot a 2D graph of χ as a function of \bar{f} and ν (Fig. 2.9). It displays a partitioning into two regions, where $\chi > 0$ corresponds to retrograde particle motion (dark shading) and $\chi < 0$ to prograde particle motion (light shading).

Three special points P_1 , P_2 and P_3 are similar to those in figure 2.3 for the homogeneous case, but their coordinates are different due to the inhomogeneous effects. The point P_1 with coordinates $(0.32, 0.22)$ bounds the domain of prograde motion on the left. The value $\bar{f} \approx 0.32$ is the maximum cut-off frequency of the fundamental mode with respect to ν , and $\nu \approx 0.22$ is a critical value of ν where the H/V -ratio begins to show prograde particle motion. In the homogeneous layer, this critical value is $\nu = 0.2026$. The point P_3 with coordinates $(0.63, 0.5)$ is the upper bound of the region of prograde motion. The prograde frequency ranges from P_1 to P_3 and the frequency of P_3 is approximately double the frequency of P_1 . This characteristic is already known from the homogeneous model.

2.3 Conclusions

The model “layer with fixed bottom” is a special case of the model “layer over half-space” which is closer to the actual structure when the impedance contrast is very large. For this model, the dispersion equation and the H/V ratio are relatively simple: they depend only on the Poisson’s ratio of the layer and do not depend on the density of mass. There are some outstanding features of this model which can be used for more general models. First,

a singularity of the H/V ratio curve exists if and only if Poisson's ratio of the layer ν is greater than 0.2026. The zero points start to appear when ν is greater than 0.25. The frequency region of the particle prograde motion can be bounded by two singularities, or by one singularity and one zero point. It is always bounded by a pole with a frequency $\bar{f} = 0.25$ and a either another pole or a zero-point for which the frequency is at most $\bar{f} = 0.5126$. These two values of the lower-bound and upper-bound frequencies define the maximum region of the prograde motion which will be shown in the next chapter for the model "layer over half-space". The retrograde motion always occurs at frequencies above $\bar{f} = 0.5126$, and for this model there is no undamped surface-wave motion for frequencies below $\bar{f} = 0.25$. This is a special feature of the fixed bottom model.

Because the Poisson's ratio of the layer is the only parameter affecting the H/V ratio, it controls the broad band of frequency for the prograde motion by a simple function of ν as in (2.49) and (2.50). At the special value of $\nu = 0.25$, where the osculation point of the phase velocity curve occurs, the property of H/V ratio changes from having two singularities to having one singularity, at $\bar{f} = 0.25$, and one zero point. Numerical calculation yields only one osculation point for the fundamental mode but many for the higher modes. In the last chapter, we prove that the osculation point of higher modes is at least countable and the Poisson's ratio corresponding to them is dense in $(0, 1/3)$.

For the inhomogeneous layer in which the shear modulus is expressed as an exponential function in (2.54), we show that the behaviour of the H/V ratio curve is quite similar to the homogeneous case. We also show that by changing the parameters in (2.54), we can get many forms of the shear modulus varying from the linear form to more complex forms. By working on a particular form, we observe that, although the fundamental mode has a cut-off frequency, both the phase velocity and H/V ratio at this frequency are finite, not infinite as for the homogeneous case. Prograde motion exists when Poisson's ratio is greater than ν_0 , which is a little greater than 0.2026. This may be an effect of the inhomogeneity.

Chapter 3

Layer over half-space (LOH)

The model "layer over half-space" is a model which approximates reality. The geometry is shown as in Fig. 3.1 and we use label 1 for the parameters of the layer and label 2 for the half-space. All the parameters in half-space are constant, but the parameters in the layer may not be. We will study the cases of both the homogeneous and the inhomogeneous layer.

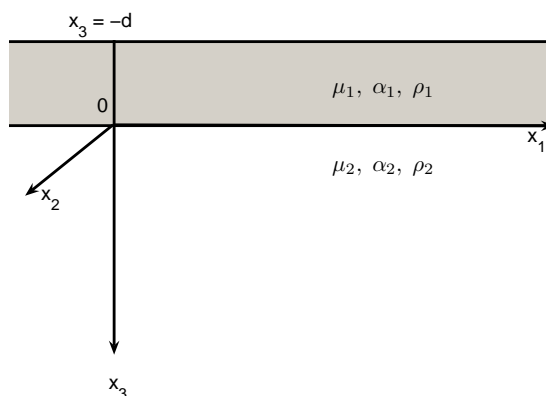


Figure 3.1: Homogeneous layer over half-space

3.1 Homogeneous layer

3.1.1 The eigen-value problem

The dispersion equation of Rayleigh waves for the LOH model is already presented in several books such as Ben-Menahem and Singh (1981) [6], but I formulate it again here in order to derive new H/V ratio formulas. These new formulas are in nature identical to Malischewsky's formula [35] but they are much more convenient for investigating H/V ratio properties.

	Model 1	Model 2	Model 3
$r_s = \beta_1/\beta_2$	0.1667	0.1667	0.2473
$r_d = \rho_1/\rho_2$	0.7406	0.7406	0.7391
ν_1	0.4375	0.5	0.4576
ν_2	0.2506	0.5	0.3449

Table 3.1: Parameters for models under consideration

We choose the expressions of complex amplitudes of potentials in the layer as

$$\begin{aligned}\varphi &= \Phi(x_3) \exp[i(kx_1 - \omega t)] , \\ \psi &= \Psi(x_3) \exp[i(kx_1 - \omega t)]\end{aligned}$$

and the solution of $\Phi(x_3)$ and $\Psi(x_3)$ which satisfies the motion equation can be expressed as

$$\begin{aligned}\Phi(x_3) &= A_1 \sinh(p_1 x_3) + A_2 \cosh(p_1 x_3) , \\ \Psi(x_3) &= A_3 \sinh(q_1 x_3) + A_4 \cosh(q_1 x_3)\end{aligned}$$

where

$$p_1^2 = k^2 - \frac{\omega^2}{\alpha_1^2} = k^2 \left(1 - \frac{c^2}{\alpha^2}\right), \quad q_1^2 = k^2 - \frac{\omega^2}{\beta_1^2} = k^2 \left(1 - \frac{c^2}{\beta^2}\right). \quad (3.1)$$

The displacements of the layer are determined by the scalar and vector potentials φ and ψ as in relation (1.7) (Chapter 1) as

$$\begin{aligned}u_1^{(1)} &= U_1^{(1)}(x_3) \exp[i(kx_1 - \omega t)] , \\ u_3^{(1)} &= U_3^{(1)}(x_3) \exp[i(kx_1 - \omega t)]\end{aligned}$$

with

$$U_1(x_3) = ik\Phi - \frac{d\Psi}{dx_3} , \quad (3.2)$$

$$U_3(x_3) = \frac{d\Phi}{dx_3} + ik\Psi . \quad (3.3)$$

The stresses are derived from displacements by Hooke's law:

$$\begin{aligned}\tau_{13}^{(1)} &= S_{13}^{(1)}(x_3) \exp[i(kx_1 - \omega t)] \\ \tau_{33}^{(1)} &= S_{33}^{(1)}(x_3) \exp[i(kx_1 - \omega t)]\end{aligned}$$

with

$$\begin{aligned}S_{31}^{(1)} &= \rho_1 \beta_1^2 \left[\frac{dU_1^{(1)}}{dx_3} + ikU_3^{(1)} \right] , \\ S_{33}^{(1)} &= \rho_1 \alpha_1^2 \left[\frac{dU_3^{(1)}}{dx_3} + ik(1 - 2\gamma_1)U_1^{(1)} \right] .\end{aligned}$$

In half-space, similar to model half-space, we choose the displacement forms as

$$\begin{aligned} U_1^{(2)} &= -i [B_1 e^{-p_2 x_3} + B_2 e^{-q_2 x_3}] \\ U_3^{(2)} &= B_1 \frac{p_2}{k} e^{-p_2 x_3} + B_2 \frac{k}{q_2} e^{-q_2 x_3} \end{aligned}$$

and stresses

$$\begin{aligned} S_{31}^{(2)} &= \rho_2 \beta_2^2 \left[\frac{dU_1^{(2)}}{dx_3} + ik U_3^{(2)} \right], \\ S_{33}^{(2)} &= \rho_2 \alpha_2^2 \left[\frac{dU_3^{(2)}}{dx_3} + ik(1 - 2\gamma_2) U_1^{(2)} \right]. \end{aligned}$$

Boundary conditions at the free surface of the layer and at the interface between the layer and the half-space are

$$\tau_{31}(-d) = \tau_{33}(-d) = 0 \quad (3.4)$$

for the free-surface condition and

$$\begin{aligned} U_1^{(1)}(0) &= U_1^{(2)}(0), \\ U_3^{(1)}(0) &= U_3^{(2)}(0), \\ S_{13}^{(1)}(0) &= S_{13}^{(2)}(0), \\ S_{33}^{(1)}(0) &= S_{33}^{(2)}(0), \end{aligned} \quad (3.5)$$

for the continuous displacements and stresses at the interface. Substituting formulas for displacement and stresses in the layer and half-space into six boundary conditions (3.4)-(3.5), we obtain a homogeneous system of six equations with respect to the six integral constants A_1, A_2, A_3, A_4 and B_1, B_2 as

$$[M] \cdot [v] = 0 \quad (3.6)$$

with

$$[M] = \begin{bmatrix} 2ie_\alpha \cosh(e_\alpha dk) & -2ie_\alpha \sinh(e_\alpha dk) & h_1 \sinh(e_\beta dk) & -h_1 \cosh(e_\beta dk) & 0 & 0 \\ -h_1 \sinh(e_\alpha dk) & h_1 \cosh(e_\alpha dk) & 2ie_\beta \cosh(e_\beta dk) & -2ie_\beta \sinh(e_\beta dk) & 0 & 0 \\ 0 & k & ie_\beta k & 0 & 1 & 1 \\ e_\alpha g_\beta k & 0 & 0 & ig_\beta k & -g_\beta g_\alpha & -1 \\ 2ie_\alpha g_\beta k & 0 & 0 & h_1 g_\beta k & -2if_1 g_\beta g_\alpha & -if_1 h_2 \\ 0 & h_1 k & 2ie_\beta k & 0 & f_1 h_2 & 2f_1 \end{bmatrix} \quad (3.7)$$

and

$$[v] = [A_1, A_2, A_3, A_4, B_1, B_2]'. \quad (3.8)$$

Setting the determinant of the matrix $[M]$ to zero results in the secular equation

$$\Delta(C, \bar{f}) = 0 \quad (3.9)$$

with

$$\begin{aligned} \Delta(C, \bar{f}) = & A_0(C) + B_0(C) \sinh\left(\frac{2\pi\bar{f}e_\beta}{C}\right) \sinh\left(\frac{2\pi\bar{f}e_\alpha}{C}\right) + C_0(C) \sinh\left(\frac{2\pi\bar{f}e_\alpha}{C}\right) \cosh\left(\frac{2\pi\bar{f}e_\beta}{C}\right) \\ & + D_0(C) \cosh\left(\frac{2\pi\bar{f}e_\alpha}{C}\right) \sinh\left(\frac{2\pi\bar{f}e_\beta}{C}\right) + E_0(C) \cosh\left(\frac{2\pi\bar{f}e_\beta}{C}\right) \cosh\left(\frac{2\pi\bar{f}e_\alpha}{C}\right) \end{aligned} \quad (3.10)$$

where the auxiliary functions are

$$\begin{aligned} A_0(C) &= 4\beta_1 h_1 [2(-1 + \beta_2)h_1 - f_1(2 + h_1)(2\beta_2 - h_2) + f_1^2(4\beta_2 - h_2^2)] , \\ B_0(C) &= 4\beta_1^2 [4(-1 + f_1)^2\beta_2 - (-2 + f_1 h_2)^2] \\ &\quad h_1^2 [(-1 + \beta_2)h_1^2 - 2h_1 f_1(2\beta_2 - h_2) + f_1^2(4\beta_2 - h_2^2)] , \\ C_0(C) &= e_\beta f_1 \beta_3 C^4 r_s^2 , \\ D_0(C) &= e_\alpha f_1 \beta_4 C^4 r_s^2 , \\ E_0(C) &= -A_0(C) - \beta_1 f_1^2(4\beta_2 - h_2^2)C^4 \end{aligned} \quad (3.11)$$

with these notations:

$$\begin{aligned} C &= \frac{c}{\beta_1}, \quad \bar{f} = \frac{df}{\lambda_{\beta_1}}, \quad e_\alpha = \sqrt{1 - C^2 \gamma_1}, \quad e_\beta = \sqrt{1 - C^2}, \\ g_\alpha &= \sqrt{1 - C^2 \gamma_2 r_s^2}, \quad g_\beta = \sqrt{1 - C^2 r_s^2}, \\ h_1 &= e_\beta^2 + 1, \quad h_2 = g_\beta^2 + 1, \quad f_1 = \frac{1}{r_s^2 r_d}, \\ \beta_1 &= e_\alpha e_\beta, \quad \beta_2 = g_\alpha g_\beta, \\ \beta_3 &= -4e_\alpha^2 g_\beta + g_\alpha h_1^2, \quad \beta_4 = -e_\beta^2 g_\alpha + g_\beta h_1^2. \end{aligned}$$

For the real solution of (3.9), the phase velocity c must be less than β_2 , which is the shear wave velocity of the substrate. If $c > \beta_2$, it causes either $A_0(C)$ or $C_0(C)$, $D_0(C)$ to become a complex number and in this case, the solution of (3.9) can not be a real number.

3.1.2 Dispersion of zero-frequency Rayleigh waves

Surface acoustic waves (SAW) play an important role in the study of the elastic properties of thin films, which have a huge number of applications in modern industry (see e. g. the monograph of Kundu [28]). The same is true for the larger-scale investigation of the Earth's interior by seismic surface waves. Like the properties of a thin layer deposited on a substrate, it is well known that the properties of the Earth's crust have a strong influence the dispersion characteristics of Rayleigh waves. A deeper theoretical analysis of the dispersion of Rayleigh waves also implies the investigation of the derivative of the phase velocity with respect to frequency for zero frequency. This is of considerable practical interest because the value of the derivative at zero frequency controls the character of dispersion: normal, anomalous or zero dispersion. Several papers have been devoted to the approximation of the influence of a

thin layer on the dispersion of Rayleigh waves. Tiersten [54] for example, introduced special boundary conditions in order to obtain a low-frequency approximation, while B6vik [12] used a perturbation technique in which the field variables were expanded in the layer thickness in the normal direction. This procedure leads to so-called $O(h)$ boundary conditions, where h stands for the layer thickness. Recently, Baron et al. [5] published a general expression for the derivative of the phase velocity at zero frequency by expanding the secular determinant into a Taylor series. This expression goes back to a similar formula of Shuvalov and Every [52]. These formulae are very general but not very convenient for practical use in the laboratory where we sometimes need to quickly determine the phase velocity's derivative in dependence on elastic parameters. Here, we fill this gap by presenting a simple analytical formula for that derivative for the Rayleigh-wave fundamental mode.

When frequency equals zero, or $\bar{f} = 0$, the secular equation becomes

$$\Delta(C, 0) = A_0(C) + E_0(C) = 0. \quad (3.12)$$

Substituting $A_0(C)$ and $E_0(C)$ from (3.11) into (3.12) yields

$$h_2^2 - 4g_\alpha g_\beta = 0, \quad (3.13)$$

or

$$(\bar{C}^2 - 2)^2 - 4\sqrt{1 - \bar{C}^2}\sqrt{1 - \gamma_2\bar{C}^2} = 0 \quad (3.14)$$

where

$$\bar{C} = \frac{c}{\beta_2} \quad (3.15)$$

and its relation to C is $\bar{C} = Cr_s$. From now on, in this section, we will use \bar{C} instead of C as usual. Eq. (3.14) is the Rayleigh wave equation for the model “half-space”, so at zero frequency, the phase velocity is the Rayleigh wave velocity of the half-space.

The Taylor expansion of (3.9) into powers of \bar{f} for $\bar{f} = 0$ is:

$$\Delta(\bar{C}, \bar{f}) = A_0(\bar{C}) + A_1(\bar{C})\bar{f} + Q_2(\bar{C})\bar{f}^2 + o(\bar{f}^3) = 0 \quad (3.16)$$

where

$$\begin{aligned} A_0(\bar{C}) &= (\bar{C}^2 - 2)^2 - 4\sqrt{1 - \bar{C}^2}\sqrt{1 - \gamma_2\bar{C}^2}, \\ A_1(\bar{C}) &= 2r_s r_d \pi \bar{C} \left[\bar{C}^2(\sqrt{1 - \bar{C}^2} + \sqrt{1 - \gamma_2\bar{C}^2}) + 4r_s^2(\gamma_1 - 1)\sqrt{1 - \bar{C}^2} \right], \\ A_2(\bar{C}) &= 4r_s^2 r_d^2 \pi^2 (\sqrt{1 - \bar{C}^2}\sqrt{1 - \gamma_2\bar{C}^2} - 1) [\bar{C}^2 + 4r_s^2(\gamma_1 - 1)], \\ P_2(\bar{C}) &= A_2(\bar{C}) + 8\pi^2 r_s^2 r_d (2\sqrt{1 - \bar{C}^2}\sqrt{1 - \gamma_2\bar{C}^2} + \bar{C}^2 - 2) \left(2\frac{r_s^2(1 - \gamma_1)}{\bar{C}^2} - \gamma_1 \right), \\ Q_2(\bar{C}) &= P_2(\bar{C}) - 2A_0(\bar{C})\pi^2 \left(1 + \gamma_1 + 4r_s^2 \frac{\gamma_1 - 1}{\bar{C}^2} \right), \end{aligned} \quad (3.17)$$

$$\gamma_1 = \frac{1 - 2\nu_1}{2(1 - \nu_1)} .$$

In the section “The impedance wave”, we determined the secular equation of the impedance wave by the Tiersten boundary condition to be

$$A_0(\bar{C}) + A_1(\bar{C})\bar{f} + A_2(\bar{C})\bar{f}^2 = 0 . \quad (3.18)$$

Bövik [12] proposed what he called the $O(h)$ boundary conditions, where h is the thickness of the layer, and derived another form of the secular equation:

$$A_0(\bar{C}) + A_1(\bar{C})\bar{f} + P_2(\bar{C})\bar{f}^2 = 0 . \quad (3.19)$$

The secular equation of Rayleigh waves for a layer over half-space is a function of two variables: phase velocity \bar{C} and frequency \bar{f} , so the derivative of this function at $\bar{f} = 0$ is

$$\left(\frac{d\bar{C}}{d\bar{f}} \right)_{\bar{f}=0} = - \frac{\partial \Delta}{\partial \bar{f}} / \frac{\partial \Delta}{\partial \bar{C}} \Big|_{\bar{C}=\bar{C}(0)} . \quad (3.20)$$

By using the Taylor expansion of $\Delta(\bar{C}, \bar{f})$ as in (3.16), we obtain

$$\left(\frac{d\bar{C}}{d\bar{f}} \right)_{\bar{f}=0} = - \frac{A_1(\bar{C})}{\frac{dA_0(\bar{C})}{d\bar{C}}} \Big|_{\bar{C}=\bar{C}(0)} \quad (3.21)$$

where $\bar{C}(0)$ refers to the Rayleigh-wave velocity for the zero-frequency, which is identical to the velocity of the half-space. Only $A_0(\bar{C})$ and $A_1(\bar{C})$ appear in (3.21), so all three approximations of the secular equations from Tiersten, Bövik and the Taylor expansion give the same result for the first derivative of the phase velocity curve at zero frequency. Using (3.17), the derivative of the phase velocity is finally obtained as

$$\frac{d\bar{C}}{d\bar{f}} \Big|_{\bar{f}=0} = \frac{1}{2} \pi r_d (1-x)^{3/2} (x-2)^2 \frac{K_1(r_s, \nu_1, \nu_2)}{K_2(\nu_2)} \quad (3.22)$$

where $r_s = \beta_1/\beta_2$ is the ratio of the shear-wave velocities in the layer and the half-space, respectively, and $r_d = \rho_1/\rho_2$ is the corresponding density ratio. The Poisson ratios of the layer and the half-space are ν_1 and ν_2 , respectively. The entity x , defined by $x = c_2^2/\beta_2^2$, refers to the Rayleigh-wave velocity of the half-space c_2 , which is identical with c for $\bar{f} = 0$. Clearly x is a function of ν_2 alone, and Malischewsky’s formula for half-space velocity (see Malischewsky [34]) can be profitably used for its determination:

$$x(\nu_2) = \frac{2}{3} \left[3 - \sqrt[3]{h_3(\gamma_2)} + \frac{2(1-6\gamma_2)}{\sqrt[3]{h_3(\gamma_2)}} \right] \quad (3.23)$$

where $\gamma_2 = \frac{1-2\nu_2}{2(1-\nu_2)}$ and with the auxiliary functions

$$\begin{aligned} h_1(\gamma_2) &= 3\sqrt{33 - 186\gamma_2 + 321\gamma_2^2 - 192\gamma_2^3} , \\ h_3(\gamma_2) &= 17 - 45\gamma_2 + h_1(\gamma_2) . \end{aligned} \quad (3.24)$$

In the formula (3.23), the main value of the cubic roots are to be used. Alternatively, x can be determined by using Malischewsky's approximation (see Pham Chi Vinh and Malischewsky [48]), which is also valid for auxetic materials with negative Poisson ratios [like the exact formula (3.23)]:

$$x(\nu_2) = 0.874 + 0.196 \nu_2 - 0.043 \nu_2^2 - 0.055 \nu_2^3 . \quad (3.25)$$

Finally, the functions K_1 and K_2 are given by:

$$K_1(r_s, \nu_1, \nu_2) = \frac{8r_1^2}{\nu_1 - 1} + \frac{8x - 8x^2 + x^3}{1 - x} , \quad (3.26)$$

$$K_2(\nu_2) = \frac{8(1 - x^2)}{1 - \nu_2} - 16x + 32x^2 - 20x^3 + 3x^4 \quad (3.27)$$

and the derivation of the phase velocity for the zero frequency can be simply determined by combining (3.26) - (3.27). It can be demonstrated after some algebra that our formula (3.22) is identical with the formula of Baron et al. [5] up to a factor 2, which must be a misprint. It should be noted that our formula is implicitly contained in the formulae of Tiersten [54] and B6vik [12] as well. For completeness, we specify the quadratic term Q_2 in expansion (3.16), which is closely connected to the second derivative of the phase velocity

$$\bar{C}''(\bar{f})|_{\bar{f}=0} = - \frac{2Q_2 + 2 \frac{dA_1}{dC} \bar{C}'(\bar{f}) + \frac{d^2(A_0)}{dC^2} \bar{C}'^2(F)}{\frac{dA_0}{dC}} . \quad (3.28)$$

The quadratic dispersion has been calculated by Shuvalov and Every [52]; however, the generality of their result does not permit a simple comparison with our explicit formula. The formula of the second derivative shows the difference among Tiersten, B6vik and our Taylor expansion secular equations in the quadratic terms A_2 , P_2 and Q_2 .

Classification of dispersion at zero frequency

It is interesting to know whether the dispersion curve starts at zero frequency with normal, anomalous or zero dispersion in dependence on material parameters. This can be simply tested by setting the derivative to zero. From (3.22) we see that we have to search for roots of $K_1 = 0$, which leads with (3.26) to

$$\frac{r_s^2}{\nu_1 - 1} + g(\nu_2) = 0 \quad (3.29)$$

where the auxiliary function g is given by

$$g(\nu_2) = \frac{1}{8} \frac{8x - 8x^2 + x^3}{1 - x} . \quad (3.30)$$

	$M1$	$M2$	$M3$
ν_1	0.25	0.3925	0.47
ν_2	0.25	0.25	0.25
r_s	0.75	0.9	0.9
r_d	0.4208	0.4208	0.4208
$\frac{d\bar{C}}{d\bar{f}} \Big _{\bar{f}=0}$	-0.1970	0	0.0790

Table 3.2: Model parameters for the models M_1 , M_2 , M_3 with the derivatives of \bar{C} for $\bar{f} = 0$

Further, we observe that $K_2(\nu_2)$ is negative for all ν_2 . It follows that the classification of dispersion for zero-frequency can be written as

$$\begin{aligned}
\frac{r_s^2}{\nu_1 - 1} + g(\nu_2) &> 0 && \rightarrow \text{normal dispersion ,} \\
\frac{r_s^2}{\nu_1 - 1} + g(\nu_2) &< 0 && \rightarrow \text{anomalous dispersion ,} \\
\frac{r_s^2}{\nu_1 - 1} + g(\nu_2) &= 0 && \rightarrow \text{zero dispersion .}
\end{aligned} \tag{3.31}$$

We observe that this classification depends on the shear-wave contrast and the Poisson ratios, but not on the density contrast.

Graphic representation

In order to demonstrate the influence of the different parameters, we have constructed isolines $K_1 = 0$ for $\nu_2 = -1, 0, 0.25, 0.4$ and present them in dependence on ν_1 and r_s in Fig. 3.2. The regions left and right from the corresponding isolines belong to normal dispersion and anomalous dispersion, respectively. The position of three models with different dispersion at zero frequency M_1 (normal), M_2 (zero), M_3 (anomalous) is indicated in Fig. 3.2. The model parameters are given in Table 3.1.2.

Fig. 3.2 shows that for $\nu_2 = 0.25$ anomalous dispersion is only possible in the right upper corner of the graphic, i. e. for higher values of r_s and ν_1 . Higher values of r_s denote a small shear-wave contrast between layer and half-space. If the half-space is auxetic with a negative Poisson ratio, the range of anomalous dispersion becomes much greater. Finally, Fig. 3.3 presents the dispersion curves in the vicinity of the zero frequency belonging to the models M_1 , M_2 , M_3 .

In Fig. 3.4 we compare Tiersten, B6vik and our Taylor expansion phase velocity curves with the exact curve in the small range of frequency for the two models M_1 and M_3 . Although all the curves have the same slope at $\bar{f} = 0$, the Tiersten curve shows a good approximation in a very small range of frequency, and the B6vik curve and Taylor expansion show better approximations in a larger range of frequencies. This difference is due to the effect of the second derivatives which are controlled by the quadratic terms A_2 , P_2 and Q_2 .

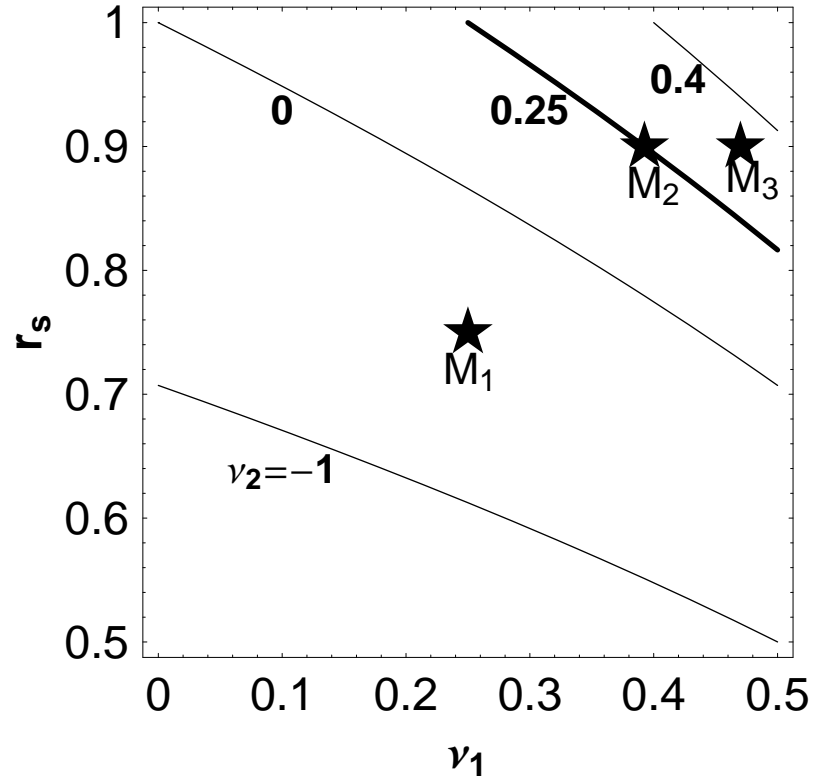


Figure 3.2: Isolines $K_1 = 0$ in dependence on ν_1 and r_s for different values of ν_2 . The position of three example models M_1 , M_2 , M_3 is indicated by stars.

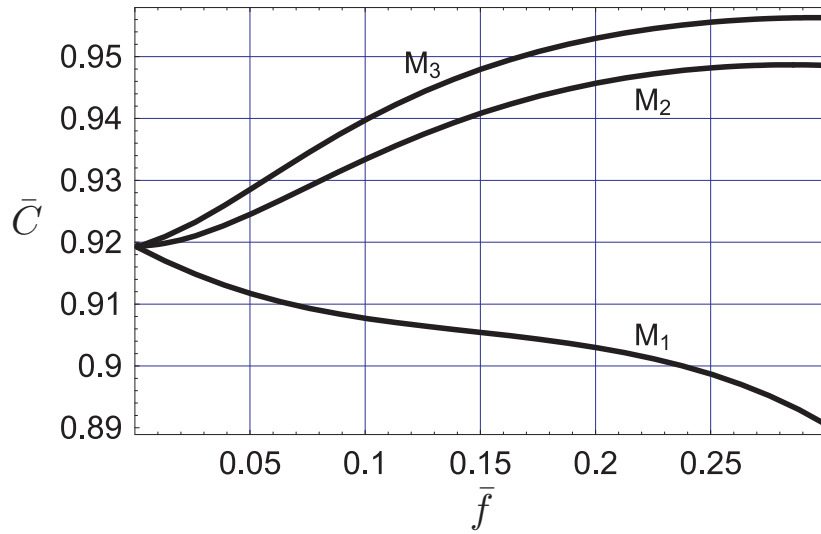


Figure 3.3: Dispersion curves $\bar{C}(\bar{f}) = c(\bar{f})/\beta_2$ for the models M_1 , M_2 , M_3

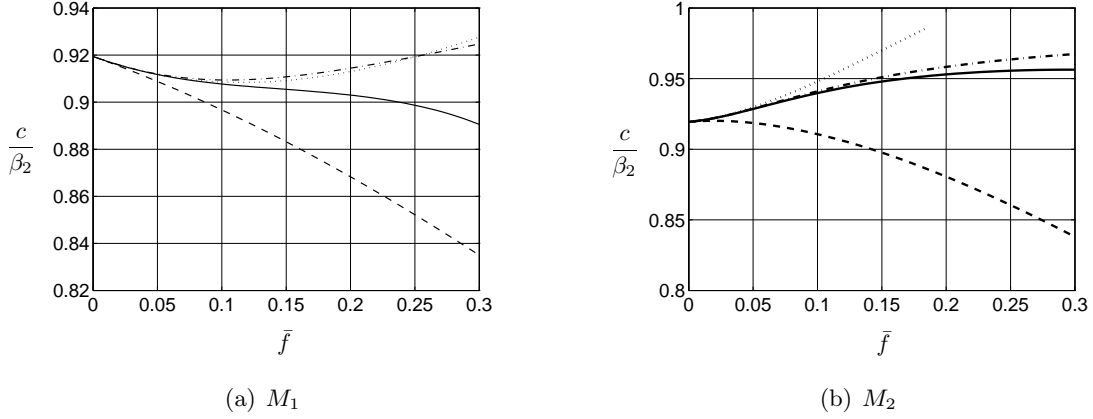


Figure 3.4: Dispersion curves $\bar{C}(\bar{f}) = c(\bar{f})/\beta_2$ for the models M_1 , M_2 : Exact (continuous), Tiersten (dash), Bövik (dot) and Taylor expansion (dash-dot)

Application for synthetic data

It is an experimental challenge to obtain phase velocities for very low frequencies. In order to confirm our theoretical results, we present here a comparison using synthetic data for a two-layer model. These data were obtained by generating a stationary stochastic wave field similar to those which are routinely used in applying ambient vibration/microtremor methods [see e. g. Wathelet et al. (2008) [60]]. The model parameters are $\beta_1 = 150$ m/s, $\rho_1 = 1.5$ g/cm³ and thickness $d = 15$ m for the layer and $\beta_2 = 350$ m/s and $\rho_2 = 2$ g/cm³ for the half-space. Poisson's ratio is about 0.25 for the layer and the half-space as well. The synthetic data were analyzed by f-k analysis [see e. g. Capon (1969) [13]] and with the Spatial Autocorrelation Method (SPAC) [see e. g. Aki (1957) [2]]. The slowness for the data as a function of frequency is presented in Fig. 3.5 together with the exact dispersion curve and our approximation. We observe a good coincidence up to 2.2 Hz.

Variation of first derivative to other parameters

Each parameters has a certain effect on the derivative of the phase velocity with respect to frequency for zero frequency, so it can affect on phase velocity curve state at zero frequency. We have

$$\left. \frac{d^2 \bar{C}}{d\bar{f} dr_s} \right|_{\bar{f}=0} = \frac{1}{2} \frac{\pi r_2 (1-x)^{3/2} (x-2)^2}{K_2(\nu_2)} \frac{dK_1}{dr_s} = 8\pi r_d r_s \frac{(1-x)^{3/2} (x-2)^2}{K_2(\nu_2)} \frac{1}{\nu_1 - 1} > 0 \quad (3.32)$$

and because $K_2(\nu_2) < 0$ for every value of ν_2 and $\nu_1 - 1 < 0$, $\left. \frac{d^2 \bar{C}}{d\bar{f} dr_s} \right|_{\bar{f}=0}$ is always positive.

By analogy, we have that

$$\left. \frac{d^2 \bar{C}}{d\bar{f} d\nu_1} \right|_{\bar{f}=0} = \frac{1}{2} \frac{\pi r_2 (1-x)^{3/2} (x-2)^2}{K_2(\nu_2)} \frac{dK_1}{d\nu_1} = 4\pi r_d r_s^2 \frac{(1-x)^{3/2} (x-2)^2}{-K_2(\nu_2)} \frac{1}{(\nu_1 - 1)^2} > 0. \quad (3.33)$$

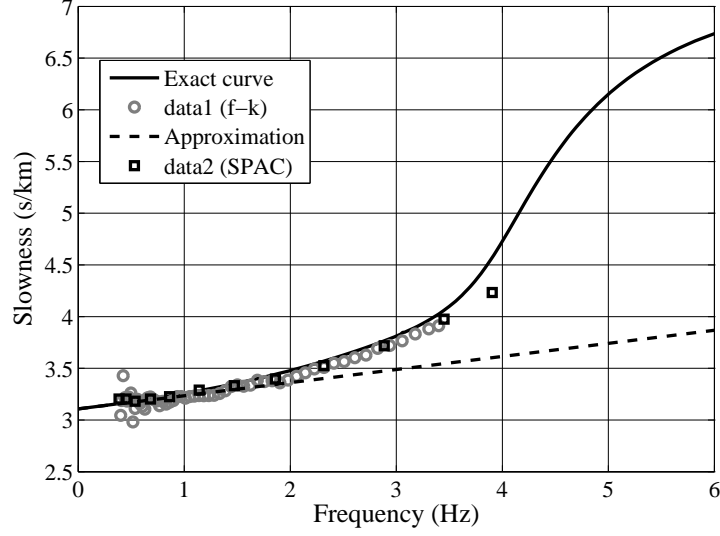


Figure 3.5: Dispersion analysis of synthetic data for a two-layer model with f-k (data1) and SPAC (data2). Comparison with the exact dispersion curve (solid) and the approximation (dashed)

We can easily see that $\left. \frac{d^2 \bar{C}}{df d\nu_1} \right|_{\bar{f}=0}$ is always greater than 0. Thus $\left. \frac{d\bar{C}}{df} \right|_{\bar{f}=0}$ is an increasing function of ν_1 and r_s or the slope of the phase velocity curve at $\bar{f} = 0$ increases with increment of ν_1 or decrement of impedance contrast.

Although ν_2 and r_d do not play important roles in the behavior of the phase velocity curve, by numerical calculation we can show that the condition for $\left. \frac{d^2 \bar{C}}{df d\nu_2} \right|_{\bar{f}=0} > 0$ with all possible parameters is $r_s < 0.2931$. In practical usage, we often choose r_s satisfying this condition.

3.1.3 Displacements

Suppose that the eigenvalue is found. From (3.2) and (3.3) we have the displacement amplitudes of the layer and the half-space, which are

$$U_1^{(1)}(x_3) = ik [A_1 \sinh(p_1 x_3) + A_2 \cosh(p_1 x_3)] - q_1 [A_3 \cosh(q_1 x_3) + A_4 \sinh(q_1 x_3)] \quad (3.34)$$

$$U_3^{(1)}(x_3) = p_1 [A_1 \cosh(p_1 x_3) + A_2 \sinh(p_1 x_3)] + ik [A_3 \sinh(q_1 x_3) + A_4 \cosh(q_1 x_3)] \quad (3.35)$$

and

$$\begin{aligned} U_1^{(2)}(x_3) &= -i [B_1 e^{-p_2 x_3} + B_2 e^{-q_2 x_3}] , \\ U_3^{(2)}(x_3) &= B_1 \frac{p_2}{k} e^{-p_2 x_3} + B_2 \frac{k}{q_2} e^{-q_2 x_3} \end{aligned} \quad (3.36)$$

with p_1, q_1 and p_2, q_2 from (3.1), respectively. The displacement amplitudes are normalized with respect to the vertical surface displacement amplitude by introducing

$$\tilde{U}_1^{(1)}(x_3) = \frac{U_1^{(1)}(x_3)}{U_3^{(1)}(-d)}, \quad \tilde{U}_3^{(1)}(x_3) = \frac{U_3^{(1)}(x_3)}{U_3^{(1)}(-d)}, \quad (3.37)$$

$$\tilde{U}_1^{(2)}(x_3) = \frac{U_1^{(2)}(x_3)}{U_3^{(1)}(-d)}, \quad \tilde{U}_3^{(2)}(x_3) = \frac{U_3^{(2)}(x_3)}{U_3^{(1)}(-d)}. \quad (3.38)$$

Each normalized displacement amplitude is a function of the frequency and the depth. The detail of these functions are presented in Appendix 3.

3.1.4 H/V -ratio

The H/V -ratio is formulated as the ratio of horizontal to vertical displacement amplitudes at the surface

$$\chi = \frac{U_1^{(1)}(-d)}{U_3^{(1)}(-d)}. \quad (3.39)$$

In terms of the formula of $U_1^{(1)}(x_3)$ and $U_3^{(1)}(x_3)$ in (3.34) and (3.35) and the relation between the integral constants A_1, A_2, A_3, A_4 in (4.61), we can determine the H/V -ratio formula. Because the relation between A_1, A_2, A_3, A_4 can be obtained from five of six boundary conditions (4.61), we can have at least five different formulations of the H/V -ratio. We will use two formulae which are rather simple in appearance. The first one is

$$\chi_1 = \frac{h_1}{2e_\alpha} \frac{A(C)}{B(C)} \quad (3.40)$$

where

$$\begin{aligned} A(C) &= t_1 \sinh\left(\frac{2\pi\bar{f}e_\alpha}{C}\right) + t_2 \sinh\left(\frac{2\pi\bar{f}e_\beta}{C}\right) + t_3 \cosh\left(\frac{2\pi\bar{f}e_\alpha}{C}\right) - t_3 \cosh\left(\frac{2\pi\bar{f}e_\beta}{C}\right), \\ B(C) &= t_1 \cosh\left(\frac{2\pi\bar{f}e_\alpha}{C}\right) + t_2 t_4 \cosh\left(\frac{2\pi\bar{f}e_\beta}{C}\right) + t_3 \sinh\left(\frac{2\pi\bar{f}e_\alpha}{C}\right) - t_3 t_4 \sinh\left(\frac{2\pi\bar{f}e_\beta}{C}\right) \end{aligned} \quad (3.41)$$

with the auxiliary functions

$$\begin{aligned} t_1 &= (-4f_1g_\alpha g_\beta + 2g_\alpha g_\beta h_1 - h_1 h_2 + f_1 h_2^2)/e_\alpha, \\ t_2 &= 2e_\beta [4(-1 + f_1)g_\alpha g_\beta + h_2(2 - f_1 h_2)]/h_1, \\ t_3 &= 2g_\beta(-2 + h_2), \quad t_4 = \frac{h_1^2}{4e_\alpha e_\beta}. \end{aligned}$$

The second formula is

$$\chi_2 = \frac{M(C)}{N(C)} \quad (3.42)$$

where

$$\begin{aligned} M(C) &= h_1 k_1 \cosh\left(\frac{2\pi \bar{f} e_\alpha}{C}\right) + 2k_2 \cosh\left(\frac{2\pi \bar{f} e_\beta}{C}\right) - \frac{h_1}{e_\alpha} k_3 \sinh\left(\frac{2\pi \bar{f} e_\alpha}{C}\right) + 2e_\beta k_3 \sinh\left(\frac{2\pi \bar{f} e_\beta}{C}\right), \\ N(C) &= -2k_3 \cosh\left(\frac{2\pi \bar{f} e_\alpha}{C}\right) + h_1 k_3 \cosh\left(\frac{2\pi \bar{f} e_\beta}{C}\right) + 2e_\alpha k_1 \sinh\left(\frac{2\pi \bar{f} e_\alpha}{C}\right) + \frac{h_1}{e_\beta} k_2 \sinh\left(\frac{2\pi \bar{f} e_\beta}{C}\right) \end{aligned}$$

and

$$\begin{aligned} k_1 &= h_1 [2 + 2(-1 + f_1)g_\alpha g_\beta - f_1 h_2], \\ k_2 &= 2[-h_1 + (-2f_1 + h_1)g_\alpha g_\beta + f_1 h_2], \\ k_3 &= f_1 g_\alpha (-2 + h_2). \end{aligned}$$

In [35], Malischewsky and Schebaum published an H/V -ratio formula, and they used this formula to compare with a simple H/V -ratio formula from Love [30] for incompressible media. However, the formula of Malischewsky and Scherbaum is rather complicated in form and would not be suitable for us to study other properties of ellipticity.

The zero-frequency H/V ratio

When $\bar{f} = 0$, using formula (3.42) of H/V ratio we have

$$\chi_2|_{\bar{f}=0} = \frac{h_1 k_1 + 2k_2}{(h_1 - 2)k_3} \Big|_{C=C(0)} = - \frac{h_2 - 2g_\alpha g_\beta}{g_\alpha (h_2 - 2)} \Big|_{C=C(0)}. \quad (3.43)$$

Furthermore, $C(0)$ is a solution of Rayleigh equation, so we have

$$h_2^2 - 4g_\alpha g_\beta = 0$$

or $g_\alpha g_\beta = h_2^2/4$. Substituting $g_\alpha g_\beta$ into (3.43) we have

$$\chi_2|_{\bar{f}=0} = \frac{h_2}{2g_\alpha} \Big|_{C=C(0)} = \frac{2 - \bar{C}^2}{2\sqrt{1 - \bar{C}^2}\gamma_2} \Big|_{\bar{C}=\bar{C}(0)} \quad (3.44)$$

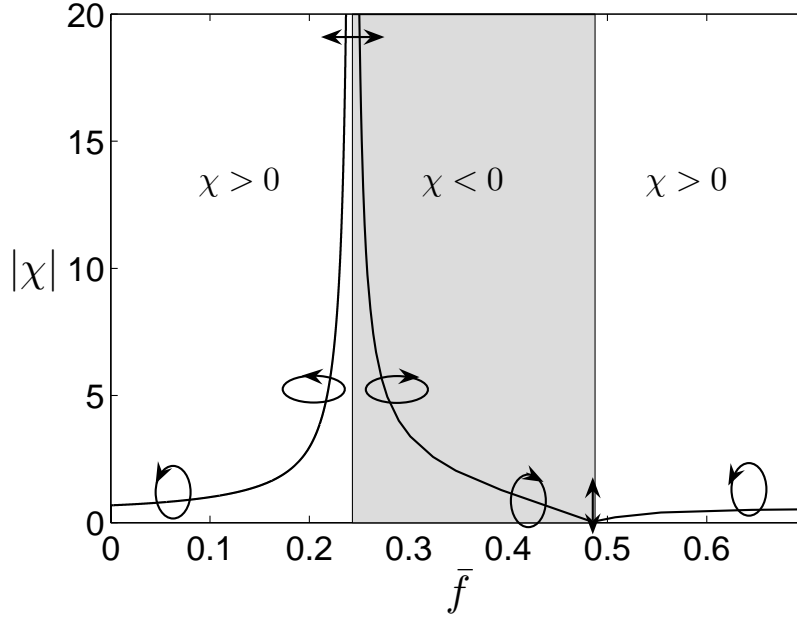
with $\bar{C} = Cr_s = c/\beta_2$ and because $\bar{C}(0)$ is Rayleigh wave of substrate, we have

$$(2 - \bar{C}^2)^2 = 4\sqrt{1 - \bar{C}^2}\sqrt{1 - \bar{C}^2}\gamma_2.$$

Substituting this equation into (3.45) we finally derive

$$\chi_2|_{\bar{f}=0} = 2 \frac{\sqrt{1 - \bar{C}^2}}{2 - \bar{C}^2} \Big|_{\bar{C}=\bar{C}(0)}. \quad (3.45)$$

This is the H/V ratio formula of the substrate.

Figure 3.6: H/V curve of Model 1 in Table 3

The first peak

A typical curve of the H/V ratio has a singularity and a zero point. Fig. 3.6 shows an H/V ratio curve with the parameters of Model 1 in Table 3. In this figure, the darker area corresponds to area in which the particle motion is prograde, the other to the area of retrograde motion. When $\bar{f} = 0$, the ellipticity is the ellipticity of the half-space and is positive. When $\bar{f} \approx 0.2434$ the H/V ratio reaches an infinite value, or the vertical motion vanishes. This causes the particle motion to change its direction to prograde, and when $\bar{f} \approx 0.4876$ the horizontal motion vanishes and the particle motion changes back to retrograde motion.

However, the H/V ratio curve does not always have a singularity or a zero point. In the model “layer with fixed bottom” which is a special case of the current model “layer over half-space”, we proved that its H/V ratio curve has singularity if the Poisson’s ratio ν is greater than 0.2026 and has zero point if ν greater than 0.25. The first singularity of the H/V ratio of LFB always occurs at $\bar{f} = 0.25$, if it exists. For model LOH the condition of existence of singularity and zero point is similar, but not identical to model LFB. With the extreme case when the impedance contrast is very high, $r_s \approx 0$, the condition of existence singularity and zero point of LOH comes back to the condition in LFB and the singularity occurs at the resonance frequency of the shear wave of the layer, $\bar{f} = 0.25$, while the zero point start to occur at $\bar{f} = \sqrt{3}/4$. But with higher r_s or moderate impedance contrast, the

condition of existence of singularity of LOH should be

$$r_s < F(\nu_1) \quad (3.46)$$

where

$$F(\nu_1) = A(\nu_2, r_d) \arctan [B(\nu_2, r_d)(\nu_1 - 0.2026)] \quad (3.47)$$

with the auxiliary functions

$$\begin{aligned} A(\nu_2, r_d) &= 0.297 + 0.061 r_d - 0.058 r_d^2 + 0.170 \nu_2 - 0.589 r_d \nu_2 \\ &\quad + 0.373 r_d^2 \nu_2 - 0.284 \nu_2^2 + 0.817 r_d \nu_2^2 - 0.551 r_d^2 \nu_2^2, \\ B(\nu_2, r_d) &= 29.708 - 42.447 r_d + 23.852 r_d^2 - 14.309 \nu_2 + 75.204 r_d \nu_2 \\ &\quad - 59.881 r_d^2 \nu_2 + 121.370 \nu_2^2 - 246.328 r_d \nu_2^2 + 170.027 r_d^2 \nu_2^2 \end{aligned}$$

where ν_1 , ν_2 are Poisson ratio of the layer and the half-space, respectively. The impedance contrast is $r_s = \beta_1/\beta_2$, and $r_d = \rho_1/\rho_2$ is the ratio between density of mass of the layer and the half-space. This formula was determined by enormous numerical calculation and it can be applied to $0 < \nu_2 < 0.5$ and $0.3 < r_d < 0.9$ at a very good approximation (often less than one or two percents of error). The value 0.2026 in formula (3.47) is the solution of equation

$$1 - 2\sqrt{\gamma} \sin(\sqrt{\gamma} \frac{\pi}{2}) = 0 \quad (3.48)$$

with $\gamma = (1 - 2\nu_1)/2/(1 - \nu_1)$. This equation is from the model “layer with fixed bottom”, and we already analytically proved that the singularity exists only if $\nu_1 > 0.2026$ (in Malischewsky et al. (2008)[38]). After deeper investigation, we can see that the function $F(\nu_1)$ barely depends on ν_2 and only slightly depends on r_d . The maximum difference of $F(\nu_1)$ on ν_2 is only about 0.55% and on r_d is about 3.3% in the whole range of r_d from 0.3 to 0.9 and ν_2 from 0 to 0.5.

Information about the S-wave velocity of the bedrock is contained in the peak of the H/V ratio at the fundamental frequency of resonance. This peak is mainly controlled by the velocity contrast between bedrock and sediment; the higher the contrast, the large the amplitude of the H/V ratio at the resonant frequency (Donat Fäh et. al 2002 [17]). When $r_s > F(\nu_1)$, the H/V ratio curve does not have a singularity, but presents a maximum point which often occurs near the resonant frequency $\bar{f} = 0.25$. Fig. 3.7 shows the frequency of singularity and the maximum point with different impedance contrast and Poisson’s ratio of the layer. The density ratio and Poisson’s ratio of the half-space was chosen as in Model 3 in Table 3. Here $\bar{f} = d/\lambda_{\beta_1}$ is the ratio of the thickness of the layer to the wavelength of S-wave of the layer, and we chose argument $\bar{f}_p/0.25$ because when $r_s = 0$, which corresponds to the model “layer with fixed bottom”, we proved that it equals 1 ([38]). In other words, when the impedance contrast is very high, the frequency of the first peak is the S-wave resonance frequency of the layer. In this figure, the blue line is the curve of the function $F(\nu_1)$, which shows when H/V ratio has singularity or only maximum point. In this case, after applying the formula (3.47) with our chosen ν_2 and r_d we get:

$$F(\nu_1) = 0.291 \arctan [18.147(\nu_1 - 0.2026)] . \quad (3.49)$$

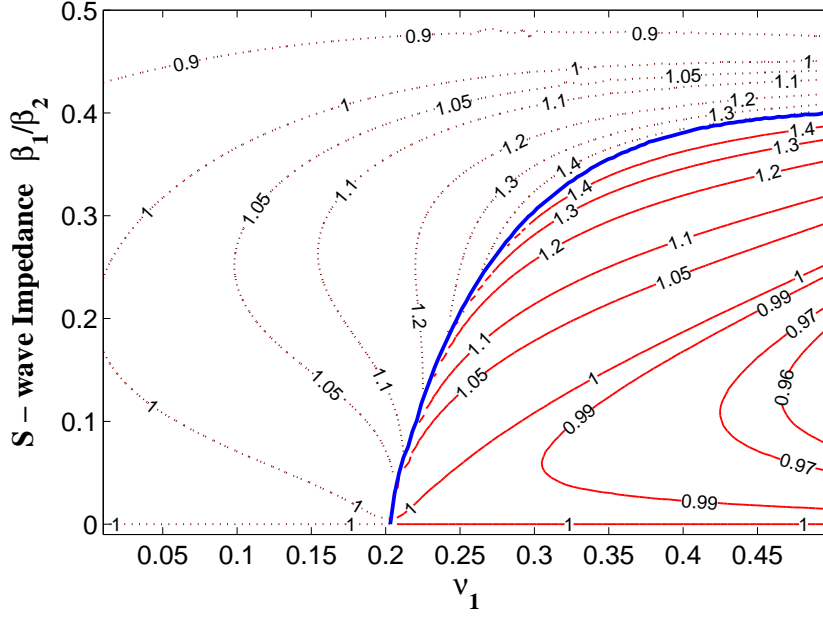


Figure 3.7: Contour of $\bar{f}_p/0.25$. The blue line is the curve of function $F(\nu_1)$ and it divides the domain into two parts: continuous red lines are for the singularities and dotted brown lines for maximum points.

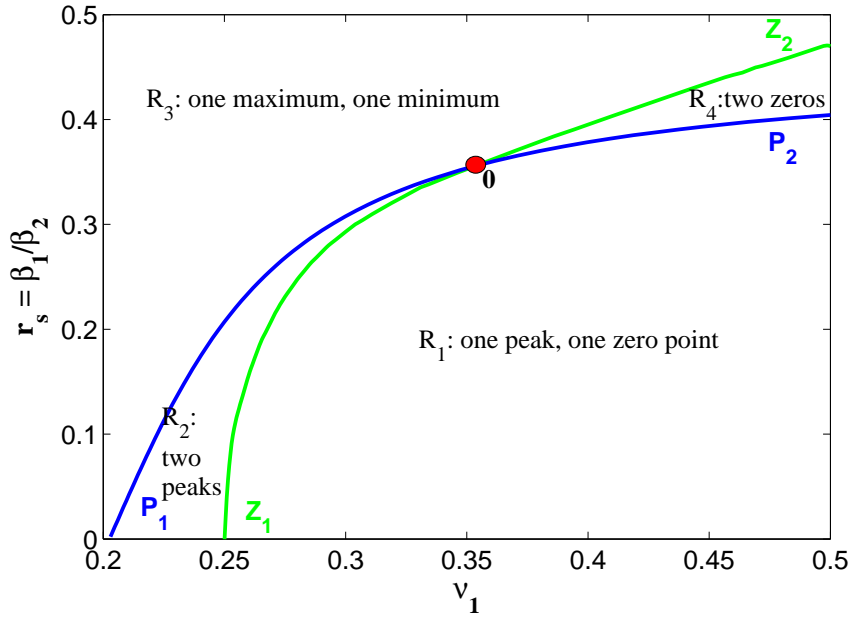


Figure 3.8: Four different characters of H/V ratio. The curve of function $F(\nu_1)$ is blue and the curve of function $G(\nu_1)$ is green.

The continuous red region is for the domain having a singularity of H/V , and the dotted brown one is for the maximum. In Bonney-Claudet et al. (2008) [11], it states that “Focusing on the fundamental mode, the vanishing of the vertical component occurs at a frequency Fr which is very close (i.e, less than 5% different) to the fundamental resonance frequency for S-waves only if the S-wave impedance contrast exceeds a value of 4”. This statement was supported in some other works such as Narayan (2002) [43]. From this figure, we can easily see that the value of $\bar{f}_p/0.25$ near 1 and within a 5% difference lies in the region of high value ν_1 and the impedance contrast. This is in agreement with other observations. We still observe another region of maxima that attain this value of $\bar{f}_p/0.25$. Because in practical data, we get only the finite peak, not the singularity, this region deserves more investigation. We also see that on the blue curve of $F(\nu_1)$, the frequency of the peak reaches its highest value. This was once discussed in Malischewsky and Scherbaum (2004) [35], who plotted a figure of the peak versus the impedance contrast. In that paper, he chose $\nu_1 = 0.4375$, and he realized that there was a value of $\beta_2/\beta_1 \approx 2.6$ where the frequency of the peak reached its highest value. At that time, this value was still strange to him and required additional investigation. But from our figure (3.7) we can see this point is on the blue curve, where the property of H/V changes and the particle motion changes, and the value $\beta_2/\beta_1 \approx 2.6$ can be obtained from equation (4.22) when $\nu_1 = 0.4375$. It gives $\beta_2/\beta_1 = 2.5637$, which is very close to the value of 2.6 that Malischewsky presented.

Zero point

The value of Poisson’s ratio of the layer where the H/V curve starts to have a zero point is 0.25. This value corresponds to $r_s = 0$. With $\nu_1 < 0.25$, the H/V curve has only the minimum point. By analogy to the singularity point, when the impedance contrast $r_s > 0$ there must be condition between r_s and ν_1 for the existence of a zero point as

$$r_s < G(\nu_1) . \quad (3.50)$$

The general form of $G(\nu_1)$ is more complicated than that of $F(\nu_1)$. In particular cases such as the Model 3 in Table 3, the curves of functions $F(\nu_1)$ and $G(\nu_1)$ are plot in Fig. 3.8. Because the Poisson’s ratio of the half-space ν_2 and the density ratio r_d do not much affect the behaviour of the H/V curve, in most cases $F(\nu_1)$ and $G(\nu_1)$ divides the domain of ν_1 and r_s into four regions. These regions correspond to four different states of the H/V ratio. In region R_1 where r_s is less than both $F(\nu_1)$ and $G(\nu_1)$, the H/V ratio has both a singularity and a zero point. This is the most interesting region, and it is close to the actual model with high impedance contrast (exceeding 2.5) and a large value of Poisson’s ratio of the layer, $\nu_1 > 0.25$. The three other regions R_1 , R_2 and R_3 correspond to three unimportant states of the H/V ratio, especially the regions R_2 and R_4 where H/V ratio curve has two singularities and two zero points, respectively.

By numerical calculation, we can find an approximation for the boundary of the region R_1 which is a combination of function $F(\nu_1)$ and $G(\nu_1)$ and is defined by

$$r_s < \min[F(\nu_1), G(\nu_1)] . \quad (3.51)$$

We call this function $K(\nu_1)$, and it can be expressed as

$$K(\nu_1) = C(\nu_2, r_d) \arctan [D(\nu_2, r_d)(\nu_1 - 0.25)] \quad (3.52)$$

with the auxiliary functions

$$\begin{aligned}
C(\nu_2, r_d) &= 0.3058 - 0.0471 r_d + 0.0092 r_d^2 - 0.0839 \nu_2 + 0.2918 r_d \nu_2 \\
&\quad - 0.2673 r_d^2 \nu_2 + 0.1538 \nu_2^2 - 0.6098 r_d \nu_2^2 + 0.5056 r_d^2 \nu_2^2, \\
D(\nu_2, r_d) &= 65.9858 - 91.2188 r_d + 47.6980 r_d^2 + 137.1766 \nu_2 - 342.7329 r_d \nu_2 \\
&\quad + 249.2955 r_d^2 \nu_2 + 67.7489 \nu_2^2 + 223.5938 r_d \nu_2^2 - 253.4675 r_d^2 \nu_2^2.
\end{aligned}$$

The accuracy of this approximation is not so good as for the function $F(\nu_1)$, for which the error is often less than 1 or 2 percent: the error of the function $G(\nu_1)$ can be up to 5 percent. In figure (3.9), we plot the contour of the zero point and minimum frequency of the H/V ratio curve. The green curve is the curve of function $G(\nu_1)$, the continuous red lines correspond to the contour lines of the zero point, and the dotted brown lines to the contour lines of the minimum. At $r_s = 0$ (corresponding to model “layer with fixed bottom”) the zero point starts at $\nu_1 = 0.25$ with $\bar{f}_z = \sqrt{3}/4 \approx 0.433$ and as proof, in that model, the frequency of the zero point in this case is

$$\bar{f}_z = 1.4136 + 1.2736 \nu_1 \quad (0.25 < \nu_1 < 0.5) .$$

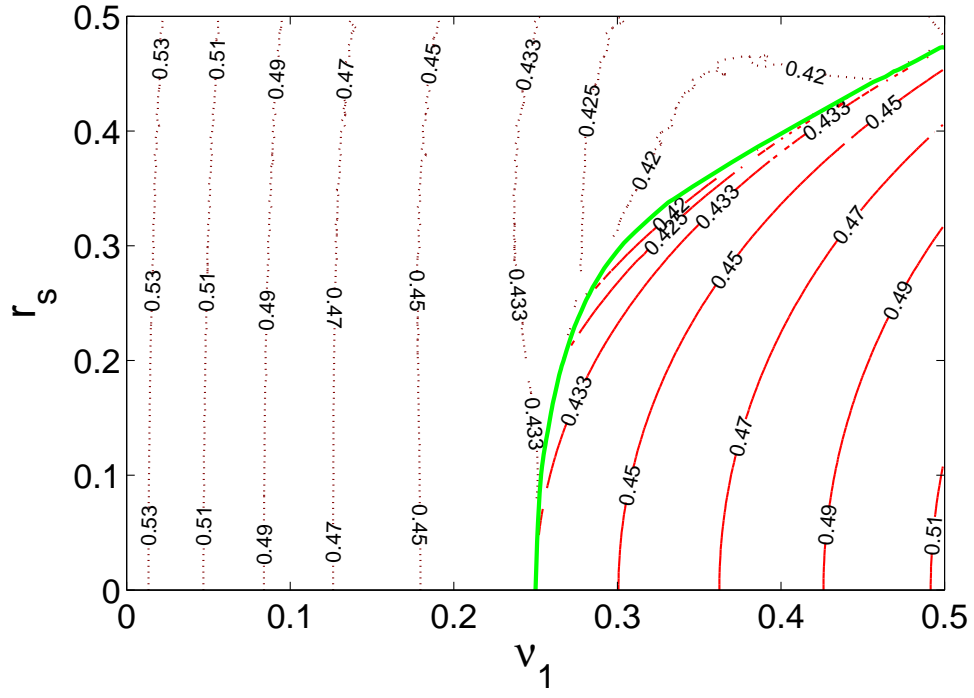
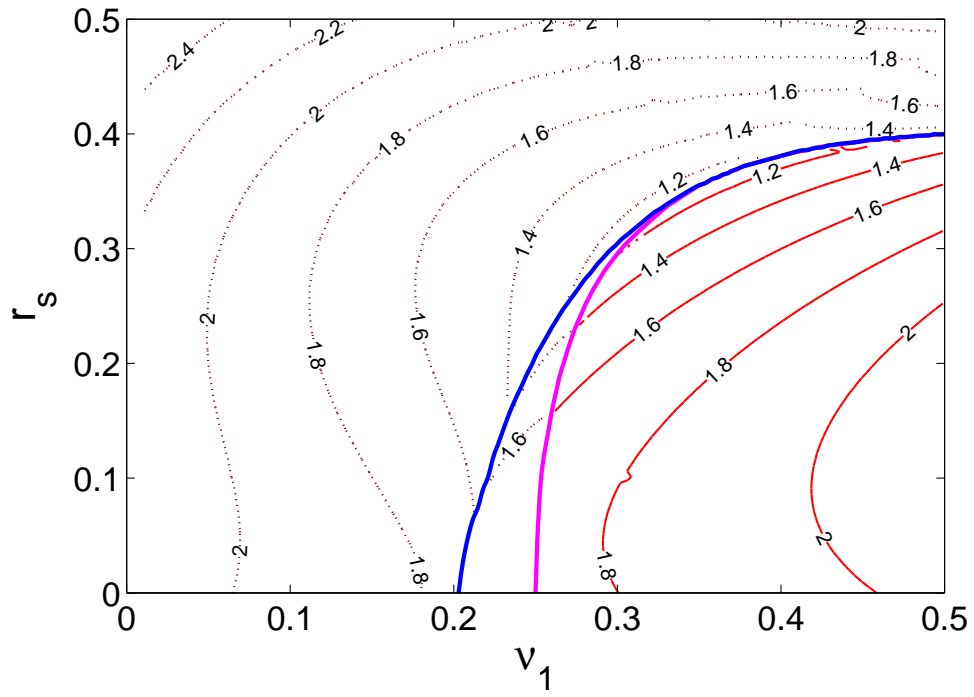
In contrast to the figure of the contour of the peak, with the trough contour, low values of \bar{f}_z concentrate around the curve of the existence of the zero condition.

When $\nu_1 < 0.25$, the H/V ratio does not have a zero point, but the minimum point and its position hardly depends on the value of r_s ; it only depends on the value of the Poisson ratio of the layer ν_1 . However, in this region, $\nu_1 < 0.25$, the minimum point is very vague. This means that although it is the minimum point mathematically, it does not differ much from its vicinity points in magnitude.

The Fig. (3.10) shows the contour of \bar{f}_z/\bar{f}_p . The blue curve is the curve of function $F(\nu_1)$, while the magenta curve is the curve of function $K(\nu_1)$, when both zero point and singularity exist, and in this particular case, it is

$$K(\nu_1) = 0.2717 \arctan [35.5473(\nu_1 - 0.25)] . \quad (3.53)$$

In some papers such as Konno and Komachi (1998) [25] or Stephenson (2003) [53], it was already noted that the ratio between trough and peak is around 2, and this can be used to obtain the resonant frequency. This is illustrated by one part of the figure in the region where H/V has both an infinite peak and a zero point with high values of the Poisson ratio of the layer and high impedance contrast. This region of the trough map is similar to the region on the peak map when the peak frequency is very near the resonant frequency of S waves in the layer. On the other hand, we can observe this value in the region where the Poisson ratio of the layer is small, and H/V has a maximum point and a minimum point. In fact, when $\nu_1 < 0.25$, the H/V ratio has a minimum point, but this point is very vague because its magnitude is not much less than the other points in its vicinity. That may be the reason why one may not notice this minimum point in measurements. The minimum point is vague not only in the region of $\nu_1 < 0.25$ but also in the region R_2 where the H/V ratio has two peaks. So in practice, the above figure of the contour of \bar{f}_z/\bar{f}_p is valid only in the region R_1 . With this observation, our numerical result is totally in accordance with result of Stephenson.

Figure 3.9: Contour of \bar{f}_z Figure 3.10: Contour of \bar{f}_z/\bar{f}_p

Application from peak and trough frequencies

The existence of non-consolidated sedimentary deposits in the shallow part of a geological structure may increase the seismic hazard, because there is the possibility of amplification of seismic waves in certain frequency bands due to the velocity contrast between soft and stiff materials. An especially dangerous situation occurs when the resonant frequency coincides with the natural periods of the buildings, and as a result additional effects of resonance appear on the edifices. For this reason, Petermans (2006) [47] used ambient noise vibrations coupled with 1D modelling to identify risky areas of a pilot zone of Brussels in different earthquake scenarios. Also, Delgado (2000) [15] constructed a map showing the resonant frequency of the soft soil in the Segura river valley (SE Spain). This frequency has been determined from the H/V ratios of microtremors measured at 180 sites in the valley. In these two studies, the resonant frequency is assumed to be the peak frequency of the H/V ratio curve and the thickness of the layer can be found by the simple relation $F_0 = V_s/4H$, where F_0 is the H/V ratio peak frequency, V_s is the shear wave velocity of the layer and H is the thickness of the layer. However, this assumption is only true when the impedance contrast and Poisson's ratio of the layer are high enough (see Fig. 3.7). In practice, soil conditions are often variable even within a relatively small areas such as a town, so the map 3.7 is helpful for us when interpreting the resonant frequency of the layer, which is considered as the dangerous frequency, from the peak frequency of the H/V ratio. In addition, information from the H/V

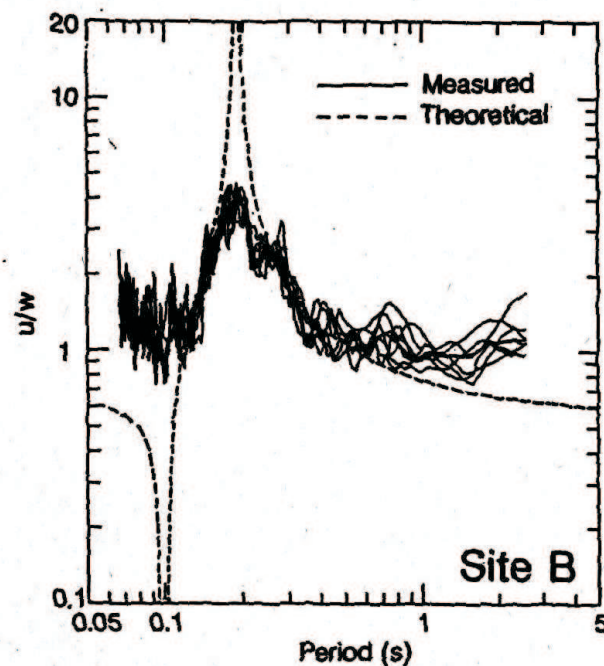


Figure 3.11: Tokimatsu[1997] [55]

spectral ratio of a noise measured from a single station can give us some information about the parameters of the structure. Fig. 3.11 is an example of H/V spectral ratio: it shows the

measured data and theoretical curves of the H/V ratio. There seems to be good agreement between them at the peak and trough frequencies. One question addressed here is that of what information we can extract from the peak and trough frequencies of an H/V spectral ratio. In this section, I create maps showing the relation between the frequencies of the peak and the trough, the Poisson's ratio of the layer, ν_1 , and the impedance contrast r_s . From these maps, and by locating the peak and trough frequencies of measured H/V ratio, we can obtain the Poisson's ratio and impedance contrast.

Fig. 3.12 is such a map for the region R_1 showing the most interesting areas, and is close to a practical model. It shows the contour line of the frequency of peak $\bar{f}_p/0.25$ as a function of

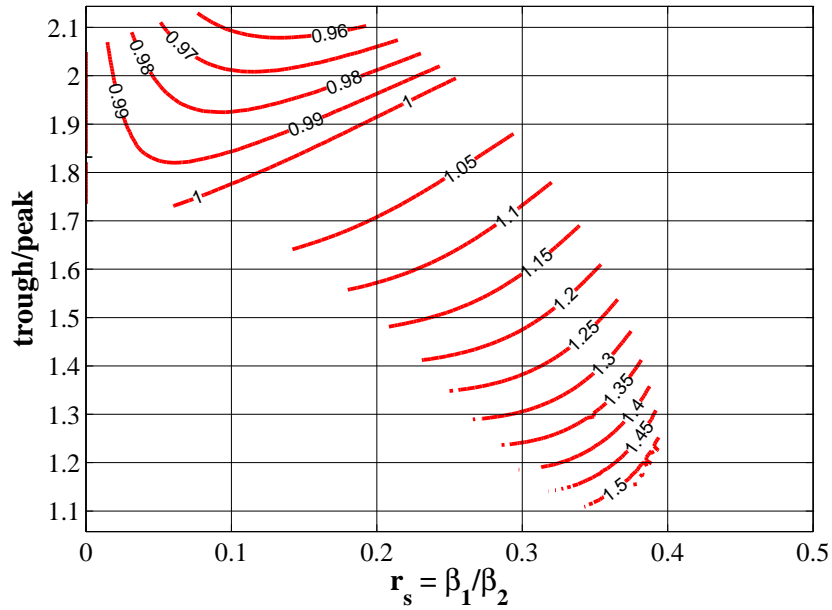


Figure 3.12: Contour of $\bar{f}_p/0.25$ as a function of r_s and \bar{f}_z/\bar{f}_p in region R_1

r_s and the ratio of trough frequency to peak frequency \bar{f}_z/\bar{f}_p . From this map we can obtain information about the impedance contrast if we know the frequency of peaks and troughs from the measurement data. For example, if $\bar{f}_p/0.25$ from measurements is 1 and \bar{f}_z/\bar{f}_p is 2, we can estimate the impedance contrast of the structure r_s to be about 0.25. The above comment about the minimum point does not clearly apply in the region R_2 and R_3 , so we will concentrate on the region R_1 , where the H/V ratio has both an infinite peak and a zero point (Fig. 3.12). From this map, we can obtain the value of r_s if we already know the value of the trough/peak and $\bar{f}_p/0.25$. Figure 3.13 shows the map for the region R_3 for which the H/V ratio has no peak and no zero point but a maximum and a minimum. The blue part corresponds to the region of $\nu_1 < 0.25$ where the minimum is very vague. The pink part delineates the rest, where both the maximum and minimum are clear. However, this map is not appropriate for applying the H/V -method, because the H/V ratio curve does not exhibit a sharp peak, which makes it difficult to identify the fundamental frequency. This fact is already reported in some papers such as Haghshenas et al. (2008) [21] and Petermans

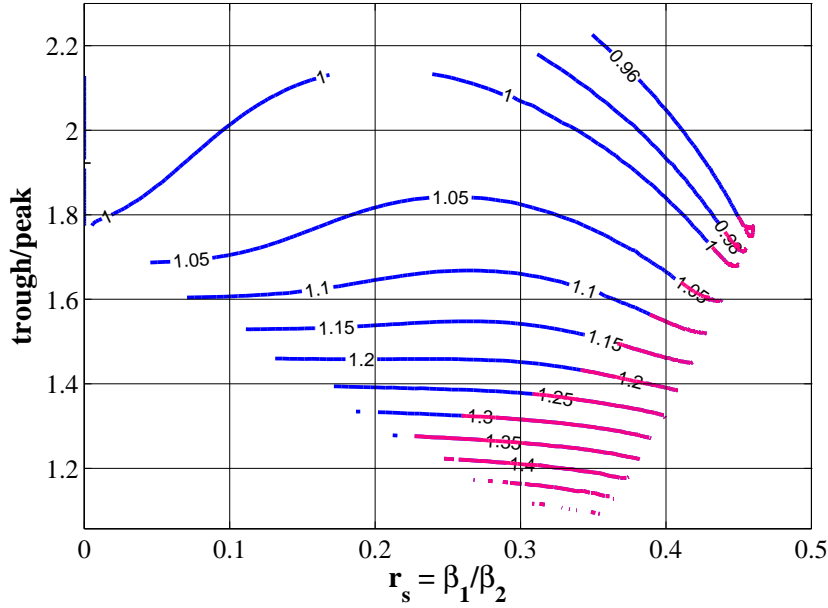
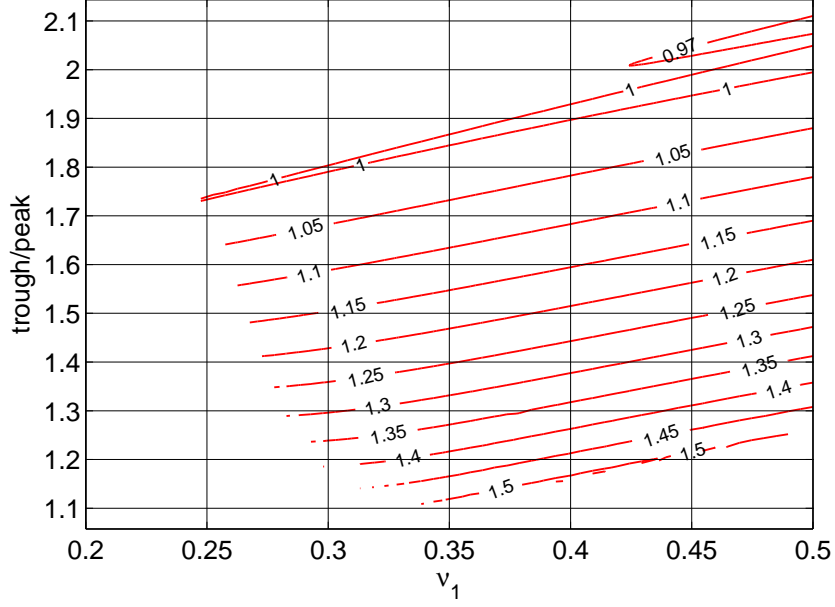
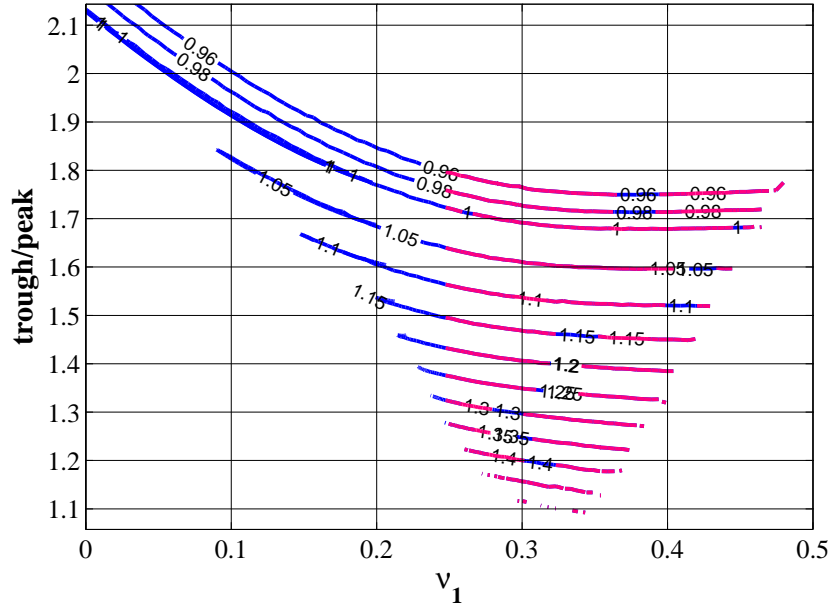


Figure 3.13: Contour of $\bar{f}_p/0.25$ as a function of r_s and \bar{f}_z/\bar{f}_p in region R_3

et al. (2006) [47]. The figures in 3.14 are similar to 3.12 and 3.13, but instead of r_s we plot versus ν_1 .

3.1.5 Particle motion

It is well established in textbooks that Rayleigh waves propagating over the surface of a homogeneous elastic half-space feature retrograde particle motion (see e.g. Achenbach [1] and Kaufman and Levshin [24]). In the model “impedance surface”, we proved that there is no possibility for prograde particle motion. However, in the inhomogeneous half-space retrograde or prograde motion is possible depending on the frequency range. In chapter 2 of model “layer with fixed bottom”, we pointed out that prograde motion exists and that it can occur in the range of frequency $\bar{f} = 0.25$ to 0.5126 . Because that this model is a particular case of the model “layer over half-space” when the impedance contrast is very high, we will consider here the prograde and retrograde particle motion of LOH. Similar to model LFB, because of the skin effect of surface waves, and recalling that the Rayleigh motion is retrograde in the homogeneous half-space, prograde motion should be expected only in a certain range of frequencies \bar{f} . Fig. 3.15 shows the regions of prograde and retrograde motion of an incompressible structural model (see Model 2 in Table 3). This figure from Malischewsky et al. (2008) [38] shows the influence of r_s and \bar{f} on the domain of prograde motion. The region of prograde Rayleigh motion ($\chi < 0$) is shown in red. The fine structure of positive H/V -values in the domain of retrograde motion is shown in shades of blue, with lighter shades corresponding to higher values. For very low r_s (i.e. for a high shear-wave contrast), we observe prograde motion approximately in the interval $0.25 \leq \bar{f} \leq 0.5126$,

(a) Region R_1 

(b) Region R_3 (The blue part corresponds to the region of $\nu_1 < 0.25$ where the minimum is very vague. The pink part delineates the rest, where both the maximum and minimum are clear)

Figure 3.14: Contour of $\bar{f}_p/0.25$ as a function of ν_1 and \bar{f}_z/\bar{f}_p .

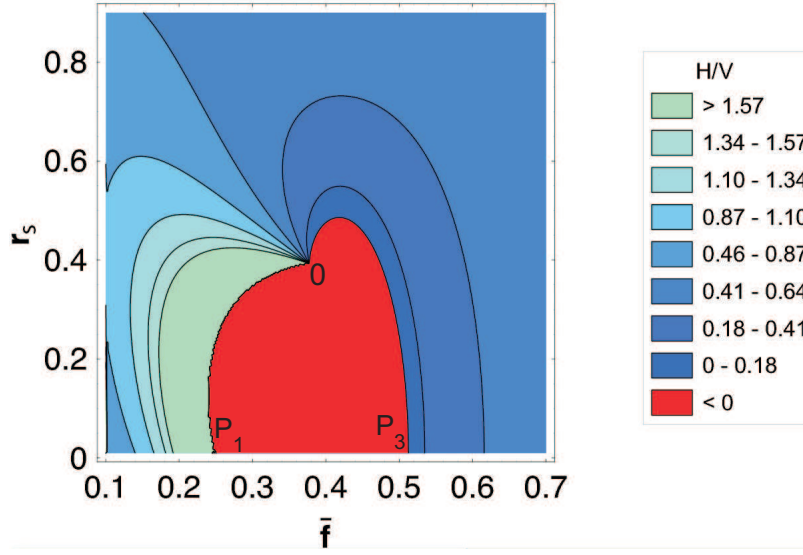


Figure 3.15: 2D graph of the domain of prograde motion (red) as a function of \bar{f} and r_s for the incompressible Model 2 (Table 3)

which is already observed in the model LFB. The value $\bar{f} = 0.25$ is the so-called fundamental frequency of the site $\beta_1/4d$ and the $\bar{f} = 0.5126$ is very close to the double site frequency $\beta_1/2d$. The fundamental site frequency is important in seismic hazard assessment as it is connected with the shear-wave resonance in the layer. In this figure, the curve P_10 represents the singularity and $0P_3$ for the zero point. The domain of prograde motion is bounded either by two zero points, by two singularities, or more commonly by a singularity and a zero point. The maximum range of this domain is bounded by P_1 and P_3 . The points P_1 and P_3 with the corresponding frequencies $\bar{f} = 0.25$ and $\bar{f} = 0.5126$, respectively, are shown in Fig. 2.3 which shows the domains of prograde and retrograde particle motion of model LFB. In Fig. 3.15, because we choose the layer to be incompressible or $\nu_1 = 0.5$, the frequency \bar{f} of P_3 is 0.5126. With other values of Poisson's ratio of the layer ν_1 , the frequency of P_3 is

$$\bar{f}_{P_3} = 0.25 + 3.861 (\nu_1 - 0.2026) \text{ when } 0.2026 \leq \nu_1 \leq 0.25 \quad (3.54)$$

and

$$\bar{f}_{P_3} = \frac{\sqrt{3}}{4} + 0.318 (\nu_1 - 0.25) \text{ when } 0.25 \leq \nu_1 \leq 0.5 \quad (3.55)$$

which are found in Chapter 2 of the model LFB.

The condition $\nu_1 > 0.2026$ is required for the existence of prograde particle motion. Otherwise, the H/V -ratio curve does not have any singularity or zero point and the particle motion is always retrograde. Fig. 3.16 shows the domain of prograde motion of Model 3 in Table 3 with many values of ν_1 from 0.21 to 0.499. Fig. 3.16 is organized as in Fig. 3.15. The red part is for singularities and the black part is for zero-points. The domain of prograde motion is white and that of retrograde motion is grey. The domain of prograde motion is bounded by the contour $\chi = 0$ for $\nu_1 = 0.499$. Thus the domain of prograde motion is maximal for an

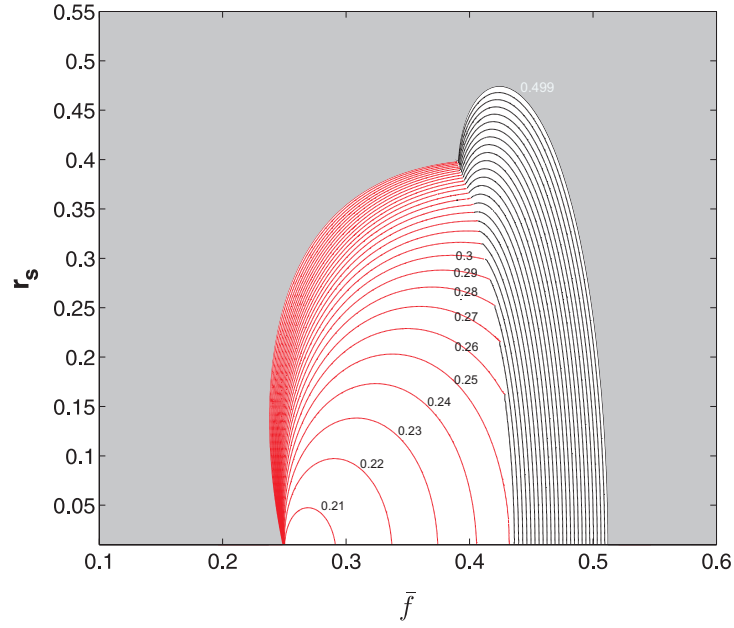


Figure 3.16: 2D graph of the domain of prograde motion (white) as a function of \bar{f} and r_s for different values of ν_1 (contours) and for r_d and ν_2 of Model 3 (Table 3)

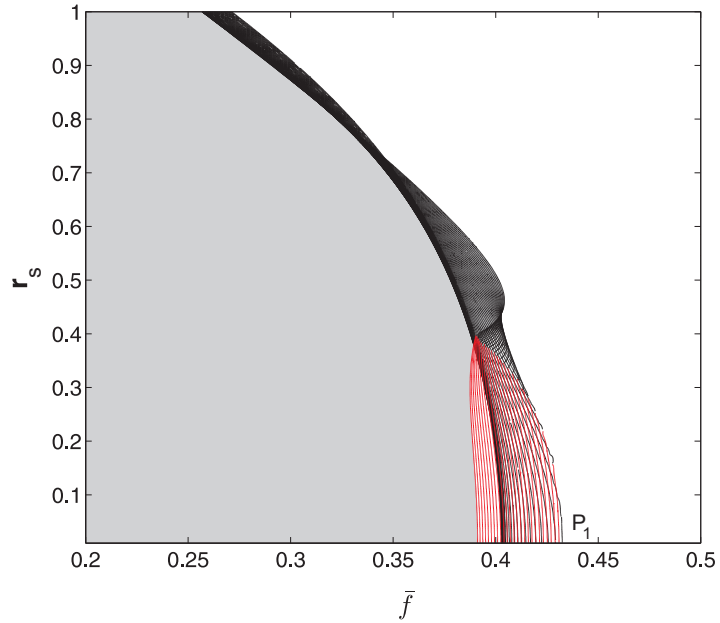


Figure 3.17: 2D graph of the domain of prograde motion (white) on the interface as a function of \bar{f} and r_s for different values of ν_1 (contours) and for r_d and ν_2 of Model 1 (Table 3)

incompressible layer. The contour of $\chi = 0$ becomes smaller for lower Poisson's ratios and disappears for $\nu_1 < 0.2026$.

3.1.6 H/V -ratio in the depth

The surface waves propagation concentrates near the surface, and it is well known that the penetration depth of the Rayleigh waves in a homogeneous half-space is about 1.5 times the wave length. Thus, studying the ellipticity in the depth has significant meaning in practice. For example, Malischewsky [37] presented an analytical approach and an approximation for the ellipticity of Rayleigh wave in a homogeneous half-space at infinitive depth in terms of Poisson's ratio. From the displacement amplitudes in the layer and in the half-space (Appendix 3) we can formulate the ellipticity of Rayleigh waves in the depth as

$$\chi^{(L)}(x_3) = \frac{\tilde{U}_1^{(1)}(x_3)}{\tilde{U}_3^{(1)}(x_3)} \quad \text{when} \quad -d \leq x_3 \leq 0 \quad (3.56)$$

and

$$\chi^{(H)}(x_3) = \frac{\tilde{U}_1^{(2)}(x_3)}{\tilde{U}_3^{(2)}(x_3)} \quad \text{when} \quad 0 \leq x_3 \leq \infty. \quad (3.57)$$

Particularly, on the interface between the layer and half-space, the H/V -ratio is

$$\chi^{(I)}(x_3) = \frac{T(x_3)}{M(x_3)} \quad (3.58)$$

where

$$\begin{aligned} T(x_3) = & T_0 + T_1 \sinh\left(\frac{2\pi\bar{f}e_\beta}{C}\right) \sinh\left(\frac{2\pi\bar{f}e_\alpha}{C}\right) + T_2 \sinh\left(\frac{2\pi\bar{f}e_\alpha}{C}\right) \cosh\left(\frac{2\pi\bar{f}e_\beta}{C}\right) \\ & + T_3 \cosh\left(\frac{2\pi\bar{f}e_\alpha}{C}\right) \sinh\left(\frac{2\pi\bar{f}e_\beta}{C}\right) + T_4 \cosh\left(\frac{2\pi\bar{f}e_\beta}{C}\right) \cosh\left(\frac{2\pi\bar{f}e_\alpha}{C}\right), \end{aligned} \quad (3.59)$$

$$\begin{aligned} M(x_3) = & M_0 + M_1 \sinh\left(\frac{2\pi\bar{f}e_\beta}{C}\right) \sinh\left(\frac{2\pi\bar{f}e_\alpha}{C}\right) + M_2 \sinh\left(\frac{2\pi\bar{f}e_\alpha}{C}\right) \cosh\left(\frac{2\pi\bar{f}e_\beta}{C}\right) \\ & + M_3 \cosh\left(\frac{2\pi\bar{f}e_\alpha}{C}\right) \sinh\left(\frac{2\pi\bar{f}e_\beta}{C}\right) + M_4 \cosh\left(\frac{2\pi\bar{f}e_\beta}{C}\right) \cosh\left(\frac{2\pi\bar{f}e_\alpha}{C}\right) \end{aligned} \quad (3.60)$$

with

$$\begin{aligned} T_0 &= 2e_\alpha e_\beta g_\beta h_1 (2 + h_1) (-2 + h_2), \\ T_1 &= g_\beta (8e_\alpha^2 e_\beta^2 + h_1^3) (-2 + h_2), \\ T_2 &= -e_\beta (-2 + h_1) h_1^2 (2g_\alpha g_\beta - h_2), \\ T_3 &= 4e_\alpha e_\beta^2 (-2 + h_1) (2g_\alpha g_\beta - h_2), \\ T_4 &= -T_0; \end{aligned}$$

and

$$\begin{aligned}
M_0 &= -2e_\alpha e_\beta h_1 [2g_\alpha g_\beta (2 - 4f_1 + h_1) + h_2(-2 - h_1 + 2f_1 h_2)] , \\
M_1 &= h_1^2 (4f_1 g_\alpha g_\beta - 2g_\alpha g_\beta h_1 + h_1 h_2 - f_1 h_2^2) + 4e_\alpha^2 e_\beta^2 [4(-1 + f_1)g_\alpha g_\beta + h_2(2 - f_1 h_2)] , \\
M_2 &= -4e_\alpha^2 e_\beta g_\beta (-2 + h_1)(-2 + h_2) , \\
M_3 &= e_\alpha g_\beta (-2 + h_1) h_1^2 (-2 + h_2) , \\
M_4 &= e_\alpha e_\beta (2h_1(2 + h_1)(2g_\alpha g_\beta - h_2) - f_1(4 + h_1^2)(4g_\alpha g_\beta - h_2^2)) .
\end{aligned}$$

Fig. 3.17 shows a 2D-graph of the prograde and retrograde domain on the interface as a function of \bar{f} and r_s for different values of ν_1 (contours) and for r_d and ν_2 of Model 3. The Poisson's ratio in this figure ν_1 from 0.01 to 0.499 with the jump is 0.01. These contour lines divide the domain into two regions: the gray region corresponds to retrograde motion, and the white region to prograde motion. The black curves are for the singularities and the red curves are for the zero points. The point P_1 with coordinates (0.43, 0) is the special point which lies on the contour line of $\nu_1 = 0.25$. When $\nu_1 < 0.25$ the H/V -ratio on the interface always has a zero-point no matter what the impedance contrast is, but when $\nu_1 > 0.25$, the H/V curve has either one singularity or one zero point depending on the impedance contrast. For each $\nu_1 > 0.25$, there exists a value of $r_s = r_s(\nu_1)$ so that H/V has singularity if $r_s < r_s(\nu_1)$ and a zero-point if $r_s > r_s(\nu_1)$. The function of $r_s(\nu_1)$ is an increasing function of ν_1 , and has a maximum at about $r_s = 0.4$ at $\nu_1 = 0.5$ or where the layer is incompressible. Hence, with low impedance contrast, e.g lower than 2.5, the H/V -ratio on the interface has only one zero point without any singularity. This conclusion is similar to that for H/V on the surface which never has a singularity with such a low impedance contrast. Comparing

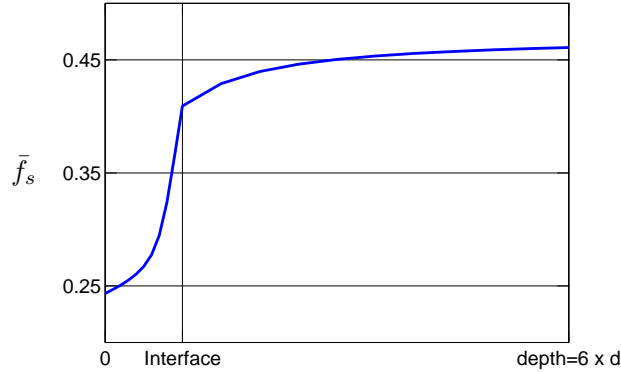


Figure 3.18: Peak frequency of H/V -ratio curve with respect to the depth

the two 2D-graphs 3.17 and 3.16, we can conclude that the peak frequency of the H/V -ratio increases with depth. On the surface, it is about $\bar{f} = 0.25$, which is the resonance frequency of shear wave in the layer, but on the interface, it is about $\bar{f} = 0.4$ to $\bar{f} = 0.43$. Fig. 3.18 illustrates this conclusion for the singularity frequency of the H/V -ratio curve as a function of depth. In this figure we choose high ν_1 and r_s as Model 1 in Table 3 to be sure that there

are singularities on the interface. The frequency of singularity increases dramatically in the layer but less in the half-space.

3.2 Inhomogeneous layer over half-space

Margery Newlands and Stoneley [39] studied the Rayleigh waves in a two-layer heterogeneous medium with the rigidity of the layer increasing linearly for both incompressible and compressible material. However, the linear variability of the shear modulus in the layer sometimes does not fit well the actual models. Recently, Vrettos [57] [58] investigated an inhomogeneous half-space where the shear modulus varies as a function of the depth

$$\mu(x_3) = \mu_0 + (\mu_\infty - \mu_0)[1 - e^{-ax_3}] , \quad 0 < \mu_0 < \mu_\infty \quad (3.61)$$

where μ_0, μ_∞ is the shear modulus at the surface and at infinitive depth, respectively, and a is a constant with the dimension of inverse length. This is an exponential function, so it increases quickly from μ_0 to a value approximating μ_∞ in a certain depth. We have

$$\mu(x_3) \approx \mu_\infty \quad \text{when} \quad x_3 > \frac{2\pi}{a} \quad (3.62)$$

with the error less than one one-thousandth. Thus we can consider this inhomogeneous half-space model as an inhomogeneous layer over homogeneous half-space where the thickness of the layer is $2\pi/a$ and the shear modulus of the homogeneous half-space is μ_∞ . This is a reasonable approximation model which seems to be close to the actual models. However, the numerical results are quite different from what we expect. For example, the H/V curve shows a maximum only at a very high frequency which is far from the resonance frequency of the shear wave in the layer. This can be explained by the mean value of the shear wave in the layer, which is calculated by

$$\bar{\beta}_1 = \frac{1}{d} \int_0^d \sqrt{\frac{\mu(x_3)}{d}} dx_3 . \quad (3.63)$$

The mean value is so large that the equivalent impedance contrast $\bar{r}_s = \bar{\beta}_1/\beta_\infty$ is greater than 0.9. If we consider this model as a homogeneous LOH with impedance contrast $r_s = \bar{r}_s$, then this large value of r_s only gives an H/V curve with a broad maximal. This is consistent with numerical results from Vrettos.

To avoid this problem, and to obtain a model which is close to reality, we will use Vrettos's idea but study an inhomogeneous layer over a homogeneous half-space. The modulus of the shear wave in the layer is as in formula (3.61), but the domain of this function is only $0 \leq x_3 \leq d$, in which d is the thickness of the layer and

$$\mu_1 = \mu(d) \quad \text{or} \quad ad = \ln \frac{\mu_\infty - \mu_0}{\mu_\infty - \mu_1} . \quad (3.64)$$

The shear modulus of the half-space is μ_2 , which is greater than μ_0 and μ_1 . The Poisson's ratio in the layer is ν_1 and in half-space is ν_2 . The densities of mass are ρ_1 and ρ_2 , respectively.

The procedure of finding the secular equation is similar to that in the model “inhomogeneous LFB” for the layer. In the layer we have

$$u_1^L(x_1, x_3, t) = \hat{u}_1(x_3) \exp[i(\omega t - kx_1)] , \quad (3.65)$$

$$u_3^L(x_1, x_3, t) = i\hat{u}_3(x_3) \exp[i(\omega t - kx_1)] \quad (3.66)$$

where i is the imaginary unit. The factor i in front of the displacement amplitude \hat{u}_3 implies that the path of a particle in the medium will be an ellipse, a property which holds for Rayleigh waves in a homogeneous half-space. The displacement amplitudes in the layer are similar to (3.67) and displayed as

$$\hat{u}_1(\xi) = A_1 \hat{u}_1^{(1)}(\xi) + A_2 \hat{u}_1^{(2)}(\xi) + A_3 \hat{u}_1^{(3)}(\xi) + A_4 \hat{u}_1^{(4)}(\xi) , \quad (3.67)$$

$$\hat{u}_3(\xi) = A_1 \hat{u}_3^{(1)}(\xi) + A_2 \hat{u}_3^{(2)}(\xi) + A_3 \hat{u}_3^{(3)}(\xi) + A_4 \hat{u}_3^{(4)}(\xi) \quad (3.68)$$

where A_1, A_2, A_3 and A_4 are integration constants. The functions $\hat{u}_i^{(j)}(\xi)$ with $i = 1, 3$ and $j = 1 - 4$ are presented in (2.72). ξ is the subsidiary depth variable as

$$\xi = H_0 \exp(-ax_3) \quad (3.69)$$

with $H_0 = 1 - \mu_0/\mu_\infty$.

The stresses in the layer are

$$\begin{aligned} \sigma_{33}^L &= i \frac{2\mu(x_3)}{1 - 2\nu_1} \left[-a\xi(1 - \nu_1)\hat{u}_3' - k\nu_1\hat{u}_1 \right] , \\ \sigma_{13}^L &= \mu(x_3) \left[-a\xi\hat{u}_1' + k\hat{u}_3 \right] . \end{aligned} \quad (3.70)$$

In the half-space we choose the displacement as

$$u_1^H(x_1, x_3, t) = U_1(x_3) \exp[i(\omega t - kx_1)] , \quad (3.71)$$

$$u_3^H(x_1, x_3, t) = iU_3(x_3) \exp[i(\omega t - kx_1)] \quad (3.72)$$

with $U_1(x_3)$ and $U_3(x_3)$ satisfying the motion equation as

$$U_1(x_3) = C_1 e^{-kg_\alpha x_3} + C_2 e^{-kg_\beta x_3} , \quad (3.73)$$

$$U_3(x_3) = -g_\alpha C_1 e^{-kg_\alpha x_3} - \frac{C_2}{g_\beta} e^{-kg_\beta x_3} \quad (3.74)$$

where C_1, C_2 are the integral constants in the half-space. The stresses in half-space are

$$\begin{aligned} \sigma_{33}^H &= i \frac{2\mu_2 k}{1 - 2\nu_2} \left[C_1 (g_\alpha^2 - \nu_2 (g_\alpha^2 + 1)) e^{-kg_\alpha x_3} + C_2 (1 - 2\nu_2) e^{-kg_\beta x_3} \right] , \\ \sigma_{13}^H &= -k\mu_2 \left[2C_1 g_\alpha e^{-kg_\alpha x_3} + C_2 (g_\beta + \frac{1}{g_\beta}) e^{-kg_\beta x_3} \right] . \end{aligned} \quad (3.75)$$

Boundary conditions at the free surface of the layer and at the interface between the layer and the half-space are

$$\sigma_{13}^L = \sigma_{33}^L = 0 \text{ at } x_3 = 0 \text{ or } \xi = H_0 \quad (3.76)$$

and at $x_3 = d$ or $\xi = H_1 = 1 - \mu_1/\mu_\infty$

$$\begin{aligned} U_1(d) &= \hat{u}_1(H_1) , \\ U_3(d) &= \hat{u}_3(H_1) , \\ \sigma_{13}^H(d) &= \sigma_{13}^L(H_1) , \\ \sigma_{33}^H(d) &= \sigma_{33}^L(H_1) . \end{aligned} \quad (3.77)$$

Substituting displacement amplitudes and stresses of the layer and half-space into six boundary conditions yields a system of equations with respect to six integral constants A_1, A_2, A_3, A_4 and C_1, C_2 as

$$[M] \cdot [v] = 0 \quad (3.78)$$

with $[v]$ is the integral constant vector and the matrix $[M]$ is

$$[M] = \begin{bmatrix} RB1(1)H_0^{m_1} & RB1(2)H_0^{m_2} & RB1(3)H_0^{m_3} & RB1(4)H_0^{m_4} & 0 & 0 \\ RB2(1)H_0^{m_1} & RB2(2)H_0^{m_2} & RB2(3)H_0^{m_3} & RB2(4)H_0^{m_4} & 0 & 0 \\ RB3(1)H_1^{m_1} & RB3(2)H_1^{m_2} & RB3(3)H_1^{m_3} & RB3(4)H_1^{m_4} & t_3HD_1 & t_3HD_2 \\ RB4(1)H_1^{m_1} & RB4(2)H_1^{m_2} & RB4(3)H_1^{m_3} & RB4(4)H_1^{m_4} & -t_4HD_3 & -t_4HD_4 \\ RB5(1)H_1^{m_1} & RB5(2)H_1^{m_2} & RB5(3)H_1^{m_3} & RB5(4)H_1^{m_4} & -e^{-kg_\alpha} & -e^{-kg_\beta} \\ RB6(1)H_1^{m_1} & RB6(2)H_1^{m_2} & RB6(3)H_1^{m_3} & RB6(4)H_1^{m_4} & g_\alpha e^{-kg_\alpha} & e^{-kg_\beta}/g_\beta \end{bmatrix} \quad (3.79)$$

where

$$RB1(i) = \nu_1 \sqrt{\beta} \sum_{n=0}^{\infty} a_n^{(i)} H_0^n + (1 - \nu_1) \sum_{n=0}^{\infty} (n + m_i) b_n^{(i)} H_0^n \quad (i = 1, 2, 3, 4) , \quad (3.80)$$

$$RB2(i) = \sum_{n=0}^{\infty} (n + m_i) a_n^{(i)} H_0^n - \sqrt{\beta} \sum_{n=0}^{\infty} b_n^{(i)} H_0^n \quad (i = 1, 2, 3, 4) , \quad (3.81)$$

$$RB3(i) = \nu_1 \sqrt{\beta} \sum_{n=0}^{\infty} a_n^{(i)} H_1^n + (1 - \nu_1) \sum_{n=0}^{\infty} (n + m_i) b_n^{(i)} H_1^n \quad (i = 1, 2, 3, 4) , \quad (3.82)$$

$$RB4(i) = \sum_{n=0}^{\infty} (n + m_i) a_n^{(i)} H_1^n - \sqrt{\beta} \sum_{n=0}^{\infty} b_n^{(i)} H_1^n \quad (i = 1, 2, 3, 4) , \quad (3.83)$$

$$RB5(i) = \sum_{n=0}^{\infty} a_n^{(i)} H_1^n \quad (i = 1, 2, 3, 4) , \quad (3.84)$$

$$RB6(i) = \sum_{n=0}^{\infty} b_n^{(i)} H_1^n \quad (i = 1, 2, 3, 4) \quad (3.85)$$

and

$$HD_1 = g_\alpha^2 - \nu_2(g_\alpha^2 + 1) , \quad (3.86)$$

$$HD_2 = 1 - 2\nu_2, \quad HD_3 = 2g_\alpha, \quad HD_4 = g_\beta + 1/g_\beta , \quad (3.87)$$

$$t_3 = \sqrt{\beta} \frac{1 - 2\nu_1}{1 - 2\nu_2} \frac{\mu_2}{\mu_1}, \quad t_4 = \sqrt{\beta} \frac{\mu_2}{\mu_1} \quad (3.88)$$

where $\beta = k^2/a^2$.

A nontrivial solution of the constants corresponds to the determinant of matrix $[M]$ equals zero which leads to the secular equation of this model as

$$\Delta(c, f) = 0. \quad (3.89)$$

For numerical calculation, we choose a model which is close to reality with these parameters: the shear wave velocity at the surface is $\beta_0 = 200$ m/s; at the interface, $\beta_1 = 800$ m/s; in the half-space, $\beta_2 = 2000$ m/s; the density of mass is $\rho_1 = 1.9$ g/cm³ in the layer and $\rho_2 = 2.1$ g/cm³ in half-space, and the thickness of the layer is $d = 20$ m. We will investigate the effect of the inhomogeneous layer on the phase velocity and on the ellipticity by choosing several different forms of μ_{x_3} in the layer, providing that they satisfy $\mu(0) = \mu_0$ and $\mu(d) = \mu_1$. As discussed in the model “inhomogeneous LFB”, we can derive various approximate forms of $\mu(x_3)$ by choosing a suitable μ_∞ as in Table 2.1. In this section, we will work on the approximations given below $G(x_3)$ of $\mu(x_3)$ as

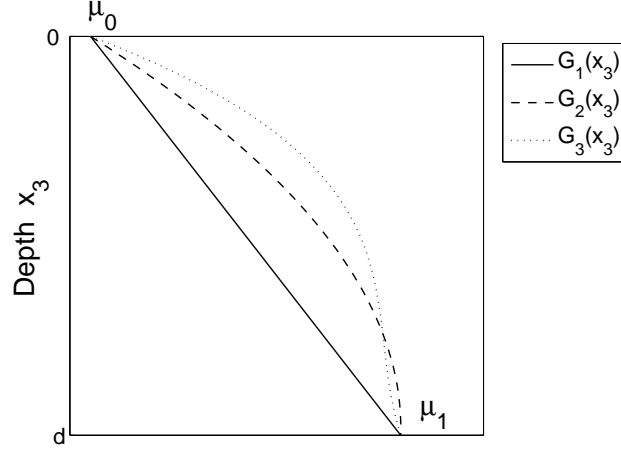


Figure 3.19: Three approximation of shear modulus in the layer: linear $G_1(x_3)$ (continuous), quadratic $G_2(x_3)$ (dashed) and third power polynomial $G_3(x_3)$ (dotted)

- linear function

$$G_1(x_3) = \mu_0 \left(1 + 15 \frac{x_3}{d} \right) \quad \text{with } \mu_\infty = 3000 \text{ m/s}, \quad (3.90)$$

- quadratic polynomial

$$G_2(x_3) = \mu_0 \left[1 + 30.566 \frac{x_3}{d} - 15.566 \left(\frac{x_3}{d} \right)^2 \right] \quad \text{with } \mu_\infty = 850 \text{ m/s}, \quad (3.91)$$

- third power polynomial

$$G_3(x_3) = \mu_0 \left[1 + 50.472 \frac{x_3}{d} - 62.195 \left(\frac{x_3}{d} \right)^2 + 26.723 \left(\frac{x_3}{d} \right)^3 \right] \quad \text{with } \mu_\infty = 810 \text{ m/s}. \quad (3.92)$$

The relative error for these above approximations can be calculated as

$$\delta_i = \frac{\int_0^d |\mu(x_3) - G_i(x_3)| dx_3}{\int_0^d \mu(x_3) dx_3} \quad (i = 1, 2, 3) \quad (3.93)$$

are 1%, 3.1% and 1.29%, respectively. Fig. 3.19 shows the three above approximation functions.

Fig. 3.20 shows the effect of the inhomogeneity on the phase velocity and H/V ratio curves. In this figure we choose $\nu_1 = 0.4375$ and $\nu_2 = 0.2506$. From the figures of phase velocity and H/V ratio curves we can see that the complexity of the inhomogeneity increases the value of phase velocity, and although it does not have much affect on the zero point frequency, the effect on the singularity frequency is remarkable. It tends to reduce the frequency region of prograde motion which lies between the the singularity and zero point.

To evaluate the difference between Vrettos's technique and Newlands's technique, we plot the phase velocity curves on a two-layer heterogeneous medium where the rigidity of the layer is of linear variability by using these two techniques. The parameters of the model are chosen from Newlands and Stoneley (1950) [39] with the thickness of the layer set at 37.5 km and its rigidity increasing linearly from 2.3×10^{11} to 4.53×10^{11} dynes/cm². The rigidity of the half-space is constant and equals 6.47×10^{11} dynes/cm². The density of mass of the layer and half-space are 2.72 and 3.40 g/cm³, respectively. The Poisson's ratios are equal for both layer and half-space and are 0.2308. With Vrettos's technique, we use $\mu_\infty = 10 \times 10^{11}$ dynes/cm². This value is high enough so that the rigidity form of the layer as in (3.61) is very close to the linear form. The error between them which is defined similarly as in (3.93) is 1.84 per cent. Figure (3.21) shows three velocity curves by using Vrettos's and Newlands's techniques and by using a package of Herrmann's program (1994) [22], which is very powerful for generating synthetic data. The x-axis is the wave-length of the Rayleigh wave multiplied with the thickness of the layer. The agreement between Vrettos's and Newlands's techniques is very good in this small range of the wavelength. The phase velocity curve plotted by Herrmann's program shows that the Vrettos's technique is more advanced than that of Newlands.

In practical measurement, when we work on the actual model with continuous shear wave velocity in the layer, one commonly used approximation for the interpretation of H/V ratios is based on the assumption of the single soft layer over a half-space showing a strong contrast. There are two common approaches for the simplification of a structure. The first one is to form the weighted average of the velocities of the layers as follows:

$$\bar{\beta} = \frac{1}{d} \int_0^d \beta(x_3) dx_3 . \quad (3.94)$$

The second approach is based on the concept that the average velocity can be computed in a way such that the travel time in an average model corresponds to the sum of the travel times in the single layers of the actual model, or

$$\frac{1}{\bar{\beta}} = \frac{1}{d} \int_0^d \frac{dx_3}{\beta(x_3)} . \quad (3.95)$$

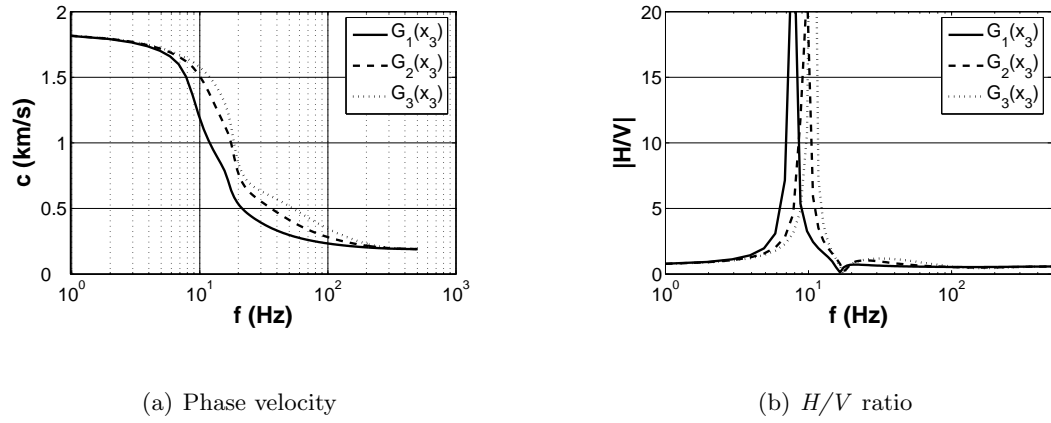
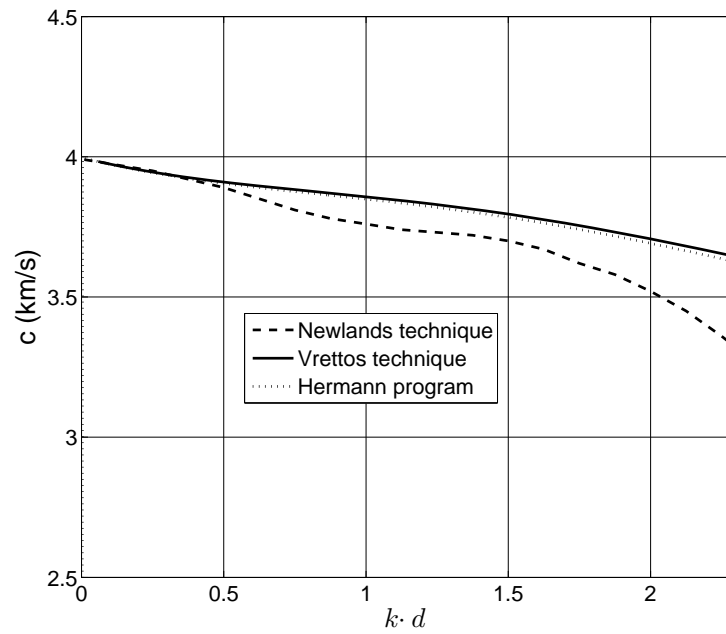
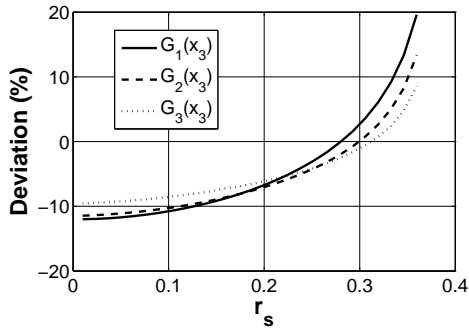
Figure 3.20: Phase velocity and H/V ratio curves of $G_1(x_3)$, $G_2(x_3)$ and $G_3(x_3)$ 

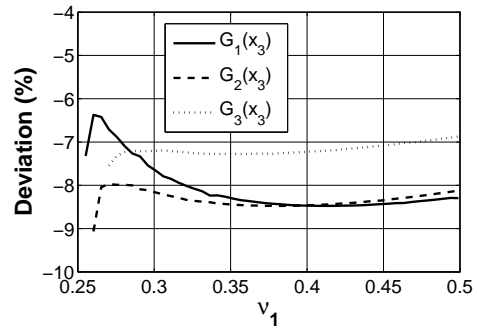
Figure 3.21: The phase velocity curve using Vrettos's technique (continuous), Newlands's (dashed) and Hermann's program (dotted)

To decide which approximation model is better, we will compare the peak and the trough frequencies of the actual model with the two simple homogeneous LOH models with the equivalent shear modulus as in (3.94) and (3.94).

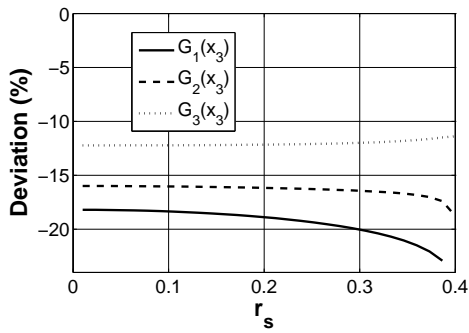
Fig. 3.22 shows the deviation of the singularity and zero point frequencies defined as $\frac{f_{p1}-f_{p2}}{f_{p2}}$ and $\frac{f_{z1}-f_{z2}}{f_{z2}}$ where f_{p1} and f_{p2} are frequencies of singularity of the equivalent homogeneous LOH with formula (3.94) and of the actual inhomogeneous model, respectively, of three above shear moduli: $G_1(x_3)$, $G_2(x_3)$ and $G_3(x_3)$. In Fig 3.22(a, c), we choose $\nu_1 = 0.4375$ and let the impedance contrast r_s vary. With such a high Poisson's ratio ν_1 , the H/V curve has a singularity with r_s up to 0.4 or when the impedance contrast exceeds 2.5. This value was already shown in Fig. 3.16. We can see that the deviation of the singularity frequency is rather small (less than 10%) and the coincidence is quite good around $r_s = 0.3$. Fig. 3.22(b, d) is similar to Fig. 3.22(a, c) but instead of letting the impedance contrast vary, we fix $r_s = 1/6$ and let ν_1 vary from 0 to 0.5, and we have similar good deviation for the singularity frequency.



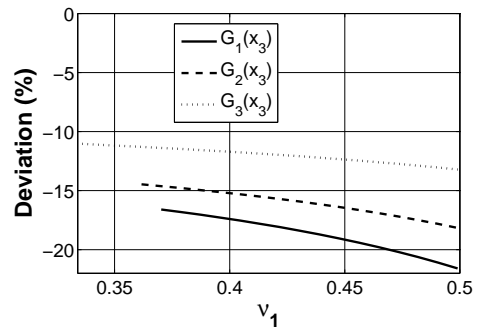
(a) Deviation of singularity frequency



(b) Deviation of singularity frequency



(c) Deviation of frequency of zero point



(d) Deviation of frequency of zero point

Figure 3.22: $\nu_1 = 0.4375$ for figure a, c and $r_s = 1/6$ for figure b, d

Although the deviation of the singularity is not big, often less than 10%, the deviation of the zero point frequency is remarkable. Hence, in practical calculations, we can replace

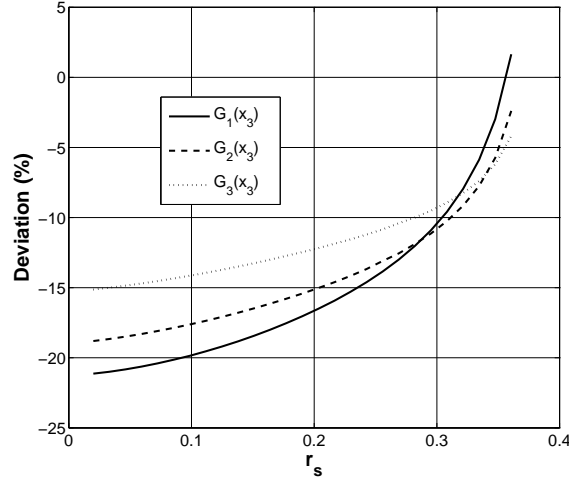


Figure 3.23: Deviation of singularity frequency between the actual model and the simple equivalent model "Layer over half-space" with the average shear wave velocity of the layer is calculated by (3.95)

a complicated inhomogeneous model by a simple homogeneous one with the average shear wave velocity of the layer as in (3.94) if we want to find the singularity with similar results. The equivalent model shows the frequency of the zero point as less than the actual model. As we know that higher r_s reduces the frequency of zero point, we can conclude that the mean of the impedance contrast \bar{r}_s is greater than the actual " r_s ". On the other hand, if we want to use an equivalent homogeneous model for an inhomogeneous actual model, we should take an equivalent impedance contrast which is less than the mean impedance contrast from the real model. Fig. 3.23 is similar to the Fig. 3.22(a) but the average phase velocity of the equivalent simple model is given by formula (3.95). We can see that the deviation between the real model and the equivalent model applying (3.95) is almost double that for the equivalent model applying (3.94). We see the same phenomenon for similar figures with Figs. 3.22(b, c, d). This fact can lead to the conclusion that the first way of taking the average shear velocity for the layer of the simple equivalent model is better than the second way, in that it gives a better approximation of the peak frequency.

3.2.1 Application for synthetic data

To illustrate that we can use the simple model "Layer over half-space" to replace a complex model with reasonable accuracy, we will work on a structure with two homogeneous layers over half-space. Because synthetic H/V -ratio data was used to constrain the velocity solutions from the H/V -ratio inversion, and it agrees well with the observed data curve, especially in the frequency range between the peak and the first trough of the H/V -ratio curve, (Donat Fäh et al. 2002 [17]), we therefore make synthetic data for the H/V -ratio for this model. We assume that this synthetic H/V curve is also of a simple model "one layer over half-space"

	Thickness (m)	P-wave (m/s)	S-wave (m/s)	Density (g/cm ³)
1st layer	7.8	310	193	2
2nd layer	20	1112	694	2
Half-space	0	2961	2086	2

Table 3.3: Parameters for the "two-layer over half-space" model in Liegé, Belgium

with constant parameters, and, by applying some of the maps given above, we obtain results for the simple structure from information about the peak and trough in the synthetic H/V curve. Afterward, we will compare the calculated results with the average actual results.

The parameters of the structure are in Table 3.2.1. These parameters are from the Liege site in Belgium and they are presented in Wathelet 2005 [59]. Synthetic data for H/V -ratio of this model was created by Matthias Ohrnberger in 2007 as presented in Fig. 3.24(a). It shows a clear peak at a frequency of about $f_p = 5.1$ Hz and a trough at about $f_z = 9.8$ Hz. If the thickness of the structure and the average of the shear wave velocity in two layers are derived from the bore-hole cores, we can determine the other parameters from the synthetic H/V -ratio data and our maps. In this case, we assume that the thickness of the layer is $d = d_1 + d_2 = 27.8$ m and the average shear wave velocity is

$$\bar{\beta} = \frac{\beta_1 d_1 + \beta_2 d_2}{d} = 553.43 \text{ (m/s)} .$$

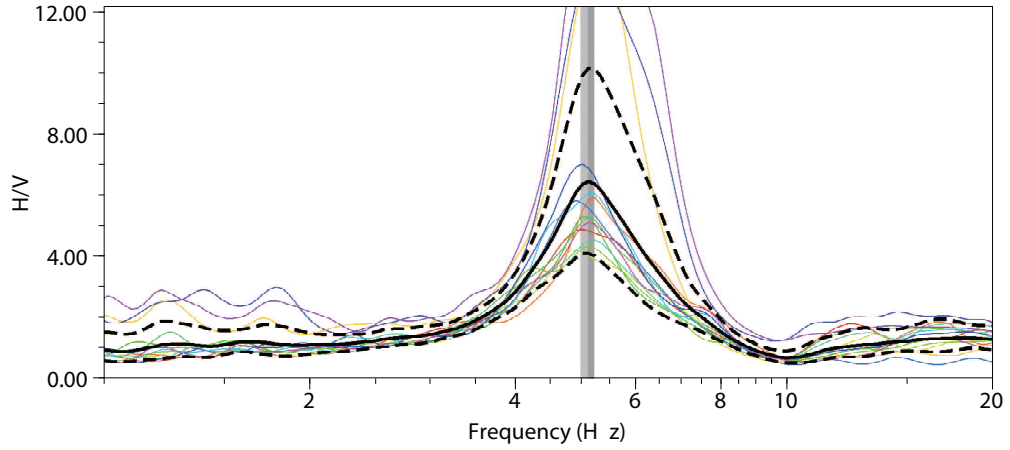
This information gives us the ratio of trough to peak frequency and ratio of the peak frequency to the resonant frequency of the layer as

$$\frac{\bar{f}_z}{\bar{f}_p} = \frac{f_z}{f_p} = 1.9216 \text{ and } \frac{\bar{f}_p}{0.25} = 1.0247$$

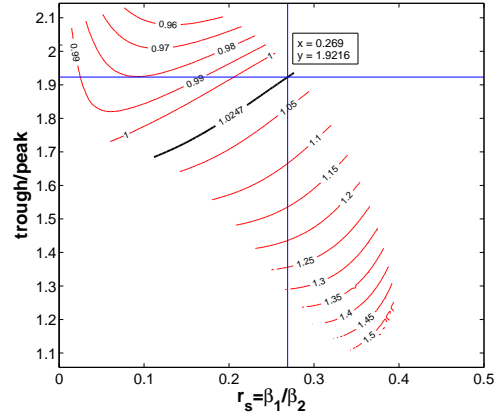
with the dimensionless frequency $\bar{f} = df/\bar{\beta}$. Fig. 3.24(b,c) depicts two maps that are similar to those in Fig. 3.12 and Fig. 3.14(a). They show the contour lines of $\bar{f}_p/0.25$ in relation to \bar{f}_z/\bar{f}_p and Poisson's ratio of the layer ν_1 or S-wave velocity contrast r_s . Comparing the contour line of $\bar{f}_p/0.25 = 1.0247$ and value of $\bar{f}_z/\bar{f}_p = 1.9216$ gives us the value of the Poisson's ratio of the layer as 0.485 and the impedance contrast of the simple model as 0.269. From the parameters of the actual model, we have the average of Poisson's ratio and impedance contrast as 0.4579 and 0.2653, respectively. These values are very close to the results from the maps: the relative error is only 1.3% for Poisson's ratio and 6% for impedance contrast.

3.3 Incident body waves

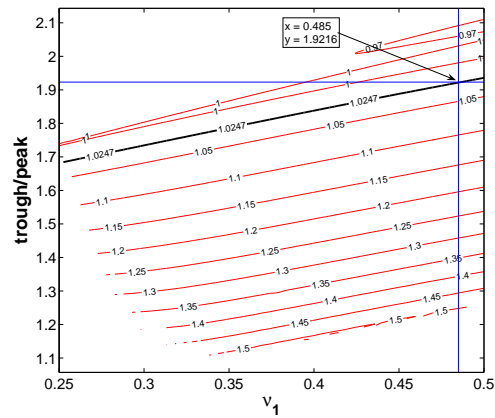
As site amplifications occurring during actual earthquakes essentially involve incoming body waves, it is clear that the horizontal and vertical components of body waves are both highly sensitive to site conditions. The proportion of body wave in the noise wavefield is still unclear



(a) Synthetic spectral ratio Horizontal to Vertical (H/V). Grey bands indicate the average and standard deviation of the frequency peak values observed for each individual time window.



(b) The maps of r_s



(c) The maps of ν_1

Figure 3.24: Synthetic H/V -ratio data and two maps defining the value of Poisson's ratio and S-wave velocity contrast

and is summarized in Bonneyfoy-Claudet et al. (2006) [9]. This depends on the location of the noise source and the distance between the noise source and the receiver. Jerez (2004) [23] compared between microtremor H/V spectral ratio and theoretical results by using the surface forces with the ratio of horizontal to vertical force between 0.75 and 1.5 concluded that: the shape of the Nakamura's ratio appears to be mainly determined by the fundamental and higher Rayleigh modes except around the predominant peak where the Love and body waves have the highest weight. So the main question to address here is the relation between H/V -ratios derived from earthquake recordings and H/V -ratios derived from ambient vibration recordings, especially around the peak frequency.

In this chapter, we continue concern a simple horizontally 2-layered structure with one soft layer over a half-space, and its response to obliquely incident S and P-plane waves. The parameters of the model and the coordinates is shown in Fig. 3.1.

3.3.1 Formulas of H/V -ratios of incident body waves

Incident SV-wave

Suppose that an plane SV wave coming from in deep half-space to the interface between the layer and the half-space. This wave can be expressed in the potential form:

$$\tilde{\psi}_0(x, z) = A_0 \mathbf{d} \exp \left[i k_{SV}^{(H)} (x_1 \sin \theta - x_3 \cos \theta) \right] \quad (3.96)$$

where θ is the incident angle, \mathbf{d} is the vector defining the directions of motion and $k_{SV}^{(H)}$ is the wave number of the incident SV-wave in the half-space. By the reflection and refraction, this incident SV-wave generates the upcoming and down-going systems of P-wave and SV-wave in the layer and down-going systems of P-wave and SV-wave in the half-space. The incident angles of these plane wave systems are based on the Schnell's law and the magnitudes depends on the reflection and refraction ratio and the magnitude of the incidence. Different from the Rayleigh wave which the phase velocity has to be found, the apparent phase velocity for incident SV-wave depends on the incident angle θ and the velocity of SV-wave in half-space β_2 as

$$c = \frac{\beta_2}{\sin \theta} \quad \text{or} \quad C = \frac{c}{\beta_1} = \frac{1}{r_s \sin \theta} \quad (3.97)$$

where β_1 is the S-wave velocity in the layer and $r_s = \beta_1/\beta_2$ is the shear wave velocity contrast. The H/V -ratio formula is found by the potential method which is presented in Appendix 4 and it is

$$\chi_{SV} = i \frac{e_\beta}{e_\alpha} \frac{TS_{SV}}{MS_{SV}} \quad (3.98)$$

with the abbreviations are

$$\begin{aligned} e_\alpha &= \sqrt{1 - C^2 \gamma_1}, \quad e_\beta = \sqrt{1 - C^2}, \\ g_\alpha &= \sqrt{1 - C^2 \gamma_2 r_s^2}, \quad g_\beta = \sqrt{1 - C^2 r_s^2}, \\ h_1 &= e_\beta^2 + 1, \quad h_2 = g_\beta^2 + 1, \quad f_1 = \frac{1}{r_s^2 r_d} \end{aligned}$$

and

$$\begin{aligned}
TS_{SV} &= e_\alpha h_1 (-2 + f_1 h_2) \cosh \left(\frac{2\pi \bar{f} e_\alpha}{C} \right) + 2e_\alpha (h_1 - f_1 h_2) \cosh \left(\frac{2\pi \bar{f} e_\beta}{C} \right) \\
&\quad + g_\alpha \left[h_1 (-2f_1 + h_1) \sinh \left(\frac{2\pi \bar{f} e_\alpha}{C} \right) + 4e_\alpha e_\beta (-1 + f_1) \sinh \left(\frac{2\pi \bar{f} e_\beta}{C} \right) \right], \\
MS_{SV} &= g_\alpha \left[-2e_\beta (2f_1 - h_1) \cosh \left(\frac{2\pi \bar{f} e_\alpha}{C} \right) + 2e_\beta h_1 (-1 + f_1) \cosh \left(\frac{2\pi \bar{f} e_\beta}{C} \right) \right] \\
&\quad + 2e_\alpha e_\beta (-2 + f_1 h_2) \sinh \left(\frac{2\pi \bar{f} e_\alpha}{C} \right) + h_1 (h_1 - f_1 h_2) \sinh \left(\frac{2\pi \bar{f} e_\beta}{C} \right).
\end{aligned}$$

The incident angle should be smaller than the critical angle so that all above wave systems exist. The condition for θ is

$$\sin \theta < \min \left[1/\sqrt{r_s^2}, \sqrt{\gamma_2}, \sqrt{\gamma_1/r_s^2} \right]. \quad (3.99)$$

Because we works on the model of soft layer over half-space or $r_s^2 < 1$, so the condition (3.99) become

$$\sin \theta < \min \left[\sqrt{\gamma_2}, \sqrt{\gamma_1/r_s^2} \right]$$

or

$$C > \max \left[\frac{1}{\sqrt{\gamma_2} r_1}, \frac{1}{\sqrt{\gamma_1}} \right]. \quad (3.100)$$

From the formula of H/V -ratio (3.98), we can realize that when $C > \frac{1}{\sqrt{\gamma_2} r_s}$, g_α becomes an imaginary number and by condition of phase velocity (3.100), H/V -ratio is always a complex value.

Incident P-wave

The P body incident wave has the potential form

$$\tilde{\varphi}_0(x, z) = A_0 \mathbf{d} \exp \left[i k_P^{(H)} (x_1 \sin \theta - x_3 \cos \theta) \right] \quad (3.101)$$

with the apparent phase velocity

$$c = \frac{\alpha_2}{\sin \theta} \quad \text{or} \quad C = \frac{1}{\sqrt{\gamma_2} r_s \sin \theta}. \quad (3.102)$$

By analogy with the SV-wave, we have the formula of H/V -ratio at the surface

$$\chi_P = i \frac{e_\beta}{e_\alpha} \frac{TS_P}{MS_P} \quad (3.103)$$

with the abbreviations are

$$\begin{aligned}
TS_P &= g_\beta \left[2e_\alpha h_1 (-1 + f_1) \cosh \left(\frac{2\pi \bar{f} e_\alpha}{C} \right) - 2e_\alpha (2f_1 - h_1) \cosh \left(\frac{2\pi \bar{f} e_\beta}{C} \right) \right] \\
&\quad + h_1 (h_1 - f_1 h_2) \sinh \left(\frac{2\pi \bar{f} e_\alpha}{C} \right) + 2e_\alpha e_\beta (-2 + f_1 h_2) \sinh \left(\frac{2\pi \bar{f} e_\beta}{C} \right), \\
MS_P &= 2e_\beta (h_1 - f_1 h_2) \cosh \left(\frac{2\pi \bar{f} e_\alpha}{C} \right) + e_\beta h_1 (-2 + f_1 h_2) \cosh \left(\frac{2\pi \bar{f} e_\beta}{C} \right) \\
&\quad + g_\beta \left[4e_\alpha e_\beta (-1 + f_1) \sinh \left(\frac{2\pi \bar{f} e_\alpha}{C} \right) + h_1 (-2f_1 + h_1) \sinh \left(\frac{2\pi \bar{f} e_\beta}{C} \right) \right].
\end{aligned}$$

The condition of θ for every incident angles do not exceed the critical angle is

$$\sin \theta_0 < \min \left[1/\sqrt{\gamma_2}, 1/\sqrt{r_s^2 \gamma_2}, \sqrt{\gamma_1/(r_s^2 \gamma_2)} \right],$$

and due to $\gamma_2, r_s^2 < 1$, so

$$\sin \theta_0 < \frac{\sqrt{\gamma_1}}{r_s \sqrt{\gamma_2}} \quad \text{or} \quad C > \frac{1}{\sqrt{\gamma_1}}. \quad (3.104)$$

In addition, if the incident angle is real then from (3.102) we have

$$C = \frac{1}{\sqrt{\gamma_2} r_s \sin \theta} > \frac{1}{\sqrt{\gamma_2} r_s}, \quad (3.105)$$

which make the final condition of phase velocity is

$$C > \max \left[\frac{1}{\sqrt{\gamma_2} r_s}, \frac{1}{\sqrt{\gamma_1}} \right]. \quad (3.106)$$

This condition is the same with one of SV-wave incidence (3.100).

When $f = 0$

With Rayleigh surface waves, when the frequency equals zero, or $\bar{f} = 0$, the phase velocity becomes the phase velocity of Rayleigh wave of the half-space and the H/V ratio is the H/V ratio of the half-space. However, with body incident wave, the phase velocity is arbitrary; it depends on the incident angle and the type of incident wave. Substituting $\bar{f} = 0$ into the formula of H/V ratio of P-wave (3.103) yields

$$H/V_P|_{\bar{f}=0} = \frac{2g_\beta}{h_2} = \frac{2\sqrt{1 - c^2/\beta_2^2}}{2 - c^2/\beta_2^2}. \quad (3.107)$$

This is exactly the H/V ratio formula for the half-space, but in this case, the phase velocity is not the Rayleigh wave but arbitrary.

By analogy, substitute $\bar{f} = 0$ into (3.98) we gain the H/V ratio of SV incident wave at zero frequency as

$$H/V_{SV}|_{\bar{f}=0} = \frac{h_2}{2g_\alpha} = \frac{2 - c^2/\beta_2^2}{2\sqrt{1 - c^2/\alpha_2^2}}. \quad (3.108)$$

If c takes the value of Rayleigh wave for the half-space, that means it satisfies the Rayleigh equation for the half-space, as

$$h_2^2 - 4g_\alpha g_\beta = 0$$

then the H/V at $\bar{f} = 0$ is the same for both P-wave and SV-wave.

When frequency is large

P-wave

If $C < 1/\sqrt{\gamma_1}$ then

$$H/V_P|_{\bar{f} \rightarrow \infty} = \frac{h_1}{2e_\alpha} = \frac{2 - c^2/\beta_1^2}{2\sqrt{1 - c^2/\alpha_1^2}}. \quad (3.109)$$

And if C takes the value of Rayleigh wave of the layer, that means it satisfies

$$h_1^2 - 4e_\alpha e_\beta = 0$$

then when $\bar{f} \rightarrow \infty$ the H/V of P-wave is the same with Rayleigh wave. If $C > 1/\sqrt{\gamma_1}$ then H/V ratio is a trigonometric function of \bar{f} , so it may have infinity number of changing the sign or number of zero point.

When $C < \sqrt{2}$ then $H/V_P|_{\bar{f} \rightarrow \infty} > 0$ and vice versa.

SV-wave

If $C < 1/\sqrt{\gamma_1}$ then

$$H/V_{SV}|_{\bar{f} \rightarrow \infty} = \frac{h_1}{2e_\alpha} = \frac{2 - c^2/\beta_1^2}{2\sqrt{1 - c^2/\alpha_1^2}}. \quad (3.110)$$

This formula is exactly the one of P-wave incidence.

3.3.2 Real incident angles

We have proved that for both P or SV-incident wave, the condition of phase velocity to satisfy the critical incident angles and being real is

$$C > \max\left[\frac{1}{\sqrt{\gamma_2}r_s}, \frac{1}{\sqrt{\gamma_1}}\right]. \quad (3.111)$$

With this condition of phase velocity C , H/V -ratio of both P and SV-incidences are complex. We will only investigate the real part of H/V -ratio and we will concentrate on the first peak and zero point and compare them to those of Rayleigh wave.

Contrast to Rayleigh wave, the phase velocity in this case is arbitrary, not dependent on frequency, and it depends on the incident angle. The smaller the incident angle is, the

bigger the phase velocity C is and when the incident wave is normal to the interface between layer and half space, the apparent phase velocity tends to infinity. From the formula of the condition for apparent phase velocity (3.111) we can see that, when one of the layer or half space becomes incompressible, that means γ_1 or γ_2 tends to zero, that makes C tends to infinity.

We showed that the Poisson's ratio of half-space ν_2 and densities of mass ratio r_d do not play important role in H/V -ratio of ambient noise. This fact keeps being true with incident body waves, although ν_2 affects on the critical angle, so we will only investigate property of H/V -ratio in dependence with Poisson's ratio of the layer ν_1 and impedance contrast r_s . The incident angle of the incoming body wave depends on the location of the source.

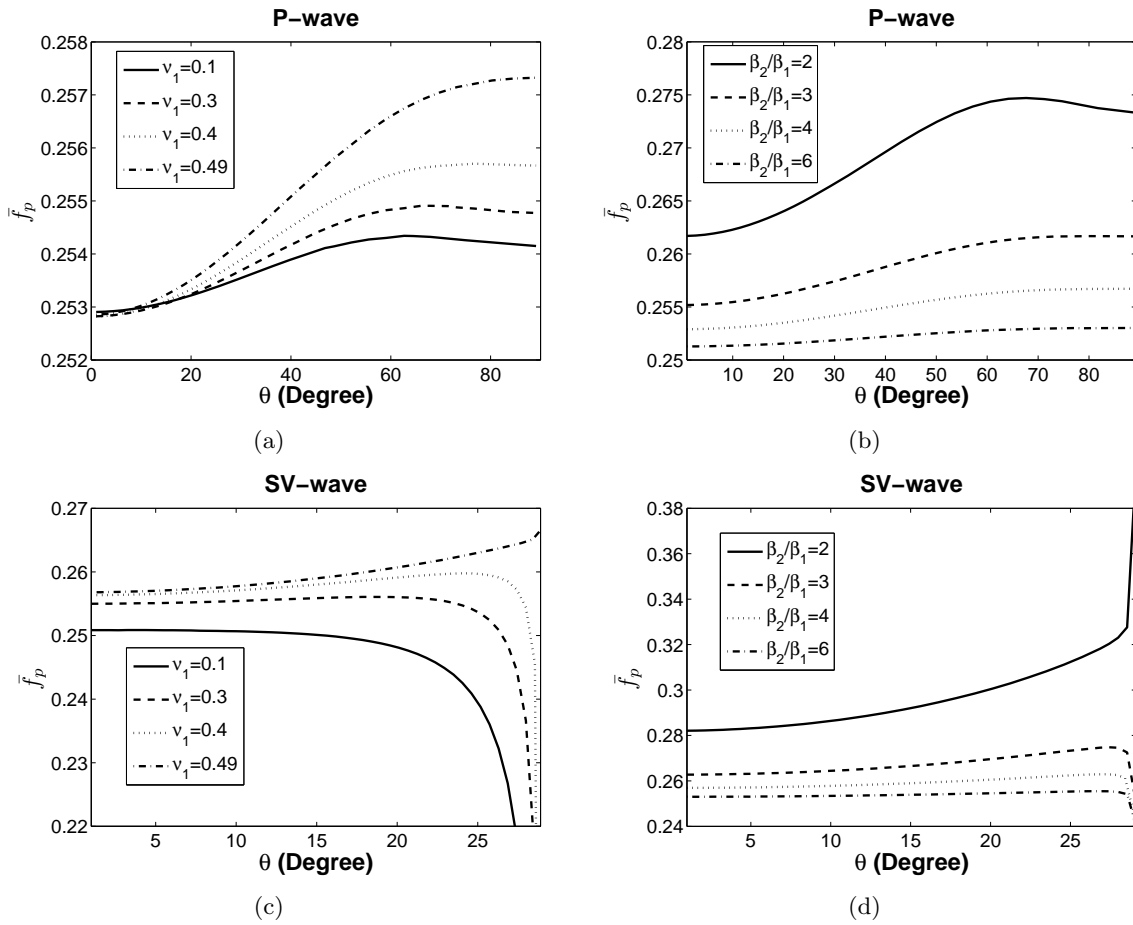
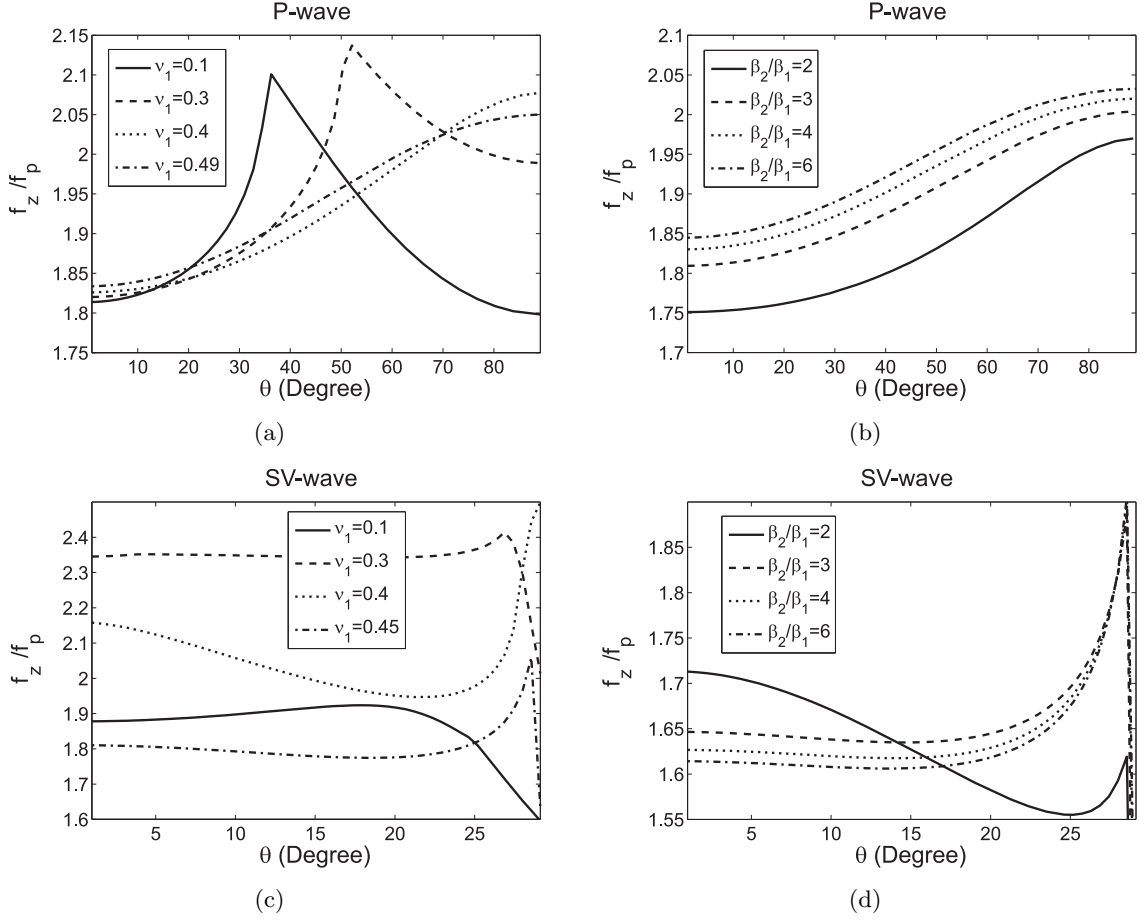


Figure 3.25: Peak frequency of H/V -ratio of incident body waves

With different incident angle, as long as it is less than the critical one, the H/V -ratio on the surface changes its properties. However, the peak and trough frequency are the most important parameter so we will concentrate on their variation. We use parameters of Model 3 (Table 3) with $\nu_1 = 0.4576$, $r_s = 0.2473$, $\nu_2 = 0.3449$, $r_d = 0.7391$. Figure 3.25.a shows the peak frequencies of H/V -ratio of incident P-wave depending on the incident angle with several cases of different $\nu_1 = 0.1, 0.3, 0.4, 0.49$ when we fix other parameters. Figure 3.25.b is similar to 3.25.a but we fix $\nu_1 = 0.4576$ and let the impedance contrast varies. In

Figure 3.26: Ratio between peak and trough frequencies of H/V -ratio of incident body wave

these two figures, the critical angle is approximately 90° and we can see that, in the case of incident P-wave, Poisson's ratio of the layer ν_1 does not affect much on the peak frequency, the maximum relative deviation is only about 2%. However, the impedance contrast has remarkable influence on peak frequency. With high impedance contrast, e.g. $\beta_2/\beta_1 = 6$, peak frequency of H/V -ratio is very close to S-wave resonant frequency of the layer, $\bar{f} = 0.25$, but with low impedance contrast, the different between them can go up to 10%. Figure 3.25.c and 3.25.d have the same manner with 3.25.a and 3.25.b but they show the peak frequency of incident SV-wave instead of P-wave. With incident SV-wave, the critical angle for this model is only approximately 29° and peak frequency changes dramatically when the incident angle is closely near to the critical one. However, if the incident angle is not close to the critical one, e.g. $\theta < 20^\circ$ for this case, the peaks of H/V -ratio curve exhibit at frequency surrounding the S-wave resonant frequency of the layer. Similar to the case of incident P-wave, the Poisson's ratio of the layer does not affect much on the peak frequency but the impedance contrast really does.

The role of the trough frequency in H/V method is remarkable and it has been proven in Konno and Ohmachi (1998) [25] and it is reported that the ratio between the trough and peak frequency to be 2 with high Poisson's ratio ν_1 and high impedance contrast. We can see

this statement again in Fig. 3.26.a and 3.26.b which plot this ratio for incident P-wave. Fig. 3.26.b shows clearly that this ratio reaches closer to value 2 with higher impedance contrast. However, this ratio of incident SV-wave behaves complicatedly and it does not often to be 2. This behaviour can be explained by the fact that, the H/V -ratio curve of incident SV-wave exhibits a very vague minimum point while one of incident P-wave often exhibits a zero point.

3.3.3 The relation between body wave and Rayleigh wave

One of well-known features of Rayleigh surface waves is that: the phase velocity is always less than shear wave of the half-space. If it is not so, there is only the leaking wave which is not interested in this thesis. With this condition, the H/V -ratio of Rayleigh waves is real. We already proved that the H/V -ratios of body incident waves are always complex when the incident angle is satisfied not to exceed the critical one. To get real value of H/V -ratio for body incident waves, some of wave systems in the layer or in the half-space must be vanished. From the formula of H/V -ratio of SV and P-incident wave (3.98) and (3.103) we have the condition of phase velocity for H/V -ratio of SV-incident wave to be real is

$$C < \frac{1}{\sqrt{\gamma_2 r_s}} , \quad (3.112)$$

and of P-wave incident wave is

$$C < \frac{1}{r_s} . \quad (3.113)$$

However, due to the formulas of phase velocity (3.97) and (3.102) of body incident wave, we can not find a real value of incident angles for these conditions. These conditions of phase velocity hold only with imaginary value of incident angles which do not happen in reality. But if we still assume that the incident angles can be imaginary numbers, there is relation among H/V -ratios of Rayleigh waves and body incident waves.

Proposition 4. *At Rayleigh wave velocity C_R , the H/V -ratios of P and SV-incident waves are equal.*

Proof. From the formulas of H/V -ratio of the body waves (3.98) and (3.103) and assume that they are equal, we have

$$\chi_{SV} = \chi_P \quad (3.114)$$

or

$$TS_{SV} \cdot MS_P = TS_P \cdot MS_{SV} . \quad (3.115)$$

But after some simple algebra manipulations, we have

$$TS_{SV} \cdot MS_P - TS_P \cdot MS_{SV} = \Delta(C_R, \bar{f}) \quad (3.116)$$

where $\Delta(C, \bar{f})$ is expressed as in (3.10). Due to

$$\Delta(C, \bar{f}) = 0$$

is the dispersion equation of Rayleigh wave and since C_R is Rayleigh wave so we have

$$TS_{SV} \cdot MS_P - TS_P \cdot MS_{SV} = \Delta(C_R, \bar{f}) = 0$$

or

$$\chi_{SV} = \chi_P . \quad (3.117)$$

□

Proposition 5. *At Rayleigh wave velocity C_R , the H/V -ratio of SV-incident waves equals H/V -ratio of Rayleigh waves.*

Proof. We use the formula χ_1 in (3.40) for H/V -ratio of Rayleigh wave and assume that

$$\chi_1 = \chi_P \quad (3.118)$$

or

$$2e_\beta TS_P \cdot B(C) = h_1 A(C) MS_P . \quad (3.119)$$

But after some simple algebra manipulations, we have

$$2e_\beta TS_P \cdot B(C) - h_1 A(C) MS_P = \frac{2g_\beta}{e_\alpha} \Delta(C, \bar{f}) \quad (3.120)$$

where $\Delta(C, \bar{f})$ is expressed as in (3.10). Due to

$$\Delta(C, \bar{f}) = 0$$

is the dispersion equation of Rayleigh wave and since C_R is Rayleigh wave so we have

$$2e_\beta TS_P \cdot B(C_R) - h_1 A(C_R) MS_P = \frac{2g_\beta}{e_\alpha} \Delta(C_R, \bar{f}) = 0$$

or

$$\chi_1 = \chi_P . \quad (3.121)$$

□

Since at Rayleigh wave phase velocity, all of three formulas of Rayleigh wave, P-wave and SV-wave get the same values, so we can use the H/V -ratio formulas of P and SV-incident body waves for H/V -ratio of Rayleigh surface wave. This kind of connection between body wave incidents and Rayleigh waves has been already reported by Malischewsky 2000 [32] but for the model "homogeneous half-space".

3.4 Conclusions

Because the dispersion equation and H/V -ratio formula for this model depend not only on the Poisson's ratio of the layer, as in model LFB, but also on other parameters such as the impedance contrast, the Poisson's ratio of the half-space and the ratio between the density of mass of the layer and half-space, it becomes difficult to investigate the behaviour of H/V -ratio curve. However, each parameter plays a different role in determining the peak and trough of the H/V -ratio curve, which are the key features used in the H/V method. I have observed that the Poisson's ratio of the half-space and the density ratio do not play an important role in most investigations. This fact has also been noted in some papers, e.g. [35], [38]. However, the Poisson's ratio of the layer ν_1 and the impedance contrast r_s are key parameters affecting the peak and the trough of the H/V -ratio curve. High values are often used for these parameters in practical applications with the assumption that the H/V spectral ratio has a peak and its frequency is very close to the resonant frequency of the layer. In this chapter, I show that this assumption is true, and I find more detailed conditions of ν_1 and r_s for this assumption. Condition (3.47) states when the H/V -ratio curve has singularity and condition (3.52) states when the H/V -ratio has both singularity and zero point. These two conditions help us to divide the domain of ν_1 and r_s into four regions corresponding to four states of the H/V -ratio curve: having two singularities, having two zero points, having one singularity and one zero point and having only maximum and minimum. For each region, the maps of the peak and trough frequencies are made and these maps will help us to find Poisson's ratio ν_1 and impedance contrast r_s from the peaks and troughs in the H/V spectral ratio measured from a single station. From these maps, we confirm that we can consider the frequency of the peak in the H/V spectral ratio to be the resonant frequency of the shear wave in layer with reasonable error if the Poisson's ratio ν_1 is high enough (e.g. greater than 0.4) and the impedance contrast is high. However, if ν_1 is not so high, for example about 0.3, the error becomes remarkable even when impedance contrast is high.

The peak frequency of the H/V -ratio in depths below the surface was also investigated, and found to increase with the depth to the interface. The peak frequency of H/V -ratio curve in the half-space is relatively stable. A figure showing the prograde and retrograde particle motion in the interface is made and we observe that the singularity only exist if $\nu_1 > 0.25$ and with high enough impedance contrast. If the impedance contrast is low, e.g less than 2.5, the H/V -ratio curve in the interface has only zero point without singularity. This conclusion is the same for the H/V -ratio curve in the surface.

For the inhomogeneous layer, we continue to investigate the layer with exponential variation of the shear modulus as in (3.61). By changing the parameters we obtain many types of variation. We particularly study three simple forms of shear modulus in the layer: the linear, the quadratic and the third power polynomial, and compare the effect of the inhomogeneity. Because of the simplicity of the homogeneous layer, we compare the peak and trough frequency of the inhomogeneous case with the that of homogeneous layer which takes the average value of the inhomogeneous model. The deviation between these is good enough for the peak frequency but is too high for the trough. This leads to the conclusion that we can use the simple homogeneous model for the inhomogeneous and apply the above maps we made above to calculate the average value.

The H/V -ratio of the incident body wave is also investigated and it shows that the first peak

frequency is very close to the S-wave resonant frequency of the layer in most cases, especially in the case of high impedance contrast. This conclusion fortifies the H/V method in using the H/V peak frequency to infer the shear wave of the layer. I also prove that when the apparent phase velocity of incident body wave equals Rayleigh wave velocity, the H/V -ratio of these two waves are identical. However, this condition exists only in theoretical manner because the apparent phase velocity of incident body wave is always greater than Rayleigh wave velocity.

Chapter 4

Osculation points

The dispersion curve is a main factor affecting the behaviour of the H/V -ratio. But one set of features, namely the osculation points, has not yet been investigated thoroughly enough with respect to H/V . The osculation point has been investigated in some papers such as Okal (1978) [45], Thomas Forbriger (2003) [18]. In this thesis, I have found the following important phenomenon: at the osculation point the H/V -ratio changes its property from having two peaks to having one peak and one zero-point. This phenomenon is proven analytically for the model "layer with fixed bottom" and checked numerically for the model "layer over half-space". That is why it is important to carefully study the osculation point of the dispersion curve. In this chapter, we use ray theory to demonstrate the existence of the three most important and interesting classes of osculation points for the model "Layer with fixed bottom". The formulae are analytically proven and are simple enough for practical calculations. It turns out that the number of osculation points is infinite. While the fundamental mode has only one osculation point, the higher modes often have more than one. For the model "layer over half-space", an approximate formula for the osculation points is presented.

4.1 Layer with fixed bottom

Tolstoy and Usdin [56] investigated the dispersion equation by ray theory. Corresponding to the model "Layer with fixed bottom" they gave the secular equation as

$$y = \frac{-2t_1x \pm \sqrt{4t_1^2x^2 - (1+x^2)^2 + t_2^2(1-x^2)^2}}{(1+x^2) + t_2(1-x^2)} \quad (4.1)$$

where

$$x = \tan\left(\frac{kdg_\beta}{2}\right) = \tan\left(\frac{\bar{f}\pi g_\beta}{C}\right), \quad y = \tan\left(\frac{kdg_\alpha}{2}\right) = \tan\left(\frac{\bar{f}\pi g_\alpha}{C}\right), \quad (4.2)$$

$$g_\alpha = \sqrt{C^2\gamma - 1}, \quad g_\beta = \sqrt{C^2 - 1}, \quad (4.3)$$

$$t_1 = \frac{(1 - g_\beta^2)^2 + 4g_\alpha^2g_\beta^2}{4g_\alpha g_\beta(1 - g_\beta^2)}, \quad t_2 = \frac{(1 - g_\beta^2)^2 + 4}{4(1 - g_\beta^2)}. \quad (4.4)$$

In (4.1), the sign (+) corresponds to non-retrograde motion, which they called M2 mode, and the sign (-) corresponds to M1 mode.

The osculation point is the point at which two modes M1 and M2 meet each other. From this condition we obtain the equations defining the osculation points

$$4t_1^2x^2 - (1+x^2)^2 + t_2^2(1-x^2)^2 = 0 \quad (4.5)$$

and

$$y = \frac{-2t_1x}{(1+x^2) + t_2(1-x^2)} . \quad (4.6)$$

Eq. (4.5) leads to

$$(t_2^2 - 1)x^4 + 2x^2(2t_1^2 - t_2^2 - 1) + (t_2^2 - 1) = 0 . \quad (4.7)$$

This is a quadratic equation of x^2 , and we have

$$\Delta' = (2t_1^2 - t_2^2 - 1)^2 - (t_2^2 - 1)^2 = 4(t_1^2 - 1)(t_1^2 - t_2^2) . \quad (4.8)$$

The condition for (4.7) having a solution is $\Delta' \geq 0$, but we will determine the special solution of (4.7) corresponding to $\Delta' = 0$ or

$$\begin{cases} t_1^2 = t_2^2 \\ t_1^2 = 1 . \end{cases} \quad (4.9)$$

4.1.1 The case: $t_1^2 = t_2^2$

If $t_1^2 = t_2^2$, (4.7) becomes

$$(t_2^2 - 1)x^4 + 2x^2(t_2^2 - 1) + (t_2^2 - 1) = 0 . \quad (4.10)$$

1. If $t_1^2 = t_2^2 \neq 1$,
(4.10) leads to: $(x^2 + 1)^2 = 0 \Rightarrow x^2 = -1 \Rightarrow \tan(sh/2) = \pm i \Rightarrow sh/2 = \pm i\infty$. It is nonsense.

2. If $t_1^2 = t_2^2 = 1$,

- if $t_2 = 1$

$$\begin{aligned} \Rightarrow (1 - g_\beta^2)^2 + 4 &= 4 - 4g_\beta^2 \Rightarrow (1 - g_\beta^2)^2 + 4g_\beta^2 = 0 \\ \Rightarrow (2 - C^2)^2 + 4C^2 - 4 &= 0 \Rightarrow C^4 + 2C^2 = 0 \Rightarrow C = 0 \end{aligned}$$

It is nonsense.

- if $t_2 = -1$

$$\begin{aligned} \Rightarrow (1 - g_\beta^2)^2 + 4 &= -4 + 4g_\beta^2 \Rightarrow (2 - C^2)^2 - 4C^2 + 12 = 0 \\ \Rightarrow C^4 - 8C^2 + 16 &= 0 \Rightarrow C = 2. \end{aligned}$$

Substituting $C = 2$ into t_1 in (4.4) we get:

$$\begin{aligned}
 t_1 &= \frac{6\gamma - 1}{-\sqrt{3}\sqrt{4\gamma - 1}} = \pm 1 \\
 &\Rightarrow 36\gamma^2 - 12\gamma + 1 = 3(4\gamma - 1) \Rightarrow (3\gamma - 1)^2 = 0 \Rightarrow \gamma = 1/3 \\
 &\Rightarrow y = \frac{1}{x} \Rightarrow x \cdot y = 1 \Rightarrow \tan\left(\frac{\bar{f}\pi g_\alpha}{C}\right) \tan\left(\frac{\bar{f}\pi g_\beta}{C}\right) = 1 \\
 &\Rightarrow \frac{\bar{f}\pi(g_\alpha + g_\beta)}{C} = \pi \left(k + \frac{1}{2}\right) \Rightarrow \bar{f} = \frac{\sqrt{3}}{2} \left(k + \frac{1}{2}\right), \quad k = 0, 1, 2, \dots
 \end{aligned}$$

Finally, the formula of osculation points in this case is

$$C = 2, \quad \bar{f} = \frac{\sqrt{3}}{2} \left(k + \frac{1}{2}\right) \quad k = 0, 1, 2, \dots \quad (4.11)$$

When $\gamma = 1/3$ or $\nu = 0.25$, the phase velocity curve has an infinite osculation point. The osculation point of the fundamental mode belongs to this class corresponding to $k = 0$ or $\bar{f} = \sqrt{3}/4$. This point was discussed by Sezawa and Kanai [51] when they investigated the discontinuity in the dispersion curves of Rayleigh waves of the model LOH having a ratio of the rigidity of the layer to the substrate of $1/\infty$. This paper showed that the fundamental mode and the first higher mode of phase velocity curves are discontinuous, but if the discontinuous part of one curve joins to the other, it becomes continuous. Okal [45] also discussed this problem, and dealt with it by redefining the fundamental mode not by the minimum phase velocity value condition, but by the continuous of the derivative of the phase velocity curve. With this criterion, we accept that the two curves of two modes can cross each other.

4.1.2 The case: $t_1^2 = 1, t_2^2 \neq 1$

From formula of t_1 (4.4) we have:

$$\begin{aligned}
 [(1 - g_\beta^2)^2 + 4g_\alpha^2 g_\beta^2]^2 &= 16g_\alpha^2 g_\beta^2 (1 - g_\beta^2)^2 \\
 &\Rightarrow (1 - g_\beta^2)^2 = 4g_\alpha^2 g_\beta^2 \\
 &\Rightarrow (2 - C^2)^2 = 4(C^2 - 1)(C^2 \gamma - 1) \\
 &\Rightarrow C^2 = \frac{4\gamma}{4\gamma - 1}.
 \end{aligned}$$

The condition for an existent solution is $\gamma > 1/4$. This is the condition for $C^2 > 0$.

From (4.7) $\Rightarrow x^2 = 1$, and from (4.4) $\Rightarrow t_1 = \text{sign}(2\gamma - 1)$, and because $\gamma < 1/2$, therefore $t_1 = -1$.

From (4.6) and because $x^2 = 1 \Rightarrow y = -t_1 x = x = \pm 1$. From formulas of x and y (4.2) and because of $g_\alpha > g_\beta$, we obtain:

$$\begin{cases} \frac{\bar{f}\pi}{C} g_\alpha = \frac{\pi}{4} + k\pi \\ \frac{\bar{f}\pi}{C} g_\beta = \frac{\pi}{4} + k\pi + l\pi \end{cases} \quad (k = 0, 1, 2, \dots, l = 1, 2, \dots) \quad (4.12)$$

or

$$\begin{cases} \frac{\bar{f}\pi}{C}g_\alpha = -\frac{\pi}{4} + k\pi \\ \frac{\bar{f}\pi}{C}g_\beta = -\frac{\pi}{4} + k\pi + l\pi \end{cases} \quad (k = 1, 2, \dots, l = 1, 2, \dots). \quad (4.13)$$

4.1.3 Solutions of (4.12)

From condition $\gamma > 1/4$, we can limit the value of k and l . From g_α and g_β in (4.12), we have

$$\frac{g_\beta}{g_\alpha} = \sqrt{\frac{C^2 - 1}{C^2\gamma - 1}} = \frac{1 + 4(k + l)}{1 + 4k}$$

and because $C^2 = 4\gamma/(4\gamma - 1)$ we obtain:

$$\frac{1}{(1 - 2\gamma)^2} = \left(\frac{1 + 4(k + l)}{1 + 4k} \right)^2. \quad (4.14)$$

With the condition that $1/4 < \gamma < 1/2$

$$\begin{aligned} \Rightarrow 0 < (1 - 2\gamma)^2 &\leq \frac{1}{4} \Rightarrow 2 \leq \frac{1 + 4(k + l)}{1 + 4k} < +\infty \\ \Rightarrow \frac{4l}{1 + 4k} &> 1 \Rightarrow l > k + \frac{1}{4} \quad (k = 0, 1, 2, \dots). \end{aligned}$$

From (4.14)

$$\Rightarrow \gamma = \frac{2l}{1 + 4(k + l)} \Rightarrow C = \sqrt{\frac{4\gamma}{4\gamma - 1}} = \sqrt{\frac{8l}{4(l - k) - 1}}$$

and from the formula for g_α in (4.12), we obtain: $\bar{f} = \sqrt{l(1 + 4k + 4l)}/2$.
The general solution of (4.12) is

$$\begin{cases} l > k + \frac{1}{4} \quad (k = 0, 1, 2, \dots) \\ \gamma = \frac{2l}{1 + 4(k + l)}, \quad C = \sqrt{\frac{8l}{4(l - k) - 1}}, \quad \bar{f} = \sqrt{\frac{l(1 + 4k + 4l)}{2}}. \end{cases} \quad (4.15)$$

4.1.4 Solution of (4.13)

Analogous with (4.13), the solution of (4.13) is:

$$\begin{cases} l > k - \frac{1}{4} \quad (k = 1, 2, 3, \dots) \\ \gamma = \frac{2l}{4(k + l) - 1}, \quad C = \sqrt{\frac{8l}{4(l - k) + 1}}, \quad \bar{f} = \sqrt{\frac{l(4k + 4l - 1)}{2}} \end{cases} \quad (4.16)$$

Proposition 6. *The set of solutions of the second class is dense in $(0, 1/3)$ of Poisson's ratio interval.*

Proof. For every value of $0.25 < \gamma < 0.5$ (or $0 < \nu < 1/3$), we can find a pair of integers (k_n, l_n) ($n \in \mathbb{R}$) with $k_n < l_n$ satisfying

$$\gamma_n = \frac{2l_n}{1 + 4(k_n + l_n)} \Rightarrow \gamma \text{ when } n \Rightarrow +\infty$$

because of the fact that the rational set Q is dense in irrational set R . \square

For example, if $\gamma = \sqrt{2}/5$, we can choose $k_n = 7678$ and $l_n = 10000$, and then $|\gamma - \gamma_n| < 10^{-5}$. However, this osculation point belongs to a very high mode which does not exist in practice. Rather, we can consider the Poisson's ratio of the layer to be a simple rational number, and we will always find a reasonable k_n and l_n so that $\gamma = \gamma_n$.

4.1.5 Numerical results

With $k = 0$, $l = 1$ in (4.15) we have

$$\gamma = \frac{2}{5}, C = \sqrt{\frac{8}{3}}, \bar{f} = \frac{\sqrt{10}}{2} = 1.5811,$$

and with $k = 1$, $l = 3$ in (4.16) we have

$$\gamma = \frac{2}{5}, C = \sqrt{\frac{8}{3}}, \bar{f} = \frac{\sqrt{10}}{2} = 1.8708.$$

We can easily observe that there is some pair of (k, l) values in (4.15) and (4.16) which give the same γ and C but different \bar{f} . Thus, for such values of γ , the phase velocity curves have more than one osculation point.

4.1.6 Get the Tolstoy's formula again from LBF's secular equation

The secular equation of the model LFB is

$$A_0(C) + B_0(C) \sin(g_\alpha dk) \sin(g_\beta dk) + C_0(C) \cos(g_\alpha dk) \cos(g_\beta dk) = 0 \quad (4.17)$$

where $A_0(C)$, $B_0(C)$ and $C_0(C)$ are presented in (2.14). We denote

$$y = \tan(g_\alpha dk/2), \quad x = \tan(g_\beta dk/2)$$

and we have

$$A_0(C) + B_0(C) \frac{2y}{1+y^2} \frac{2x}{1+x^2} + C_0(C) \frac{1-y^2}{1+y^2} \frac{1-x^2}{1+x^2} = 0 \quad (4.18)$$

or

$$\begin{aligned} & y^2 [(A_0(C) - C_0(C)) + (A_0(C) + C_0(C))x^2] \\ & + 2y [2xB_0(C)] + [A_0(C) + C_0(C) + x^2(A_0(C) - C_0(C))] = 0. \end{aligned} \quad (4.19)$$

This is a quadric equation of variable y and its solution is

$$y = \frac{-2xB_0(C) \pm \sqrt{\delta'}}{[A_0(C) - C_0(C)] + [A_0(C) + C_0(C)]x^2} \quad (4.20)$$

with

$$\begin{aligned} \delta' = & 4x^2 B_0(C)^2 - (A_0(C)^2 - C_0(C)^2)(1 + x^4) \\ & + x^2 [(A_0(C) - C_0(C))^2 + (A_0(C) + C_0(C))^2]. \end{aligned} \quad (4.21)$$

Denote

$$t1 = B_0(C)/C_0(C), \quad t2 = -C_0(C)/A_0(C)$$

and note that $\gamma = \frac{1+g_\alpha^2}{1+g_\beta^2}$ so we can again get formula (4.1).

4.2 Osculation points of LOH

Similar to the model LFB, we can obtain the equations defining two modes M_1 and M_2 of the dispersion curves for model LOH as in [56]. However, these two equations are both complicated and cumbersome, and it is almost impossible to get such simple formulas defining the osculation point as we have in the model LFB. In this section, we will use our observation regarding the special property of the osculation point to find such a formula. The key property is that the H/V -ratio changes from having two singularities to having one singularity and one zero point at the osculation point. This property is analytically proven for model LFB and numerically checked for model LOH.

Fig. 3.8 shows the domain of Poisson's ratio ν_1 and impedance contrast r_s for the four states of the H/V -ratio. From the above observation, we can see that the curve Z_1O is the collection of the osculation points because it is the border of the region R_1 and R_2 . This curve is a part of curve Z_1Z_2 for which the formula is presented in (3.52). Our problem here is that we have to find the coordinate of the point O which is the upper bound of curve Z_1O . This point separates the curve Z_1Z_2 into Z_1O and the curve OZ_2 which is a collection of points with similar properties to those of the osculation point. At these similar points, the H/V -ratio changes its state from having one singularity to having two zero points. Let ν_0 be the Poisson's ratio value of the point O . The set of osculation points (ν_1^0, r_s^0) of model LOH is presented as

$$\begin{aligned} r_s^0 &= C(\nu_2, r_d) \arctan [D(\nu_2, r_d)(\nu_1^0 - 0.25)] \\ \nu_1^0 &< \nu_0 \end{aligned} \quad (4.22)$$

with the auxiliary functions

$$\begin{aligned} C(\nu_2, r_d) &= 0.3058 - 0.0471 r_d + 0.0092 r_d^2 - 0.0839 \nu_2 + 0.2918 r_d \nu_2 \\ &\quad - 0.2673 r_d^2 \nu_2 + 0.1538 \nu_2^2 - 0.6098 r_d \nu_2^2 + 0.5056 r_d^2 \nu_2^2, \\ D(\nu_2, r_d) &= 65.9858 - 91.2188 r_d + 47.6980 r_d^2 + 137.1766 \nu_2 - 342.7329 r_d \nu_2 \\ &\quad + 249.2955 r_d^2 \nu_2 + 67.7489 \nu_2^2 + 223.5938 r_d \nu_2^2 - 253.4675 r_d^2 \nu_2^2. \end{aligned}$$

The condition $\nu_1^0 < \nu_0$ is similar to the condition of $0 < \nu < 1/3$ in model LFB. For model LOH, the value of ν_0 depends on Poisson's ratio of the half-space ν_2 and the density ratio r_d . By numerical calculation, we can represent the function $\nu_0(r_d, \nu_2)$ in a simple form,

$$\nu_0(r_d, \nu_2) = 0.3019 + 0.0511 r_d - 0.0183 \nu_2 - 0.0444 r_d \nu_2 , \quad (4.23)$$

which shows very good accuracy – about 2 percent error – in the domain of $0.3 < r_d < 0.9$ and $0 < \nu_2 < 0.5$. The maximum and minimum values of function $\nu_0(r_d, \nu_2)$ are 0.353 and 0.2929, respectively. These values are very close to $1/3 = 0.333$, which is the upper bound of ν in model LFB.

General conclusions and perspectives

In the framework of investigating the ellipticity of Rayleigh surface waves, the objective of this thesis was to improve some aspects of the theoretical basis of the H/V method. The H/V -method, based on ambient noise recordings, has become more and more popular over the last decades, as it offers a convenient, practical and low-cost tool to be used in urbanized areas. The simple horizontal-to-vertical Fourier amplitude spectral ratio is used to determine site response parameters. Although the theoretical basis of this method is still unclear, the ability of the H/V -method to provide a reliable information related to site response has been repeatedly shown in the past (Nakamura, 1989 [40]; Lachet and Bard, 1994 [29]; Kudo, 1995 [27]; Bard, 1998 [4]). In this thesis, considering that the most dominant contributions to ambient vibrations are known to come from surface waves, although the exact composition may change depending on the particular site, I study characteristics of the ellipticity of Rayleigh waves which are actually analysed in the H/V -method. Studying the ellipticity of Rayleigh waves gives a better fundamental theoretical understanding about this method.

In studying this issue, several models with increasing complexity have been investigated. Although the real model is very complicated, in some cases it can be approximated by a simpler model which makes it easier to study. This observation has been reported in Fäh et al. (2001) [16]. In this thesis, I begin from the simplest model “homogeneous half-space” and worked up to the model “inhomogeneous layer over half-space”, which is nearest to reality, and tried to answer the following questions:

1. What is the relationship between the H/V peak frequency and the peak frequency of the transmission response of a medium where the shakeability of the site would be expected to be enhanced? Under what conditions is it allowed to assume their approximate equivalence?
2. What is the role of the trough frequency in the H/V spectral ratio to the H/V -method, and how can it be used?
3. When does the H/V -ratio curve have a sharp peak, and when only a broad maximum point? When does it have both a sharp peak and a clear trough? Which parameters affect most this character?
4. What is the frequency bound of the prograde particle motion?

5. How the inhomogeneity affects on the peak and trough frequency of the H/V -ratio curve compare to the homogeneous case?
6. What (primarily) controls the variation of phase velocity at zero frequency? When the phase velocity curve has osculation points?
7. How does the incident body wave affect the H/V -ratio?

The most prominent of the above questions is that of the relationship between the H/V peak frequency and the S-wave resonant frequency of the layer, and when we can assume their approximate equivalence. These questions turn out to be surprisingly challenging theoretically, even for very simple models and they have only rarely been addressed in the literature (e. g. Malischewsky and Scherbaum, 2004 [35], Malischewsky et al., 2008 [38]). In this thesis, by studying the ellipticity of the model “layer with fixed bottom”, I analytically prove that we can approximate the S-wave resonant frequency of the layer with the H/V peak frequency when the impedance contrast between the layer and the substrate is high enough. This conclusion has been noted in numerical calculations and recorded data such as in Tokimatsu 1997 [55], Scherbaum et al. 2002 [49], Parolai et al. 2004 [46], Bonnefoy-Claudet et al. 2006 [9], Souriau et al. 2007 [3]. However, when the impedance of the layer and the substrate is not so high, the relationship between the H/V peak frequency and the S-wave resonant frequency of the layer becomes much more complicated. In this case, we can not simply assume that they are approximately equal. I found that this relationship is sensitive to Poisson’s ratio of the layer and the variation of the impedance contrast; however, it only depends slightly on Poisson’s ratio of the half-space and the density of mass. In this thesis, I present some maps showing this relationship in dependence on the key parameters. From these maps, we can infer the S-wave resonant frequency of the layer from peak frequency of H/V spectral ratio.

The role of the trough frequency has been reported to be useful and applicable as in Konno and Ohmachi (1998) [25]. In this thesis, I integrate trough frequency information along with peak frequency information into one map in dependence on key parameter such as Poisson’s ratio of the layer or impedance contrast. From these maps, I propose a way to infer the Poisson’s ratio of the layer and the impedance contrast by observing informations from the H/V spectral ratio.

The maps considered above are not only for the cases in which the H/V -ratio curve has singularities and zero-points, but also for the cases in which it has maximum and minimum points. I also present in this thesis two simple functions of model parameters classifying when the H/V -ratio curve has sharp peaks or a only broad maximum point, and when it has a zero-point or only minimum points. These functions were determined by enormous numerical calculations, but they show a very good approximation.

The singularity and zero-point frequencies are associated with the particle motion in the sense that the direction of this motion changes at these frequencies. With the simple model “homogeneous half-space”, it is well-known that the motion of a particle at the surface is always retrograde. The prograde motion starts to be observed in the model “layer with fixed bottom”, which is a special case of the more general model “layer over half-space” when the impedance contrast is very high. By studying this model, I found the bound of the prograde motion frequency band in relation to the thickness and shear wave velocity of the layer. These bound frequency values depend on Poisson’s ratio of the layer, and can be used to infer this

ratio.

If the layer is inhomogeneous, in some cases, we can approximate this inhomogeneous layer with a simple homogeneous layer without any great difference in the peak frequency of the H/V -ratio curve. In this thesis, I only consider the inhomogeneous layer in which the shear modulus varies while the other parameters remain constant. The simple homogeneous replaced layer takes an equivalent shear modulus which can be calculated either by the mean of the shear wave velocity or by the mean travel time of the S-wave in the layer. I illustrate that taking the equivalent shear modulus by the first method gives a better approximation of the peak frequency than is given by the second method.

The phase velocity is a key factor affecting the H/V -ratio, and it is well-known that at the zero frequency, the phase velocity takes on the characteristics of the Rayleigh wave of the half-space. The slope of the phase velocity at zero frequency decides whether it decreases or increases at this frequency. In this thesis, I present a simple formula of this slope dependent on different parameters. However, only the impedance contrast and Poisson's ratio of the layer and half-space affect the sign of the slope, and we can easily use this formula to determine that the surface wave will exhibit normal, anomalous or no dispersion at the zero frequency.

The osculation point is a special feature of the phase velocity curve where two separate modes seem to meet each other. I find a special property of the H/V -ratio of fundamental mode at this point: the H/V -ratio curve changes its property from having two singularities to having one singularity and one zero point. This property is analytically proven in the simple model "layer with fixed bottom" and numerically illustrated in model "layer over half-space". I also present the exact formulae of the three most interesting classes of osculation points of the model "layer with fixed bottom" and an approximated formula of the osculation point for the model "layer over half-space".

Although it is not the aim of this thesis to resolve questions about the content of ambient noise (body waves and surface waves), I also study the effects of body waves on the H/V spectral ratio. It turns out that, the first peak frequency of H/V -ratio contributed by the incident body wave is very near to the S-wave resonant frequency of the layer in most the cases. I also found that the H/V -ratio of incident body wave becomes identical with that of the Rayleigh wave if their velocities are equal. This happens only in theory, because the apparent velocity of the incident body wave is always greater than those of the Rayleigh surface waves.

These are the main results which I obtain in this thesis. However, there are many problems which are not addressed in this thesis, and could be addressed and resolved in the future. The first that I would mention here is the determination of the first higher mode. Although the peak frequency of the first higher mode is presented in this thesis by a simple formula for the model "layer with fixed bottom", there has been nothing achieved for the model "layer over half-space". This problem should be solved in the future because the first higher mode affects the H/V spectral ratio in some cases such as in Konno and Ohmachi (1998) [25], in which it was reported that the H/V spectral ratio does not show a clear trough because the peak frequency of the first higher mode is close to the trough frequency of the fundamental mode, and it may contribute some energy to the H/V spectral ratio.

The second issue is that we approximate a complex inhomogeneous layer by a homogeneous layer with the equivalent shear modulus calculated by taking the mean shear wave in the whole

layer. However, this procedure can only be applied when the other parameters are constant. If they are not, we need to find a better procedure to find the equivalent parameters in order to use all results of simple model “homogeneous layer over half-space” which were found in this thesis.

The last issue which I can address here is: in some cases, the model “layer over half-space” is not enough to explain the more complicated H/V spectral ratio which has, for example, more than one peak and more than one zero point. We need a more complex model to explain this phenomenon such as “two layers over half-space”. Although this model is complicated to investigate, the model “two layers with fixed bottom” is simple enough to do, and the knowledge of this model can give us a general look on the more complex model. One example for this model is to solve the problem of velocity inversion when the shear wave velocity does not increase with depth as in typical case but decrease with depth. We can have this situation when a hard thin artificial layer lies on soft soil, as is very popular in urban areas.

Appendix

Appendix 1

By substituting the auxiliary $A_0(C)$, $B_0(C)$ and $C_0(C)$ from (2.14) into the secular equation (2.12) we have

$$\Delta(C, \bar{f}) = (1 + g_\alpha^2)\Delta_1(C, \bar{f}) + \gamma\Delta_2(C, \bar{f}) \quad (4.24)$$

with

$$\Delta_1(C, \bar{f}) = -2g_\alpha g_\beta + (-1 + g_\beta^2) [\sin(g_\alpha dk) \sin(g_\beta dk) - g_\alpha g_\beta \cos(g_\alpha dk) \cos(g_\beta dk)] \quad (4.25)$$

and

$$\begin{aligned} \Delta_2(C, \bar{f}) = & -2g_\alpha g_\beta (-3 + g_\beta^2) [1 - \cos(g_\alpha dk) \cos(g_\beta dk)] \\ & + [2 + (-2 + 4g_\alpha^2)g_\beta^2] \sin(g_\alpha dk) \sin(g_\beta dk) . \end{aligned} \quad (4.26)$$

Because $\chi_2(C, \bar{f}) = 0$ and $\chi_3(C, \bar{f}) = 0$ and from their formulas (2.33)-(2.34) we have

$$\sin(g_\alpha dk) = \frac{2g_\alpha g_\beta}{-1 + g_\beta^2} \sin(g_\beta dk) , \quad (4.27)$$

$$\cos(g_\alpha dk) = -\frac{2}{-1 + g_\beta^2} \cos(g_\beta dk) . \quad (4.28)$$

Substituting $\sin(g_\alpha dk)$ and $\cos(g_\alpha dk)$ from (4.27) into $\Delta_1(C, \bar{f})$ (4.25) and $\Delta_2(C, \bar{f})$ (4.26) yields

$$\Delta_1(C, \bar{f}) = -2g_\alpha g_\beta [1 - \sin^2(g_\beta dk) - \cos^2(g_\beta dk)] = 0 \quad (4.29)$$

and

$$\Delta_2(C, \bar{f}) = -\frac{8g_\alpha g_\beta C^2}{-1 + g_\beta^2} [\gamma(1 - C^2) + C^2/4 - \cos^2(g_\beta dk)(g(1 - C^2) + 1)] . \quad (4.30)$$

In (2.41) we have

$$\cos^2(g_\beta dk) = \frac{\gamma(1 - C^2) + C^2/4}{\gamma(1 - C^2) + 1} \quad (4.31)$$

which gives $\Delta_2(C, \bar{f}) = 0$. Thus, $\Delta(C, \bar{f}) = 0$.

Appendix 2

Because $1/\chi_2(C, \bar{f}) = 0$ and $1/\chi_3(C, \bar{f}) = 0$ and from their formulas (2.33)-(2.34) we have

$$\sin(g_\beta dk) = \frac{2g_\alpha g_\beta}{-1 + g_\beta^2} \sin(g_\alpha dk) , \quad (4.32)$$

$$\cos(g_\beta dk) = -\frac{2}{-1 + g_\beta^2} \cos(g_\alpha dk) . \quad (4.33)$$

Substituting $\sin(g_\beta dk)$ and $\cos(g_\beta dk)$ from (4.32) into $\Delta_1(C, \bar{f})$ (4.25) and $\Delta_2(C, \bar{f})$ (4.26) yields

$$\Delta_1(C, \bar{f}) = -2g_\alpha g_\beta [1 - \sin^2(g_\alpha dk) - \cos^2(g_\alpha dk)] = 0 \quad (4.34)$$

and

$$\Delta_2(C, \bar{f}) = -\frac{8g_\alpha g_\beta C^2}{-1 + g_\beta^2} [\gamma(1 - C^2) + C^2/4 - \cos^2(g_\alpha dk)(\gamma(1 - C^2) + 1)] . \quad (4.35)$$

In (2.47) we have

$$\cos^2(g_\alpha dk) = \frac{\gamma(1 - C^2) + C^2/4}{\gamma(1 - C^2) + 1} \quad (4.36)$$

which gives $\Delta_2(C, \bar{f}) = 0$. Thus, $\Delta(C, \bar{f}) = 0$.

Appendix 3

The normalized horizontal displacement amplitude of the layer in LOH is given by given by

$$\tilde{U}_1^{(1)}(x_3) = \frac{N(x_3)}{H(x_3)} \quad (4.37)$$

where

$$N(x_3) = e_\beta N_1 \cosh(e_\beta k x_3) + N_2 \cosh(e_\alpha k x_3) + N_3 \sinh(e_\beta k x_3) + N_4 \sinh(e_\alpha k x_3) \quad (4.38)$$

for

$$\begin{aligned} N_{10} &= 2e_\alpha g_\beta (-2 + h_2) h_1^2 , \\ N_{11} &= 8e_\alpha^2 g_\beta (-2 + h_2) e_\beta , \\ N_{12} &= h_1^2 (4f_1 g_\alpha g_\beta - 2g_\alpha g_\beta h_1 + h_1 h_2 - f_1 h_2^2) , \\ N_{13} &= -4e_\alpha e_\beta (4f_1 g_\alpha g_\beta - 2g_\alpha g_\beta h_1 + h_1 h_2 - f_1 h_2^2) , \\ N_{14} &= -2e_\alpha g_\beta h_1^2 (-2 + h_2) , \\ N_1 &= N_{10} + N_{11} \sinh(de_\alpha k) \sinh(de_\beta k) + N_{12} \sinh(de_\alpha k) \cosh(de_\beta k) \\ &\quad + N_{13} \cosh(de_\alpha k) \sinh(de_\beta k) + N_{14} \cosh(de_\alpha k) \cosh(de_\beta k) , \end{aligned}$$

$$\begin{aligned}
N_{20} &= 4h_1 e_\alpha e_\beta g_\beta (-2 + h_2) , \\
N_{21} &= g_\beta (-2 + h_2) h_1^3 , \\
N_{22} &= -e_\beta h_1^2 (4(-1 + f_1) g_\alpha g_\beta + h_2(2 - f_1 h_2)) , \\
N_{23} &= 2e_\alpha e_\beta^2 (4(-1 + f_1) g_\alpha g_\beta + h_2(2 - f_1 h_2)) , \\
N_{24} &= -4e_\alpha e_\beta g_\beta h_1 (-2 + h_2) , \\
N_2 &= N_{20} + N_{21} \sinh(de_\alpha k) \sinh(de_\beta k) + N_{22} \sinh(de_\alpha k) \cosh(de_\beta k) \\
&\quad + N_{23} \cosh(de_\alpha k) \sinh(de_\beta k) + N_{24} \cosh(de_\alpha k) \cosh(de_\beta k) ,
\end{aligned}$$

$$\begin{aligned}
N_{30} &= 2e_\alpha e_\beta^2 h_1 (4(-1 + f_1) g_\alpha g_\beta + h_2(2 - f_1 h_2)) , \\
N_{31} &= e_\beta h_1^2 (4f_1 g_\alpha g_\beta - 2g_\alpha g_\beta h_1 + h_1 h_2 - f_1 h_2^2) , \\
N_{32} &= 8e_\alpha^2 e_\beta^2 g_\beta (-2 + h_2) , \\
N_{33} &= -2e_\alpha e_\beta g_\beta h_1^2 (-2 + h_2) , \\
N_{34} &= 4e_\alpha e_\beta^2 (-4f_1 g_\alpha g_\beta + 2g_\alpha g_\beta h_1 - h_1 h_2 + f_1 h_2^2) , \\
N_3 &= N_{30} + N_{31} \sinh(de_\alpha k) \sinh(de_\beta k) + N_{32} \sinh(de_\alpha k) \cosh(de_\beta k) \\
&\quad + N_{33} \cosh(de_\alpha k) \sinh(de_\beta k) + N_{34} \cosh(de_\alpha k) \cosh(de_\beta k) ,
\end{aligned}$$

$$\begin{aligned}
N_{40} &= 2e_\beta h_1 (4f_1 g_\alpha g_\beta - 2g_\alpha g_\beta h_1 + h_1 h_2 - f_1 h_2^2) , \\
N_{41} &= 4e_\alpha e_\beta^2 (4(-1 + f_1) g_\alpha g_\beta + h_2(2 - f_1 h_2)) , \\
N_{42} &= -4e_\alpha e_\beta g_\beta h_1 (-2 + h_2) , \\
N_{43} &= g_\beta h_1^3 (-2 + h_2) , \\
N_{44} &= e_\beta h_1^2 (4(-1 + f_1) g_\alpha g_\beta + h_2(2 - f_1 h_2)) , \\
N_4 &= N_{40} + N_{41} \sinh(de_\alpha k) \sinh(de_\beta k) + N_{42} \sinh(de_\alpha k) \cosh(de_\beta k) \\
&\quad + N_{43} \cosh(de_\alpha k) \sinh(de_\beta k) + N_{44} \cosh(de_\alpha k) \cosh(de_\beta k) ,
\end{aligned}$$

and

$$\begin{aligned}
H &= -e_\alpha (-2 + h_1) (H_1 \cosh(de_\alpha k) + H_2 \cosh(de_\beta k) \\
&\quad + H_3 \sinh(de_\alpha k) + H_4 \sinh(de_\beta k))
\end{aligned} \tag{4.39}$$

for

$$\begin{aligned}
H_1 &= -2e_\beta (4f_1 g_\alpha g_\beta - 2g_\alpha g_\beta h_1 + h_1 h_2 - f_1 h_2^2) , \\
H_2 &= e_\beta h_1 (4(-1 + f_1) g_\alpha g_\beta + h_2(2 - f_1 h_2)) , \\
H_3 &= 4e_\alpha e_\beta g_\beta (-2 + h_2) , \\
H_4 &= -h_1^2 g_\beta (-2 + h_2) .
\end{aligned}$$

The vertical displacement amplitude is given by:

$$\tilde{U}_3^{(1)}(x_3) = \frac{K(x_3)}{H(x_3)} \tag{4.40}$$

where

$$K(x_3) = K_1 \cosh(e_\beta k x_3) + e_\alpha K_2 \cosh(e_\alpha k x_3) + K_3 \sinh(e_\beta k x_3) + K_4 \sinh(e_\alpha k x_3) \quad (4.41)$$

for

$$\begin{aligned} K_{10} &= 2h_1 e_\alpha e_\beta (4(-1 + f_1)g_\alpha g_\beta + h_2(2 - f_1 h_2)) , \\ K_{11} &= h_1^2 (4f_1 g_\alpha g_\beta - 2g_\alpha g_\beta h_1 + h_1 h_2 - f_1 h_2^2) , \\ K_{12} &= 8e_\alpha^2 e_\beta g_\beta (-2 + h_2) , \\ K_{13} &= -2e_\alpha g_\beta h_1^2 (-2 + h_2) , \\ K_{14} &= -4e_\alpha e_\beta (4f_1 g_\alpha g_\beta - 2g_\alpha g_\beta h_1 + h_1 h_2 - f_1 h_2^2) , \\ K_1 &= K_{10} + K_{11} \sinh(de_\alpha k) \sinh(de_\beta k) + K_{12} \sinh(de_\alpha k) \cosh(de_\beta k) \\ &\quad + K_{13} \cosh(de_\alpha k) \sinh(de_\beta k) + K_{14} \cosh(de_\alpha k) \cosh(de_\beta k) , \end{aligned}$$

$$\begin{aligned} K_{20} &= 2e_\beta h_1 (4f_1 g_\alpha g_\beta - 2g_\alpha g_\beta h_1 + h_1 h_2 - f_1 h_2^2) , \\ K_{21} &= 4e_\alpha e_\beta^2 (4(-1 + f_1)g_\alpha g_\beta + h_2(2 - f_1 h_2)) , \\ K_{22} &= -4e_\alpha e_\beta g_\beta h_1 (-2 + h_2) , \\ K_{23} &= g_\beta h_1^3 (-2 + h_2) , \\ K_{24} &= -e_\beta h_1^2 (4(-1 + f_1)g_\alpha g_\beta + h_2(2 - f_1 h_2)) , \\ K_2 &= K_{20} + K_{21} \sinh(de_\alpha k) \sinh(de_\beta k) + K_{22} \sinh(de_\alpha k) \cosh(de_\beta k) \\ &\quad + K_{23} \cosh(de_\alpha k) \sinh(de_\beta k) + K_{24} \cosh(de_\alpha k) \cosh(de_\beta k) , \end{aligned}$$

$$\begin{aligned} K_{30} &= 2e_\alpha g_\beta h_1^2 (-2 + h_2) , \\ K_{31} &= 8e_\alpha^2 g_\beta (-2 + h_2) , \\ K_{32} &= h_1^2 (4f_1 g_\alpha g_\beta - 2g_\alpha g_\beta h_1 + h_1 h_2 - f_1 h_2^2) , \\ K_{33} &= 4e_\alpha e_\beta (-4f_1 g_\alpha g_\beta + 2g_\alpha g_\beta h_1 - h_1 h_2 + f_1 h_2^2) , \\ K_{34} &= -2e_\alpha g_\beta h_1^2 (-2 + h_2) , \\ K_3 &= K_{30} + K_{31} \sinh(de_\alpha k) \sinh(de_\beta k) + K_{32} \sinh(de_\alpha k) \cosh(de_\beta k) \\ &\quad + K_{33} \cosh(de_\alpha k) \sinh(de_\beta k) + K_{34} \cosh(de_\alpha k) \cosh(de_\beta k) , \end{aligned}$$

$$\begin{aligned} K_{40} &= 4e_\alpha^2 e_\beta g_\beta h_1 (-2 + h_2) , \\ K_{41} &= e_\alpha g_\beta h_1^3 (-2 + h_2) , \\ K_{42} &= e_\alpha e_\beta h_1^2 (4(-1 + f_1)g_\alpha g_\beta + h_2(2 - f_1 h_2)) , \\ K_{43} &= 4e_\alpha^2 e_\beta^2 (4(-1 + f_1)g_\alpha g_\beta + h_2(2 - f_1 h_2)) , \\ K_{44} &= -4e_\alpha^2 e_\beta g_\beta h_1 (-2 + h_2) , \\ K_4 &= K_{40} + K_{41} \sinh(de_\alpha k) \sinh(de_\beta k) + K_{42} \sinh(de_\alpha k) \cosh(de_\beta k) \\ &\quad + K_{43} \cosh(de_\alpha k) \sinh(de_\beta k) + K_{44} \cosh(de_\alpha k) \cosh(de_\beta k) . \end{aligned}$$

The normalized horizontal displacements in the half-space is

$$\tilde{U}_1^{(2)}(x_3) = -e^{(g_\alpha + g_\beta)kx_3} \frac{T(x_3)}{M} \frac{D}{H(x_3)f_1} \quad (4.42)$$

where

$$\begin{aligned} M = & M_0 + M_1 \sinh(de_\alpha k) \sinh(de_\beta k) + M_2 \sinh(de_\alpha k) \cosh(de_\beta k) \\ & + M_3 \cosh(de_\alpha k) \sinh(de_\beta k) + M_4 \cosh(de_\alpha k) \cosh(de_\beta k) \end{aligned} \quad (4.43)$$

for

$$\begin{aligned} M_0 = & -2e_\alpha e_\beta h_1 (2 + h_1 - 2f_1 h_2) , \\ M_1 = & 4e_\alpha^2 e_\beta^2 (-2 + f_1 h_2) + h_1^2 (-h_1 + f_1 h_2) , \\ M_2 = & 4e_\alpha^2 e_\beta g_\beta (-2 + h_1) , \\ M_3 = & -e_\alpha g_\beta (-2 + h_1) h_1^2 , \\ M_4 = & -e_\alpha e_\beta [-4h_1 + 4f_1 h_2 + h_1^2 (-2 + f_1 h_2)] \end{aligned}$$

and

$$\begin{aligned} D = & D_0 + D_1 \sinh(de_\alpha k) \sinh(de_\beta k) + D_2 \sinh(de_\alpha k) \cosh(de_\beta k) \\ & + D_3 \cosh(de_\alpha k) \sinh(de_\beta k) + D_4 \cosh(de_\alpha k) \cosh(de_\beta k) \end{aligned} \quad (4.44)$$

for

$$\begin{aligned} D_0 = & 4e_\alpha e_\beta g_\beta h_1 (-2h_1 + f_1(2 + h_1)) , \\ D_1 = & g_\beta (16e_\alpha^2 e_\beta^2 (-1 + f_1) + (2f_1 - h_1)h_1^3) , \\ D_2 = & -e_\beta f_1 (-2 + h_1) h_1^2 h_2 , \\ D_3 = & 4e_\alpha e_\beta^2 f_1 (-2 + h_1) h_2 , \\ D_4 = & -4e_\alpha e_\beta g_\beta h_1 (-2h_1 + f_1(2 + h_1)) \end{aligned}$$

and

$$T(x_3) = T_1 e^{g_\beta k x_3} + T_2 g_\beta e^{g_\alpha k x_3} \quad (4.45)$$

for

$$\begin{aligned} T_{10} = & -2e_\alpha e_\beta h_1 (2 + h_1 - 2f_1 h_2) , \\ T_{11} = & 4e_\alpha^2 e_\beta^2 (-2 + f_1 h_2) + h_1^2 (-h_1 + f_1 h_2) , \\ T_{12} = & 4e_\alpha^2 e_\beta g_\beta (-2 + h_1) , \\ T_{13} = & -e_\alpha g_\beta (-2 + h_1) h_1^2 , \\ T_{14} = & e_\alpha e_\beta [4h_1 - 4f_1 h_2 + h_1^2 (2 - f_1 h_2)] , \\ T_1 = & T_{10} + T_{11} \sinh(de_\alpha k) \sinh(de_\beta k) + T_{12} \sinh(de_\alpha k) \cosh(de_\beta k) \\ & + T_{13} \cosh(de_\alpha k) \sinh(de_\beta k) + T_{14} \cosh(de_\alpha k) \cosh(de_\beta k) , \end{aligned}$$

$$\begin{aligned}
T_{20} &= 2e_\alpha e_\beta g_\alpha h_1 (2 - 4f_1 + h_1) , \\
T_{21} &= -g_\alpha [8e_\alpha^2 e_\beta^2 (-1 + f_1) + (2f_1 - h_1)h_1^2] , \\
T_{22} &= -4e_\alpha^2 e_\beta (-2 + h_1) , \\
T_{23} &= e_\alpha (-2 + h_1)h_1^2 , \\
T_{24} &= 2e_\alpha e_\beta g_\alpha [-h_1(2 + h_1) + f_1(4 + h_1^2)] , \\
T_2 &= T_{20} + T_{21} \sinh(de_\alpha k) \sinh(de_\beta k) + T_{22} \sinh(de_\alpha k) \cosh(de_\beta k) \\
&\quad + T_{23} \cosh(de_\alpha k) \sinh(de_\beta k) + T_{24} \cosh(de_\alpha k) \cosh(de_\beta k) .
\end{aligned}$$

Vertical displacement in the half-space is given by

$$\tilde{U}_3^{(2)}(x_3) = e^{(g_\alpha + g_\beta)kx_3} \frac{K(x_3)}{M} \frac{D}{H(x_3)f_1} \quad (4.46)$$

where

$$K = T_1 e^{g_\beta kx_3} g_\alpha + T_2 e^{g_\alpha kx_3} . \quad (4.47)$$

Appendix 4: Incident SV-wave

By reflection and refraction, the SV incident wave generates the upward and downward systems of P-wave and SV-wave in the layer and downward systems of P-wave and SV-wave in the half-space. Hence, the expression of complex amplitudes of potentials in the layer are

$$\Phi^H(x_3) = L_1 \sinh(p_1 x_3) + L_2 \cosh(p_1 x_3) , \quad (4.48)$$

$$\Psi^H(x_3) = L_3 \sinh(q_1 x_3) + L_4 \cosh(q_1 x_3) \quad (4.49)$$

and in the half-space

$$\Phi^L(x_3) = A_1 \exp(-p_2 x_3) , \quad (4.50)$$

$$\Psi^L(x_3) = A_2 \exp(-q_2 x_3) + A_0 \exp(q_2 x_3) \quad (4.51)$$

for

$$p_1 = ke_\alpha , \quad q_1 = ke_\beta ,$$

$$p_2 = kg_\alpha , \quad q_2 = kg_\beta .$$

The amplitude of displacements in the layer are

$$U_1^{(L)}(x_3) = ik\Phi^{(L)}(x_3) - \frac{d\Psi^{(L)}(x_3)}{dx_3} , \quad (4.52)$$

$$U_3^{(L)}(x_3) = \frac{d\Phi^{(L)}(x_3)}{dx_3} + ik\Psi^{(L)}(x_3) \quad (4.53)$$

and in the half-space

$$U_1^{(H)}(x_3) = ik\Phi^{(H)}(x_3) - \frac{d\Psi^{(H)}(x_3)}{dx_3} , \quad (4.54)$$

$$U_3^{(H)}(x_3) = \frac{d\Phi^{(H)}(x_3)}{dx_3} + ik\Psi^{(H)}(x_3) . \quad (4.55)$$

The amplitude of stresses in layer can be expressed due to amplitudes of displacement as

$$S_{31}^{(L)} = \rho_1 \beta_1^2 \left[\frac{dU_1^{(L)}}{dx_3} + ikU_3^{(L)} \right], \quad (4.56)$$

$$S_{33}^{(L)} = \rho_1 \alpha_1^2 \left[\frac{dU_3^{(L)}}{dx_3} + ik(1 - 2\gamma_1)U_1^{(L)} \right] \quad (4.57)$$

and in half-space as

$$S_{31}^{(H)} = \rho_2 \beta_2^2 \left[\frac{dU_1^{(H)}}{dx_3} + ikU_3^{(H)} \right], \quad (4.58)$$

$$S_{33}^{(H)} = \rho_2 \alpha_2^2 \left[\frac{dU_3^{(H)}}{dx_3} + ik(1 - 2\gamma_1)U_1^{(H)} \right]. \quad (4.59)$$

The boundary conditions are free at the surface of the layer, and the continuity of the displacements and stresses between the layer and half-space at the interface are given by

$$S_{31}^{(L)}(-d) = S_{33}^{(L)}(-d) = 0$$

and

$$U_1^{(L)}(0) = U_1^{(H)}(0),$$

$$U_3^{(L)}(0) = U_3^{(H)}(0),$$

$$S_{13}^{(L)}(0) = S_{13}^{(H)}(0),$$

$$S_{33}^{(L)}(0) = S_{33}^{(H)}(0).$$

By substituting the displacement and stress formulas of the layer and half-space into these six boundary conditions yields, after some simple algebraic modification:

$$[M][l] = [n] \quad (4.60)$$

with vector $[l] = [L_1, L_2, L_3, L_4, A_1, A_2]'$, which is a column vector of the unknown integration constants. The matrix $[M]$ with the size 6×6 is

$$\begin{bmatrix} 2ie_\alpha \cosh(e_\alpha dk) & -2ie_\alpha \sinh(e_\alpha dk) & h_1 \sinh(e_\beta dk) & -h_1 \cosh(e_\beta dk) & 0 & 0 \\ -h_1 \sinh(e_\alpha dk) & h_1 \cosh(e_\alpha dk) & 2ie_\beta \cosh(e_\beta dk) & -2ie_\beta \sinh(e_\beta dk) & 0 & 0 \\ 0 & i & -e_\beta & 0 & -i & -g_\beta \\ e_\alpha g_\beta & 0 & 0 & ig_\beta & g_\beta g_\alpha & -ig_\beta \\ 2ie_\alpha g_\beta & 0 & 0 & -h_1 g_\beta & 2if_1 g_\beta g_\alpha & f_1 g_\beta h_2 \\ 0 & h_1 & 2ie_\beta & 0 & -f_1 h_2 & 2if_1 g_\beta \end{bmatrix} \quad (4.61)$$

and the column vector $[n]$ is

$$[n] = A_0 \cdot [0, 0, -g_\beta, ig_\beta, -f_1 g_\beta h_2, 2if_1 g_\beta]'. \quad (4.62)$$

The H/V ratio is formulated by

$$\begin{aligned}\chi_{SV} &= \frac{U_1^{(L)}(-d)}{U_3^{(L)}(-d)} \\ &= \frac{iL_2 \cosh(e_\alpha dk) - e_\beta L_3 \cosh(e_\beta dk) - iL_1 \sinh(e_\alpha dk) + e_\beta L_4 \sinh(e_\beta dk)}{e_\alpha L_1 \cosh(e_\alpha dk) + iL_4 \cosh(e_\beta dk) - e_\alpha L_2 \sinh(e_\alpha dk) - iL_3 \sinh(e_\beta dk)}. \quad (4.63)\end{aligned}$$

The integration constants L_1, L_2, L_3, L_4 can be found in relation to A_0 by (4.60). After substituting these into (4.63) we obtain the H/V ratio formula for the incident SV body wave as in (3.98).

Bibliography

- [1] Achenbach J. D. (1973). *Wave Propagation in Elastic Solids*, North-Holland Publishing Company.
- [2] Aki K., Paul G. Richards (2002). *Quantitative Seismology*. University Science Books.
- [3] Annie Souriau, Agathe Roulle, Christian Ponsolles (2007). Site effects in the city of Lourdes, France, from H/V measurements: Implications for seismic-risk evaluation, *Bulletin of the Seismological Society of America*, Vol. 97, No. 6, 2118-2136.
- [4] Bard P.Y. (1998). Microtremor measurement: a tool for site effect estimation?. In: Irikura, K., Kudo, K., Okada, H. and Sasatani, T., Editors, 1998. The Effects of Surface Geology on Seismic Motion, Balkema, Rotterdam, Yokohama, December 13, 1998, pp. 1251-1279.
- [5] Baron C., A.L. Shuvalov, O. Poncelet (2007). Impact of localized inhomogeneity on the surface-wave velocity and bulk-wave reflection in solids, *Ultrasonics* 46, 1-12.
- [6] Ben-Menahem A., S. J. Singh (1981). *Seismic Waves and Sources*, Springer-Verlag, New York.
- [7] Bergman L., *Ultrasonic and the Scientific*, John Wiley Sons, New York, 1948.
- [8] Bonnefoy-Claudet S., C. Cornou, M. Ohrnberger, M. Wathelet, P.-Y. Bard, F. Cotton, and D. Fäh (2004). H/V ratio and seismic noise wavefield, *Geophysical Research Abstracts*, 6, EGU04-A-05057.
- [9] Bonnefoy-Claude S., Cecile Cornou, Pierre-Yves Bard, Fabrice Cotton, Peter Moczo, Jozef Kristek, Donat Fäh (2006). H/V ratio: a tool for site effects evaluation. Results from 1-D noise simulations, *Geophys. J. Int.*, 1-11.
- [10] Bonnefoy-Claudet S., Fabrice Cotton, Pierre-Yves Bard (2006). The nature of noise wavefield and its applications for site effects studies: A literature review, *Earth-Science Reviews* 79, 205-227.
- [11] Bonnefoy-Claudet S., A. Köhler, C. Cornou, M. Wathelet, and P.-Y. Bard (2008). Effects of Love waves on microtremor H/V ratio. *Bulletin of the Seismological Society of America* 98(1), pp. 288-300.

- [12] Bovik P. (1996). A comparison between the Tiersten model and $O(h)$ boundary conditions for elastic surface waves guided by thin layers, *ASME J. Appl. Mech.* Vol. 63, 162-167.
- [13] Capon J. (1969). High-resolution frequency-wavenumber spectrum analysis, *Proc. IEEE*, 57, 1408-1418.
- [14] Dao Huy Bich (2000). *Elasticity Theory*, (in Vietnamese), Hanoi National University Publishing House.
- [15] Delgado J., C. Lpez Casado, A. Estvez, J. Giner, A. Cuenca, S. Molina (2006). Mapping soft soils in the Segura river valley (SE Spain): a case study of microtremors as an exploration tool, *Journal of Applied Geophysics* 45, 19-32.
- [16] Donat Fh, Fortunat Kind and Domenico Giardini (2001). A theoretical investigation of average H/V ratios, *Geophys. Int.* 145, 535-549.
- [17] Donat Fh, Fortunat Kind and Domenico Giardini (2002). Inversion of local S-wave velocity structures from average H/V ratios, and their use for the estimation of site-effects, *Journal of Seismology* 7, 449-467.
- [18] Forbriger T. (2003). Inversion of shallow-seismic wavefields: I. Wavefield transformation, *Geophysical Journal International*, 153, 719-734.
- [19] Giese P. (1957). Determination of elastic properties and thickness of friable soils by using special Rayleigh waves (in German), *Gerl. Beitr. Geophysik* 66, 274-312.
- [20] Giuseppe Di Giulio, Cecile Cornou, Matthias Ohrnberger, Marc Wathelet, Antonio Rovelli (2006). Deriving wavefield characteristics and shear-velocity profiles from two dimensional small-aperture arrays analysis of ambient vibrations in a small-size alluvial basin, Colfiorito, Italy, *Bulletin of the Seismological Society of American*, Vol. 96, No. 5, 1915-1933.
- [21] Haghshenas E., P.-Y. Bard, N. Theodulidis, SESAME WP04 Team (2008). Empirical evaluation of microtremor H/V spectral ratio, *Bull Earthquake Eng* (2008) 6: 75-108.
- [22] Herrmann R. B. (1994). Computer programs in seismology, vol IV, St Louis University.
- [23] Jerez A. G., M. Navarro, F. Luzon (2004). Comparison between microtremor H/V spectral ratio and theoretical results by using a surface wave scheme, [At http://www.esc-web.org/papers/potsdam_2004/scf_3-jerez.pdf]
- [24] Kaufman A.A., Levshin A.L. (2005). *Acoustic and Elastic Wave Fields in Geophysics III*, Elsevier.
- [25] Konno K. and Ohmachi T. (1998). Ground-motion characteristics estimated from spectral ratio between horizontal and vertical components of microtremor. *Bull. Seism. Soc. Am.*, 88, 228-241.

- [26] Kreyszig E. (1983). *Advanced Engineering Mathematics*, Wiley, New York.
- [27] Kudo K. (1995). Practical estimates of site response. State-of-art report, *Proceedings of the fifth International Conference on Seismic Zonation*, Nice, France.
- [28] Kundu T., (2004). *Ultrasonic Nondestructive Evaluation*, CRC Press, London.
- [29] Lachet C., Bard P.-Y. (1994). Numerical and theoretical investigations on the possibilities and limitations of Nakamura's technique, *Journal of Physics of the Earth* 42 (4), 377-397.
- [30] Love A.E.H. (1911). *Some Problems of Geodynamics*, Cambridge University Press, Cambridge (republished by Dover, New York, 1967).
- [31] Malischewsky P. G. (1987). *Surface Waves and Discontinuities*, Amsterdam, Elsevier.
- [32] Malischewsky P. G. (2000). Some special solutions of Rayleigh's equation and the reflections of body waves at a free surface, *Geofísica Internacional*, Vol. 39,2, pp. 155-160.
- [33] Malischewsky P. G., Frank Wuttke, Albrecht Ziegert (2002). Use of acoustic surface waves for non-destructive material testing (in German), *Thüringer Werkstofftag*, Verlag Dr. Köster, Berlin 2002.
- [34] Malischewsky P. G. (2004). A note on Rayleigh-wave velocities as a function of the material parameters, *Geofísica Internacional* 45, 507-509.
- [35] Malischewsky P.G., Frank Sherbaum (2004). Love's formula and H/V-ratio (ellipticity) of Rayleigh waves, *Wave Motion* 40, 57-67.
- [36] Malischewsky P. G., C. Lomnitz, F. Wuttke, R. Saragoni (2006). Prograde Rayleigh-wave motion in the valley of Mexico, *Geofísica Internacional* 45, 149-162.
- [37] Malischewsky P. G. (2008). The ellipticity of Rayleigh waves at infinitive depth, *Geofísica Internacional* 47(1), 77-79.
- [38] Malischewsky P.G., Frank Scherbaum, Cinna Lomnitz, Tran Thanh Tuan, Frank Wuttke, Gadi Shamir (2008). The domain of existence of prograde Rayleigh-wave particle motion for simple models, *Wave Motion* 45, 556-564.
- [39] Margery Newlands, Robert Stoneley (1950). Rayleigh waves in a two-layer heterogeneous medium, *Geophysical Journal International*, Vol. 6, 109-124.
- [40] Nakamura Y. (1989). A method for dynamic characteristics estimation of sub-surface using microtremor on the ground surface, *Quarterly Report of Railway Technical Research Institute (RTRI)* Vol. 30, No. 1, 25-33.

- [41] Nakamura Y. (1996). Real-time information systems for hazards mitigation, *Proceedings of the 11th World Conference on Earthquake Engineering*, Aca-pulco, Mexico.
- [42] Nakamura Y. (2000). Clear identification of fundamental idea of Nakamura's technique and its applications, *Proceeding of the 12th World Conference on Earthquake Engineering*, Auckland, New Zealand.
- [43] Narayan J. P. (2002). H/V ratio and amplification factor: a numerical experiment using 2.5D modelling, *GEOFIZIKA*, Vol. 18-19, 1-16.
- [44] Nogoshi M., Igarashi T. (1971). On the amplitude characteristics of microtremor (part2), *Journal of Seismological Society of Japan* 24, 26-40 (In Japanese with English abstract).
- [45] Okal E.A. (1978). A physical classification of the Earth's spheroidal modes, *J. Phys. Earth* 26, 75-103.
- [46] Parolai S., Sandra M. Richwalski, Claus Milkereit, Peter Mormann (2004). Assessment of the stability of H/V spectral ratios from ambient noise and comparison with earthquake data in the Cologne area (Germany), *Tectonophysics* 390, 57-73.
- [47] Petermans T., Xavier Devleeschouwer, Franck Pouriel, Phillipe Rosset (2006). Mapping the local seismic hazard in the urban area of Brussels, Belgium, *IAEG2006* Paper number 424, 1-11.
- [48] Pham Chi Vinh, P. G. Malischewsky (2006). Explanation for Malischewsky's approximate expression for the Rayleigh wave velocity, *Ultrasonics* 45, 77-81.
- [49] Scherbaum F., Klaus-G. Hinzen and Matthias Ohrnberger (2002). Determination of shallow shear wave velocity profiles in the Cologne, Germany area using ambient vibrations, *Geophys. J. Int.* 152, 597-612.
- [50] Scherbaum F., K. G. Hinzen, and M. Ohrnberger (2003). Determination of shallow shear wave velocity profiles in the Cologne Germany area using ambient vibrations, *Geophysical Journal International*, 152, 597-612.
- [51] Sezawa K., K. Kanai (1935). Discontinuity in the dispersion curves of Rayleigh waves, *Bull. Earthquake Res.* Vol. XIII, 237-243.
- [52] Shuvalov A. L., A.G. Every (2002). Some properties of surface acoustic waves in anisotropic coated solids studied by the impedance method, *Wave Motion* 36, 257-273.
- [53] Stephenson W. R (2003). Factors bounding prograde Rayleigh-wave particle motion in a soft-soil layer. *Pacific Conference on Earthquake Engineering*, 13-15 February, Christchurch, New Zealand.
- [54] Tiersten H. F. (1969). Elastic surface waves guided by thin films, *J. Appl. Phys.* Vol. 40, 770-790.

- [55] Tokimatsu K. (1997). Geotechnical site characterization using surface waves, *Earthquake Geotechnical Engineering*, Ishihara (ed.), Balkema, Rotterdam, ISBN 905410578X, 1333-1367.
- [56] Tolstoy I., Eugene Usdin (1953). Dispersive properties of stratified elastic and liquid media: A ray theory, *Geophysics* 18, 844-870.
- [57] Vrettos CH. (1990). In-plane vibrations of soil deposits with variable shear modulus: I. Surface waves, *International journal for numerical and analytical methods in geomechanics*, Vol. 14, 209-222.
- [58] Vrettos CH. (1990). In-plane vibrations of soil deposits with variable shear modulus: II. Line load, *International journal for numerical and analytical methods in geomechanics*, Vol. 14, 649-662.
- [59] Wathelet M. (2005). Array recordings of ambient vibrations: surface-wave inversion. *PhD thesis from University of Lige*, Belgium, 177 pages.[Available at: <http://marc.geopsy.org/publications.html>]
- [60] Wathelet M., Jongmans D., Ohrnberger M., Bonnefoy-Claudet S. (2008). Array performances for ambient vibrations on a shallow structure and consequences over V_s inversion, *J. Seismol.*, 12, 1-19.

Curriculum Vitae

Personal details

Name: Tran Thanh Tuan

Date of birth: September 09, 1980

Place of birth: Hanoi, Vietnam

Nationality: Vietnamese

Marital status: Married, 1 child

Education

09/1986-09/1991 Primary and Secondary School, Hai Duong province, Vietnam

09/1991-09/1998 High School, Hai Duong province, Vietnam

09/1998-09/2002 Undergraduate student, Hanoi University of Sciences
Major: *Mathematical Mechanics*, Grade: *Very good*

09/2002-09/2004 Master thesis at Hanoi University of Sciences
Major: *Mechanics of Deformable Solids*

since 02/2006 PhD student at Department of Applied Geophysics,
Institute of Geosciences, Friedrich-Schiller-University Jena

Contracts

09/2002-02/2006 Assistant teacher, Mechanics department,
Mathematics, Mechanics and Informatics Faculty,
Hanoi University of Sciences

since 02/2006 Research Associate in working group "Applied Geophysics" at
the Institute of Geosciences, Friedrich-Schiller-University Jena

Jena, 05th November 2008.

Tran Thanh Tuan

Acknowledgements

Firstly, I am immensely grateful to my supervisor, Prof. Peter Malischewsky (Institute of Geosciences, Friedrich-Schiller-University Jena), for his constant guidance, valuable suggestions and supervision, not only in research work but also during my three years of social life in Jena, which have made it possible to complete this dissertation.

Secondly, I am thankful to my second supervisor, Prof. Frank Scherbaum (Institute of Geosciences, University of Potsdam) for many valuable suggestions and new ideas for the thesis.

I would like to thank also Dr. Frank Wuttke from Bauhaus-University Weimar for his assistance in applying Herrmann's program and Dr. Matthias Ohrnberger from Institute of Geosciences, University of Potsdam for his help in making some important figures.

It is my privilege to express my deep and sincere gratitude towards Prof. Pham Chi Vinh for introducing me to Jena and for good advice in the time I have worked in Jena.

I use this opportunity to express my sincere gratitude towards Prof. Gerhard Jentzsch, Dr. Thomas Jahr and other members in Department of Applied Geophysics, Institute of Geosciences, Friedrich-Schiller-University Jena for valuable comments and ideas in the weekly group seminars.

I am also grateful to Andre Gebauer and Marco Naujoks for many supports which help me to integrate into the social life in Germany.

Thanks also go to all my friends in Vietnamese community living in Jena for their kind support and help.

And most importantly, I would like to express my deepest gratitude to my parents, and my family members for their endless support and love.

Lastly I must also thank those whose names are not appearing, but who have offered their help.

Thank you.

Selbstständigkeitserklärung

Ich erkläre, dass ich die vorliegende Arbeit selbstständig und unter Verwendung der angegebenen Hilfsmittel, persönlichen Mitteilungen und Quellen angefertigt habe.

Jena, den 05. November 2008.

Tran Thanh Tuan